Nonlinear wave collapse and strong turbulence

P. A. Robinson*

School of Physics, University of Sydney, NSW 2006, Australia

The theory and applications of wave self-focusing, collapse, and strongly nonlinear wave turbulence are reviewed. In the last decade, the theory of these phenomena and experimental realizations have progressed rapidly. Various nonlinear wave systems are discussed, but the simplest case of collapse and strong turbulence of Langmuir waves in an unmagnetized plasma is primarily used in explaining the theory and illustrating the main ideas. First, an overview of the basic physics of linear waves and nonlinear wave-wave interactions is given from an introductory perspective. Wave-wave processes are then considered in more detail. Next, an introductory overview of the physics of wave collapse and strong turbulence is provided, followed by a more detailed theoretical treatment. Later sections cover numerical simulations of Langmuir collapse and strong turbulence and experimental applications to space, ionospheric, and laboratory plasmas, including laser-plasma and beam-plasma interactions. Generalizations to self-focusing, collapse, and strong turbulence of waves in other systems are also discussed, including nonlinear optics, solid-state systems, magnetized auroral and astrophysical plasmas, and deep-water waves. The review ends with a summary of the main ideas of wave collapse and strong-turbulence theory, a collection of open questions in the field, and a brief discussion of possible future research directions. [S0034-6861(97)00502-3]

CONTENTS

*Electronic address: robinson@physics.usyd.edu.au

I. INTRODUCTION

In a nonlinear medium, the refractive index depends on the intensity of waves present. This allows waves to interact with waves, mediated by these refractive-index variations. One such interaction is the phenomenon of *self-focusing* in which an intense wave packet raises the refractive index of the medium, leading to an increasing tendency for the waves to refract and be trapped in regions of highest intensity. In one dimension, this effect can be balanced by dispersion, leading to the formation of stable solitons (Bullough and Caudrey, 1980). However, in two or three dimensions, self-focusing can dominate over dispersion, beyond a threshold intensity, leading to runaway wave collapse. A collapsing wave packet self-focuses to ever shorter scales and higher intensities until other physical effects intervene to arrest it, most often by means of dissipation. Figure 1 shows the contraction of the core of an intense Langmuir wave packet seen in a three-dimensional simulation of an unmagnetized plasma by Robinson *et al.* (1988).

It is possible to sustain many coexisting collapsing wave packets by supplying energy from an external source, or pump, to balance losses incurred when collapsing packets are arrested. This case corresponds to *strong turbulence*, which is chiefly distinguished from its better-known counterpart *weak turbulence* by the dominance of phase-coherent four-wave or many-wave interactions (rather than three-wave interactions and/or random-phase interactions), as discussed in Sec. III. Figures 2(a) and 2(b) show ensembles of intense, coherent wave packets amid background turbulence, as seen in two- and three-dimensional simulations, respectively, of strong turbulence in an unmagnetized plasma (Robinson and Newman, 1990a).

The main aims of this review are to explain the physics behind wave collapse and strong turbulence, to provide an overview of recent developments in the field, and to show how these ideas can be applied more widely. A decade has passed since the publication of the last general reviews of wave collapse and strong turbulence aimed at a broad audience (Rudakov and Tsytovich, 1978; Sagdeev, 1979; Thornhill and ter Haar, 1978; Zakharov, 1984; Goldman, 1984; Shapiro and Shevchenko, 1984; Kuznetsov *et al.*, 1986), although some more specialized reviews have appeared (e.g., ter Haar and Tsytovich, 1981; Zakharov *et al.*, 1985; Rubenchik and Zakharov, 1991; Sagdeev *et al.*, 1991;

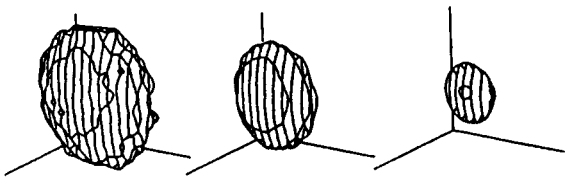

FIG. 1. Collapse of a three-dimensional Langmuir wave packet seen in numerical simulations (Robinson *et al.*, 1988). A surface of constant electric-field strength is drawn at 80% of the maximum value at the center of the packet. Time increases to the right and each frame has linear dimensions of 80 Debye lengths [see Eq. (2.1) for definition] in each direction.

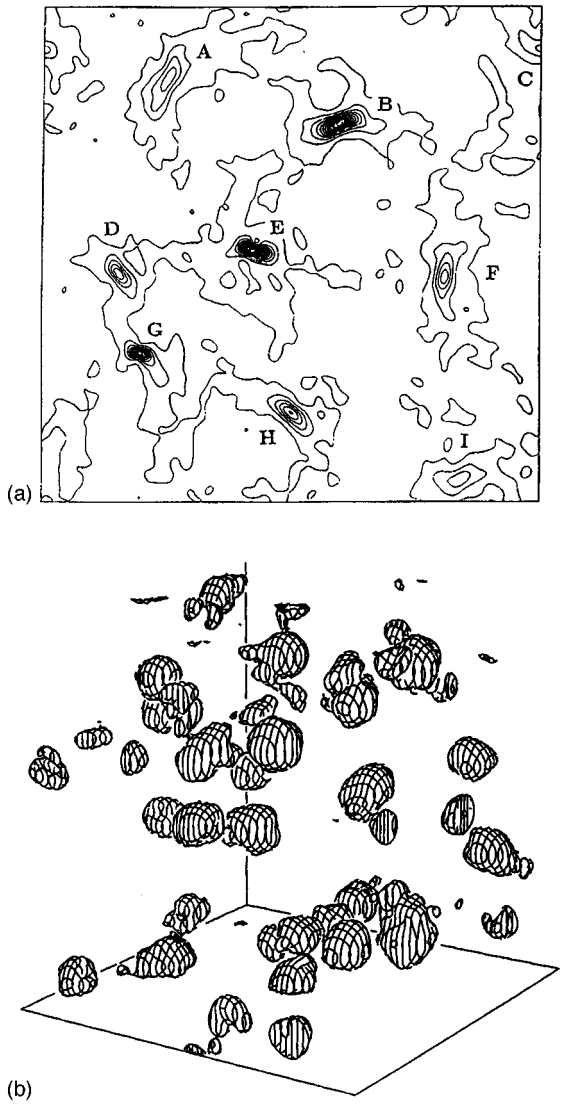

FIG. 2. Strong Langmuir turbulence from numerical simulations by Robinson and Newman (1990a). (a) Two-dimensional case, showing contours of constant Langmuir energy density. The lettered peaks are localized, coherent wave packets, subject to collapse. Regions in between are filled with low-level incoherent waves. The system has dimensions of 1340 Debye lengths [see Eq. (2.1) for definition] in each direction. (b) Three-dimensional case, showing a surface of constant energy density at 10% of the maximum value, enclosing the high-field regions of localized, coherent wave packets. Regions in between are filled with low-level incoherent waves. The system has dimensions of 800 Debye lengths in each direction.

DuBois and Rose, 1991). In this interval, many advances in the theory of such phenomena have occurred, rendering obsolete some previous pictures. In parallel, there has been major progress in two- and three-dimensional numerical simulations of such systems, with massive increases in computing power leading to many significant new insights. In addition, a variety of applications of wave collapse to phenomena in the laboratory and nature have been carried out, yielding a far wider range of tests of the theory than was previously possible. All these aspects point to the need for a fresh review.

One problematic area in the literature is that some recent applications and theoretical works have relied on outmoded or purely one-dimensional results, without the benefit of recent theoretical insights into multidimensional turbulence. This situation also motivates this review, in particular the inclusion of a section (Sec. VIII.A) covering common misconceptions and misunderstandings of wave collapse and strong-turbulence phenomena.

To minimize the mathematical and physical ''overhead'' required, attention is concentrated chiefly on the simplest and best understood case of Langmuir waves, which are electrostatic waves near the plasma frequency in an unmagnetized plasma. In solid-state physics, analogous waves in metals and semiconductors are called plasma waves (Kittel, 1976). Collapse and strong turbulence of Langmuir waves are reasonably well understood after many years of study, which began in earnest with the work of Zakharov (1972), although Hasegawa (1970) analyzed a related system involving cyclotron waves somewhat earlier. Study of the Langmuir wave system provides a relatively simple illustration of the relevant effects, a strong basis for study of other collapsing and turbulent systems, and many useful tools with which to do so. Nonlinear Langmuir waves are also important in their own right, with numerous applications in the laboratory and nature, including ionospheric-modification experiments, planetary radio emissions, relativistic-electron-beam systems, and laser-plasma experiments, as discussed in Sec. VIII. It should be emphasized, however, that other wave systems are also discussed (chiefly in Sec. IX). These include waves in nonlinear optical media (Chiao *et al.*, 1964; Sodha *et al.*, 1976; Shen, 1984; Boyd, 1992; Saleh and Teich, 1991), upper- and lower-hybrid plasma waves (Sturman, 1976; Lipatov, 1977), and deep-water waves (Davey and Stewartson, 1974).

Sections II and III of this paper introduce the essential background physics of linear waves, nonlinear refractive-index variations, and weak-turbulence theory. These sections also introduce the Zakharov equations (Zakharov, 1972), which describe the nonlinearities essential to Langmuir collapse and strong turbulence. The derivation of these equations is briefly outlined, their regimes of validity are delimited, and the limit in which they reduce to the standard (cubic) nonlinear Schrödinger equation is discussed, emphasizing the physics in each case.

Section IV briefly outlines the current picture of the physics of wave collapse and strong turbulence to orient the reader prior to the more detailed material that follows. This section introduces the key ideas of self-focusing, collapse, and arrest. It then goes on to outline the wave-packet cycle of accumulation, or nucleation, of energy into localized packets, followed by nonlinear collapse, arrest, relaxation, and renucleation, that has emerged as a key element of strong-turbulence theory (Doolen *et al.*, 1985). The basic elements of a statistical theory of strong turbulence are also laid out in this section. Together, Secs. II–IV provide a mini-review of the main ideas. Readers who are not concerned with the detailed theory can skip Secs. V–VII and proceed directly to discussion of experimental applications.

Wave collapse is considered in detail in Sec. V, tracking a packet through the cycle of nucleation, collapse, arrest, relaxation, and renucleation. The structure of nucleating packets and their coupling to an external pump is addressed. A means of calculating collapse thresholds by Hamiltonian methods is also briefly reviewed. Collapse evolution is discussed in detail, along with the arrest of collapse and subsequent relaxation of remnant structures. Throughout this section, comparisons with numerical simulations are made.

Strong turbulence is the focus of Sec. VI, which concentrates particularly on statistical properties of plasmas containing a multitude of collapsing wave packets. Calculations of such properties primarily use a two-component model of the waves in which the collapsing packets make up one component, amid a sea of lower-level incoherent waves that constitute the second (Robinson and Newman, 1990a, 1990b; Robinson, 1996a). Properties such as the scalings of averaged quantities, power spectra, and distributions of field strengths are calculated for equilibrium and nonequilibrium plasmas pumped by a variety of energy sources. Again, numerical evidence for the picture presented is discussed.

Numerical simulations of wave collapse and strong turbulence have confirmed many theoretical predictions and have led to additional insights that have then been incorporated in further theoretical work—a particularly fruitful interplay for the nonlinear wave interactions considered here. In Sec. VII the results of numerical simulations in one to three dimensions are discussed, with emphasis on key advances. This section covers results obtained using solutions of the Zakharov, nonlinear Schrödinger, and Vlasov partial differential equations, and particle-in-cell methods.

Common misconceptions surrounding strong turbulence and wave collapse are discussed in Sec. VIII.A. We then discuss a selection of applications and experimental evidence for wave collapse and strong turbulence. These applications include electron-beam experiments (e.g., Quon *et al.*, 1974; Janssen, Bonnie, Granneman, Krementsov, and Hopman, 1984; Wong and Cheung, 1984; Levron *et al.*, 1987; Robinson and Newman, 1990c; Melatos *et al.*, 1996), the ionosphere (e.g., Cheung *et al.*, 1989, 1992; DuBois *et al.*, 1990, 1993a, 1993b), planetary foreshocks (Newman, 1985;

Robinson and Newman, 1991a; Cairns and Robinson, 1992a, 1995a), type-III radio bursts in the solar wind (e.g., Papadopoulos *et al.*, 1974; Nicholson *et al.*, 1978; Robinson, Willes, and Cairns, 1993), and laser-plasma interactions (e.g., Kruer, 1988; Baldis *et al.*, 1991; Rubenchik and Zakharov, 1991). Some of the applications in this section are to plasmas in which there is a weak magnetic field, but magnetic effects in general do not dominate collapse.

Section IX outlines generalizations of the basic theory to include waves governed by the nonlinear Schrödinger equation, optical systems (some of which historically preceded Zakharov's, 1972, work on plasmas), magnetized-plasma waves in auroral, solar, and astrophysical contexts where magnetic effects dominate, electromagnetic waves in dielectrics and semiconductors, and deep-water waves. Some of these generalizations have been explored in great detail, while others remain at the cutting edge of research. Hence, when concluding, Sec. X briefly reviews some of the main results and open questions, as well as some promising future research directions.

Before proceeding, it is worth noting some of the limitations of the present review. First, it does not pretend to be exhaustive. Rather, it concentrates on the current state of the theory and applications and some of the most important inputs that have led to that state. Peripheral material, historical curiosities, and apparent dead ends have been largely omitted. Second, it does not deal with the substantial body of literature on wave collapse in systems of arbitrary dimensionality (e.g., Kuznetsov *et al.*, 1986; Zakharov, Kosmatov, and Shvets, 1989, and references cited therein). Instead, it focuses solely on one- to three-dimensional systems. Third, it deemphasizes somewhat some applications that have been discussed in excellent recent reviews and other major papers. Of note in this context are applications to Langmuir turbulence excited by ionospheric-modification experiments, which were discussed in detail by DuBois *et al.* (1990, 1993b). Laser-plasma interactions also fall into this category, and the reader is referred to the book by Kruer (1988) and recent reviews for further information (Baldis *et al.*, 1991; Rubenchik and Zakharov, 1991). Fourth, because of the emphasis here on wave physics, particle acceleration by waves is not discussed in detail, although it is an extremely important aspect of nonlinear wave physics. Nor are nonlinear processes that result in emission of secondary waves treated in much detail, despite their central significance in many applications.

II. BASIC PHYSICS

This section briefly reviews the essential linear and nonlinear wave physics and discusses the nonlinear wave equations most commonly used to study wave collapse and strong turbulence. Nonlinear wave equations governing strong turbulence are then derived heuristically, emphasizing the main physical effects, and some of their main properties are summarized. In this and subsequent sections, SI units are used, except in rescaled dimensionless equations.

A. Linear waves

A fully ionized unmagnetized plasma, in which electrons and ions individually have velocity distributions near thermal equilibrium, supports three weakly damped linear wave modes—Langmuir, ion sound, and electromagnetic waves. (Additional modes associated with the presence of intense particle beams or other strongly non-Maxwellian features of electron or ion distributions are not considered here.) These waves are essential elements of the theory and we review their properties next.

(i) Langmuir, or electron-plasma, waves are waves in which electrons and ions oscillate out of phase. Electrostatic forces resulting from charge separation provide the restoring force, while electrons provide inertia. In a thermal plasma, the frequency ω_L and wave number k of this high-frequency electrostatic wave satisfy the dispersion relation

$$\omega_L \approx \omega_p(1+3k^2\lambda_D^2/2) \tag{2.1}$$

(Tonks and Langmuir, 1929; Melrose, 1986a; Swanson, 1989; Stix, 1992; Bittencourt, 1995), where the plasma frequency ω_p is given by $\omega_p^2=N_e e^2/m_e\epsilon_0$, N_e is the number density of electrons, $\lambda_D=V_e/\omega_p$ is the electron Debye length, $V_e=(k_B T_e/m_e)^{1/2}$ is the electron thermal velocity, T_e is the electron temperature, and m_e is the electron mass. Analogous waves exist in metals and semiconductors (Sodha *et al.*, 1976; Kittel, 1976).

Dissipation of linear Langmuir waves results from Landau damping due to resonance with electrons moving at the phase velocity of the waves. The temporal damping rate $\gamma_L(\mathbf{k})$ of Langmuir waves can be calculated from kinetic theory, giving (Melrose, 1986a; Swanson, 1989; Stix, 1992)

$$\gamma_L(\mathbf{k})=\omega_p\left(\frac{\pi}{8}\right)^{1/2}(k\lambda_D)^{-3}\exp\left(-\frac{1}{2k^2\lambda_D^2}\right), \tag{2.2}$$

in a Maxwellian (i.e., thermal) plasma for $(k^2\lambda_D)^2 \ll 1$, where damping is small. Note that throughout this paper, damping coefficients are defined in terms of wave amplitudes; energy damping coefficients are exactly twice as big.

(ii) Ion sound waves are low-frequency (i.e., $\omega_S \ll \omega_p$) electrostatic waves with the dispersion relation (Tonks and Langmuir, 1929; Melrose, 1986a; Swanson, 1989; Stix, 1992; Bittencourt, 1995)

$$\omega_S = k v_S, \tag{2.3}$$

$$v_S=(\gamma m_e/m_i)^{1/2}V_e, \tag{2.4}$$

where m_i is the ion mass and γ is the ratio of specific heats of the plasma, with

$$\gamma = 1+3T_i/T_e, \tag{2.5}$$

where T_i is the ion temperature. In these waves electrons and ions oscillate almost in phase, corresponding to density perturbations, with ions providing the inertia, and electron and ion pressures providing the restoring force. These waves have a damping coefficient (Melrose, 1986a; Swanson, 1989; Stix, 1992)

$$\frac{\gamma_S(\mathbf{k})}{\omega_S(\mathbf{k})}=\left(\frac{\pi\gamma}{8}\right)^{1/2}\left[\left(\frac{m_e}{m_i}\right)^{1/2}+\gamma\left(\frac{T_e}{2T_i}\right)^{3/2}e^{-\gamma T_e/T_i}\right], \quad (2.6)$$

where the first and second terms in the brackets arise from electron and ion Landau damping, respectively. Equation (2.6) implies that ion sound waves are heavily damped except for $T_e \gg T_i$.

(iii) Transverse electromagnetic waves are high-frequency waves that obey the dispersion relation

$$\omega_T=(\omega_p^2+k^2c^2)^{1/2}. \quad (2.7)$$

These waves are undamped in a collisionless unmagnetized plasma because their phase velocity always exceeds the speed of light and, hence, they cannot resonate with plasma particles.

B. Nonlinear effects: heuristic

The Langmuir and transverse wave frequencies, Eqs. (2.1) and (2.7), depend on the plasma density through ω_p, with a larger density corresponding to a smaller refractive index. Hence density fluctuations, such as those associated with ion sound waves, will affect the high-frequency waves, causing them to refract into regions of low density and high refractive index. This provides a nonlinear mechanism to couple high-frequency waves to ion sound waves.

A heuristic derivation of the equation obeyed by Langmuir waves in the presence of density fluctuations can be made by generalizing Eq. (2.1) to

$$\omega_L \approx \omega_p+\frac{3k^2V_e^2}{2\omega_p}+\frac{\delta N_e}{2N_e}\omega_p-i\gamma_L(\mathbf{k}), \quad (2.8)$$

where ω_p denotes the *unperturbed* plasma frequency here, $\delta N_e \ll N_e$ is a small density perturbation, $(k\lambda_D)^2 \ll 1$ has been assumed, and the damping has been included. For waves near the plasma frequency ω_p, the electric field $\boldsymbol{\mathcal{E}}$ can be approximated by

$$\boldsymbol{\mathcal{E}}=\tfrac{1}{2}[\mathbf{E}\exp(-i\omega_p t)+\mathbf{E}^*\exp(i\omega_p t)], \quad (2.9)$$

where the complex envelope field $\mathbf{E}$ varies slowly compared with ω_p. If we Fourier-transform Eq. (2.8) to coordinate space and apply an additional divergence operator, acting on the left, we find

$$\nabla\cdot\left(i\frac{\partial}{\partial t}+\frac{3V_e^2}{2\omega_p}\nabla^2+i\hat{\gamma}_L\right)\mathbf{E}=\nabla\cdot\left(\frac{\omega_p\delta N_e}{2N_e}\mathbf{E}\right), \quad (2.10)$$

where $\hat{\gamma}_L$ is an appropriate Langmuir damping operator, which can also be used to incorporate instabilities ($\gamma_L(\mathbf{k})<0$). Note that the additional divergence operators acting on the left of both sides of Eq. (2.10) ensure that the Langmuir field remains electrostatic, despite the coupling to density perturbations (the quantity $\delta N_e\mathbf{E}$ is not necessarily curl free). Equation (2.10) is the *first (electrostatic) Zakharov equation* (Zakharov, 1972). This must be supplemented by an auxiliary equation for the spatially uniform component of $\mathbf{E}$, $i\partial_t\mathbf{E}_0=\omega_p(\delta N_e\mathbf{E}/2N_e)_0$, where the subscript 0 denotes the $k=0$ component.

The first Zakharov equation shows how density fluctuations affect Langmuir waves. To obtain a closed system of equations, the effect of Langmuir waves on density fluctuations must also be included. An intense packet of coherent Langmuir waves can produce a density depression via the ponderomotive force, which reproduces the expression for wave pressure in the incoherent case. To zeroth order, a particle of charge q and mass m in such a field oscillates about a fixed mean position. However, when nonuniformities of the field are accounted for, the mean position (averaged over a time scale $\sim\omega_p^{-1}$) drifts slowly out of the packet as if subject to the force (Boot and Harvie, 1957; Gaponov and Miller, 1958; Melrose, 1986a)

$$\mathbf{F}_P=-\frac{q^2}{4m\omega_p^2}\nabla|\mathbf{E}|^2=-\nabla\phi_P, \quad (2.11)$$

where ϕ_P is the ponderomotive potential energy. This force is much stronger for electrons than ions, owing to the inverse dependence on mass in Eq. (2.11). Hence electrons are expelled from the packet, setting up an ambipolar field, which then drags ions out to maintain quasineutrality (i.e., equality of electron and ion number densities to zeroth order). This indirect effect on ions is a factor m_i/m_e greater than the direct ion ponderomotive force. There is thus an acceleration $\mathbf{F}_P/m_i$ of the entire plasma.

The divergence of the ponderomotive force enters as a forcing term in the linear ion-sound-wave equation, because the net force on an infinitesimal volume depends on variations of $\mathbf{F}_P$ across that volume. This gives

$$\left(\frac{\partial^2}{\partial t^2}+2\hat{\gamma}_S\frac{\partial}{\partial t}-v_S^2\nabla^2\right)\delta N_e=\frac{\epsilon_0}{4m_i}\nabla^2|\mathbf{E}|^2, \quad (2.12)$$

where setting the right-hand side to zero gives the linear ion-sound-wave equation with damping. Equation (2.12) is the *second Zakharov equation* (Zakharov, 1972).

The Zakharov equations (2.10) and (2.12) are often rewritten in dimensionless form by introducing the rescaled variables

$$\mathbf{r}'=\left(\frac{4m_e}{9m_i}\right)^{1/2}\frac{\mathbf{r}}{\lambda_D}, \quad (2.13)$$

$$t'=\frac{2m_e}{3m_i}\omega_p t, \quad (2.14)$$

$$n'=\frac{3m_i}{4m_e}\frac{\delta N_e}{N_e}, \quad (2.15)$$

$$|\mathbf{E}'|^2=\frac{3m_i}{4m_e}\frac{\epsilon_0|\mathbf{E}|^2}{4N_e k_B T_e}, \quad (2.16)$$

where $\mathbf{r}$ denotes position. Making these replacements, then omitting the primes, yields

$$\nabla\cdot\left(i\frac{\partial}{\partial t}+\nabla^2+i\hat{\gamma}_L\right)\mathbf{E}=\nabla\cdot(n\mathbf{E}), \tag{2.17}$$

$$\left(\frac{\partial^2}{\partial t^2}+2\hat{\gamma}_S c_S\frac{\partial}{\partial t}-c_S^2\nabla^2\right)n=\nabla^2|\mathbf{E}|^2, \tag{2.18}$$

with $i\partial_t\mathbf{E}_0=(n\mathbf{E})_0$, where all quantities are expressed in the rescaled units and c_S is the ratio of the sound speed to its value at $T_i=0$. In this review we use both dimensional and dimensionless units, distinguishing them where necessary.

In the *adiabatic* or *subsonic* limit in which density perturbations are changing slowly, the time derivatives in Eq. (2.18) can be neglected, yielding

$$n=-c_S^{-2}|\mathbf{E}|^2. \tag{2.19}$$

Substitution into Eq. (2.18) then shows that the Langmuir waves obey the electrostatic (cubic) nonlinear Schrödinger equation

$$\nabla\cdot\left(i\frac{\partial}{\partial t}+\nabla^2+i\hat{\gamma}_L+c_S^{-2}|\mathbf{E}|^2\right)\mathbf{E}=0, \tag{2.20}$$

in the adiabatic limit. This equation is extremely useful for understanding many qualitative features of wave collapse and strong-turbulence phenomena, as we shall see below.

The nonlinear Schrödinger equation is commonly used in nonlinear optics to approximate the response of nonlinear media. In this context, n corresponds to a refractive-index perturbation (with positive n giving a negative perturbation). In Kerr media, one has $n\propto-|\mathbf{E}|^2$ and Eq. (2.20) follows in appropriately rescaled units. We consider Kerr media further in Sec. IX.A.

For many years it was thought that the condition $W\ll1$ was required for the validity of the Zakharov equations, with

$$W=\frac{\epsilon_0|\mathbf{E}|^2}{4N_e k_B T_e}. \tag{2.21}$$

[Alternatively, in terms of the root-mean-square (rms) field $E_{\rm rms}$, one has $W=\epsilon_0 E_{\rm rms}^2/2N_e k_B T_e$.] However, it has more recently been shown that the correct condition is

$$W(k\lambda_D)^2\lesssim1, \tag{2.22}$$

if damping is ignored, where W and k are the characteristic energy density and wave number, respectively, of the Langmuir waves in question, i.e., not necessarily of the entire spectrum (Newman *et al.*, 1990; Mounaix *et al.*, 1991; DuBois *et al.*, 1995a; Vladimirov *et al.*, 1995); this point is discussed further in Sec. V.F. It has been extensively verified by Newman *et al.* (1990) that $W\ll1$ is not required, but that dissipation indirectly imposes the condition $W\lesssim1$ in practice; otherwise localized heating can change the local electron temperature and hence the coefficients of the wave equation. The Zakharov equations require $\delta N_e\ll N_e$ for their validity. This can also indirectly restrict W by requiring that the Langmuir ponderomotive force not be so strong as to produce an unacceptably large density well. These two "indirect" constraints are thus the more relevant, practically.

In addition to the above conditions, the nonlinear Schrödinger equation requires that velocities associated with changes in the Langmuir envelope be smaller than the sound velocity. Comparison of the characteristic sizes of the terms in Eq. (2.18) shows that this requires $W<Cm_e/m_i$, where C is a constant. Crude estimates yield $C\approx1$, but simulations and more careful analyses seem to imply a much larger value (see Sec. VI.C for further discussion).

C. Nonlinear effects: systematic

This section briefly outlines a more formal derivation of the Zakharov equations. The details are not necessary and it can be omitted on a first reading.

The effect of density fluctuations on Langmuir and transverse waves can be studied by treating the plasma as a fluid and linearizing the hydrodynamic equations (Zakharov, 1972, 1984; Škorić and ter Haar, 1980), along with Maxwell's equations, subject to quasineutrality of the low-frequency oscillations. These steps yield

$$\frac{1}{c^2}\left(\frac{\partial^2\mathbf{E}}{\partial t^2}+\omega_p^2\mathbf{E}\right)+\nabla\times(\nabla\times\mathbf{E})-3\frac{V_e^2}{c^2}\nabla\nabla\cdot\mathbf{E}=-\omega_p^2\frac{\delta N_e}{N_e}\mathbf{E}, \tag{2.23}$$

in dimensional form. For $\delta N_e=0$ this equation has both Eqs. (2.1) and (2.7) as solutions.

If beats at $2\omega_p$ and zero frequency are neglected, along with the term $\partial^2\mathbf{E}/\partial t^2$, Eq. (2.23) becomes

$$-2i\frac{\omega_p}{c}\frac{\partial\mathbf{E}}{\partial t}+\nabla\times(\nabla\times\mathbf{E})-3\frac{V_e^2}{c^2}\nabla\nabla\cdot\mathbf{E}=-\omega_p^2\frac{\delta N_e}{N_e}\mathbf{E}. \tag{2.24}$$

Equation (2.24) is the first *electromagnetic* Zakharov equation, which incorporates the effects of density fluctuations on both Langmuir and transverse waves.

In a nonrelativistic plasma V_e^2/c^2 is small and the Langmuir waves are longitudinal waves that can be described by an electrostatic potential Φ, with $\mathbf{E}=-\nabla\Phi$ (Zakharov, 1972, 1984; Kuznetsov *et al.*, 1986; Melrose, 1986a). If we introduce Φ into Eq. (2.24) and take the divergence of both sides to project out the electrostatic Langmuir component of the equation, we obtain Eq. (2.17) in dimensionless units. The condition $V_e^2/c^2\ll1$ is thus an additional requirement for the validity of the electrostatic Zakharov equation (2.17).

The second Zakharov equation (2.18) can be derived more rigorously by noting that low-frequency oscillations involve slight charge separations, despite quasineutrality, because electrons have less inertia than do ions (Zakharov, 1984). This leads to the appearance of an ambipolar potential energy in addition to the ponderomotive potential ϕ_P of Eq. (2.11). If the electrons are distributed in the resulting potential according to a

Boltzmann distribution, it can then be shown that Eq. (2.18) results (Zakharov, 1984).

Before leaving this section, we note that Melrose (1987b) derived the Zakharov equations by calculating the quadratic and cubic plasma response tensors from kinetic theory, then making suitable approximations. This route is more complicated than the ones outlined here, but has the advantage that the approximations are more explicit. Goodman (1991), DuBois *et al.* (1995a), and Vladimirov *et al.* (1995) also carried out kinetic theory derivations of generalized Zakharov equations.

D. Conserved quantities

In the absence of damping, the nonlinear Schrödinger equation (2.20) can be written in terms of the Hamiltonian H and the potential Φ

$$i\frac{\partial}{\partial t}\nabla^2\Phi=\frac{\delta H}{\delta\Phi^*}, \tag{2.25}$$

where the right-hand side is the functional derivative

$$\frac{\delta}{\delta\Phi^*}=\frac{\partial}{\partial\Phi^*}-\sum_j\frac{d}{dx_j}\frac{\partial}{\partial(\partial\Phi^*/\partial x_j)}. \tag{2.26}$$

In a D-dimensional system the Hamiltonian H in Eq. (2.21) is (Gibbons *et al.*, 1977; Zakharov *et al.*, 1985)

$$H=\int\mathcal{H}d^D\mathbf{r}, \tag{2.27}$$

$$\mathcal{H}=|\nabla^2\Phi|^2-\tfrac{1}{2}|\nabla\Phi|^4 \tag{2.28}$$

$$=|\nabla\cdot\mathbf{E}|^2-\tfrac{1}{2}|\mathbf{E}|^4. \tag{2.29}$$

The first term on the right of the Hamiltonian density $\mathcal{H}$ in Eq. (2.28) or Eq. (2.29) corresponds to wave dispersion, while the second represents nonlinear self-focusing. The negative sign indicates that self-focusing tends to oppose dispersion, a point discussed in detail below.

In the absence of damping, the nonlinear Schrödinger equation (2.20) conserves the Hamiltonian, the total number of Langmuir quanta N, the total Langmuir momentum $\mathbf{P}$, and the total angular momentum $\mathbf{M}$ (Gibbons *et al.*, 1977),

$$N=\int|\mathbf{E}|^2d^D\mathbf{r}, \tag{2.30}$$

$$P_j=\int\frac{i}{2}\sum_{l=1}^{3}(E_l\partial_jE_l^*-E_l^*\partial_jE_l)d^D\mathbf{r}, \tag{2.31}$$

$$\mathbf{M}=\int(i\mathbf{E}\times\mathbf{E}^*+\mathbf{r}\times\mathcal{P})d^D\mathbf{r}, \tag{2.32}$$

where $\mathcal{P}$ is the integrand in Eq. (2.31). These conserved quantities, and the Hamiltonian formulation in general, prove to be of great use in studying nonlinear phenomena in later sections.

If the initial divergence operators on both sides of the first Zakharov equation (2.17) are omitted, the Zakharov equations can also be written as Hamiltonian equations, with

$$\mathcal{H}=|\nabla\cdot\mathbf{E}|^2+n|\mathbf{E}|^2+\tfrac{1}{2}n^2+\tfrac{1}{2}|\nabla u|^2, \tag{2.33}$$

for $c_S=1$. The hydrodynamic flux potential u has been introduced, which satisfies $u_t=n+|\mathbf{E}|^2$ and $n_t=\nabla^2u$. The first term on the right of Eq. (2.33) represents dispersion, while the others are nonlinear contributions. The Zakharov equations conserve H, N, $\mathbf{P}$, and $\mathbf{M}$, with the definitions as above, except that

$$P_j=\int\left(\frac{i}{2}\sum_{l=1}^{3}(E_l\partial_jE_l^*-E_l^*\partial_jE_l)-n\partial_ju\right)d^D\mathbf{r}. \tag{2.34}$$

Although the version of the first Zakharov equation without initial divergence operators may ultimately develop nonelectrostatic fields with nonzero curl, it can yield significant insights into the stability and short-term dynamics of an initially curl-free system, as will be seen in later sections. Setting $n=-|\mathbf{E}|^2$ and $u=0$ in Eqs. (2.33) and (2.34) reproduces the nonlinear Schrödinger forms of these quantities. Adding a term $\alpha(\nabla\times\mathbf{E}^*)\cdot(\nabla\times\mathbf{E})$ to $\mathcal{H}$ yields the dimensionless form of the electromagnetic Zakharov equation (2.23) for $\alpha=c^2m_e/3k_BT_e$ (Gibbons *et al.*, 1977).

III. WAVE-WAVE INSTABILITIES AND WEAK TURBULENCE

The Zakharov equations contain terms describing both three- and four-wave interactions between plane waves, including decay of two waves to produce a third, the inverse process of coalescence, and four-wave modulational instability, which leads to breakup of a uniform wave envelope into localized packets. These processes are important in many weak-turbulence and strong-turbulence contexts, and modified forms play a role in the formation and collapse of wave packets. This section first briefly reviews the phase-coherent plane-wave instabilities, involving Langmuir waves and ion sound waves, that are relevant to strong turbulence. It then turns to weak turbulence, in which phase relationships (and, usually, four-wave interactions) are unimportant and the Langmuir waves can be described by their intensities. Finally, the crossover from weak to strong turbulence is discussed, along with conditions under which both regimes can coexist.

A. Phase-coherent plane-wave instabilities

A monochromatic plane Langmuir wave of field strength $|\mathbf{E}|$ is not necessarily stable in the presence of the nonlinear terms in Eqs. (2.17) and (2.18). Such a plane wave can be represented by the potential

$$\Phi_0(t,\mathbf{r})=\frac{|\mathbf{E}|}{|k|}\exp[i\mathbf{k}\cdot\mathbf{r}-i\omega(\mathbf{k})t]. \tag{3.1}$$

The first step in a linear stability analysis of this wave is to add a small perturbation $\delta\Phi(t,\mathbf{r})$ such that

$$\Phi = \Phi_0 + \delta\Phi. \tag{3.2}$$

The density response n to this potential has the general form in Fourier space

$$n(\Omega,\mathbf{K}) = \frac{T_e}{N_e} G(\Omega,\mathbf{K})\phi_P(\Omega,\mathbf{K}), \tag{3.3}$$

where ϕ_P is given by Eq. (2.11) and $G(\Omega,\mathbf{K})$ is the appropriate Green function, which can be calculated from plasma kinetic or fluid theory in various limits (e.g., Tsytovich, 1977, 1995; Zakharov *et al.*, 1985; Vladimirov *et al.*, 1995). Equation (3.3) generalizes the relationship obtained by Fourier-transforming Eq. (2.12), for example.

Linearization of Eq. (2.10) about Φ_0 using Eq. (3.3) yields the following dispersion equation for the density response at Ω and $\mathbf{K}$ (Zakharov, 1984; Zakharov *et al.*, 1985):

$$1 + \frac{\omega_p}{4} W G(\Omega,\mathbf{K}) \left(\frac{\cos^2\theta_+}{\omega(\mathbf{k}+\mathbf{K}) - \omega(\mathbf{k}) - \Omega} + \frac{\cos^2\theta_-}{\omega(\mathbf{k}-\mathbf{K}) - \omega(\mathbf{k}) + \Omega} \right) = 0, \tag{3.4}$$

where $\theta_\pm$ is the angle between $\mathbf{k}$ and $\mathbf{k}\pm\mathbf{K}$, and W is the ratio of Langmuir wave energy density to thermal energy density, given by Eq. (2.21). Equation (3.4) generalizes earlier dispersion equations (e.g., Bardwell and Goldman, 1976) by including the general Green function $G(\Omega,\mathbf{K})$. In the limit $W\to 0$ the only solutions of Eq. (3.4) are linear ion sound waves, which correspond to a pole of the Green function. Note that ω and Ω can be complex in Eq. (3.4), to incorporate growth and damping.

Zakharov *et al.* (1985) showed that five different instability regimes exist for monochromatic waves, depending on the values of W and k. These regimes are summarized in Fig. 3 and discussed briefly below. This discussion outlines the main physical features and clarifies the terminology, which has been the source of much confusion in the literature. In general, this article follows the terminology of Zakharov *et al.* (1985), but the instability regimes in Fig. 3 are numbered differently from those in this reference. Linear damping is ignored in this section, to concentrate attention on the nonlinear processes. This precludes detailed discussion here of the case of heavily damped density responses for $T_e \lesssim T_i$ (the reader should see Zakharov *et al.*, 1985, and the references cited therein for more detail); such regimes are, however, encountered in some applications covered in Secs. VIII and IX, such as ionospheric-modification experiments (DuBois *et al.*, 1993a). Linear damping tends to raise the thresholds for nonlinear processes.

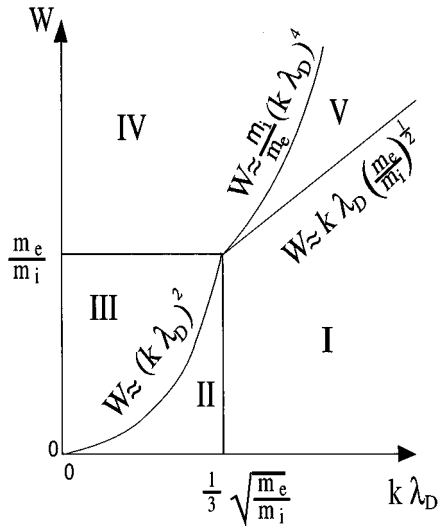

FIG. 3. Regimes of monochromatic, plane-wave Langmuir instabilities as functions of $k\lambda_D$ and W. Approximate boundaries are as labeled. Region I: Electrostatic decay. Region II: Modulational instability. Region III: Subsonic modulational instability. Region IV: Supersonic modulational instability. Region V: Modified decay instability.

1. Electrostatic decay instability

The electrostatic decay instability dominates in Region I of Fig. 3, where $k > k_*/2$ and $W < k\lambda_D(m_e/m_i)^{1/2}$, with

$$k_* \approx \frac{2}{3}\left(\frac{\gamma m_e}{m_i}\right)^{1/2} k_D, \tag{3.5}$$

$k_D = 1/\lambda_D$, and γ given by Eq. (2.5). In this regime, a Langmuir wave L decays into another, L', and an ion sound wave S in the process $L \to L' + S$ illustrated in Fig. 4 (Oraevskii and Sagdeev, 1962; Silin, 1965; DuBois and Goldman, 1967; Nishikawa, 1968a, 1968b). Zakharov *et al.* (1985) discussed the threshold and maximum growth rate of this instability, finding that the growth rate peaks with a value $\Gamma_{\max}$ at $\mathbf{K} = \mathbf{K}(\Gamma_{\max})$ with

$$\Gamma_{\max} \approx \frac{\omega_p}{2}\left(\frac{\gamma m_e}{m_i}\right)^{1/4} (k\lambda_D)^{1/2} W^{1/2} < \Omega, \tag{3.6}$$

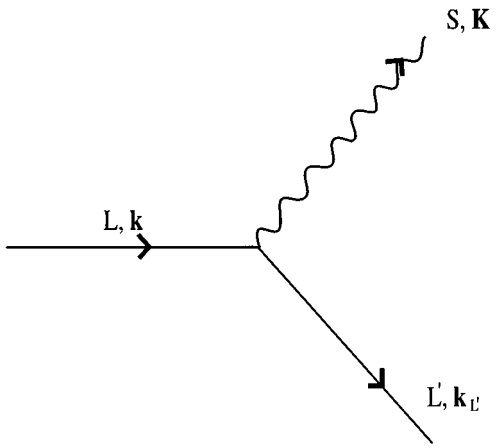

FIG. 4. Quantum view of the decay instability, showing decay of a Langmuir quantum L of wave vector $\mathbf{k}$ into a product Langmuir quantum L' of wave vector $\mathbf{k}_{L'}$ and ion sound quantum S of wave vector $\mathbf{K}$.

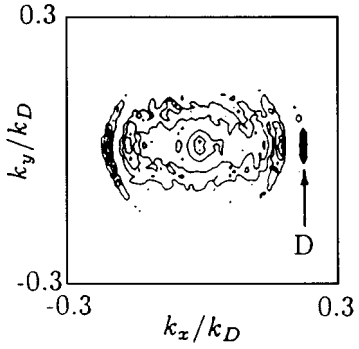

FIG. 5. Langmuir wave-number spectrum from two-dimensional strong turbulence pumped by a driver, labeled "D," at $\mathbf{k}=0.225k_D\hat{\mathbf{x}}$ (logarithmic scale, highest three decades), from Robinson and Newman (1989).

$$\mathbf{K}(\Gamma_{\max})\approx 2\mathbf{k}-\hat{\mathbf{k}}k_* . \tag{3.7}$$

Hence the most rapidly growing product Langmuir wave's wave vector satisfies $\mathbf{k}_{L'}\approx -\mathbf{k}+\hat{\mathbf{k}}k_*$, implying that L' is backscattered relative to L for $k_L>k_*$. The wave number of the product Langmuir wave is reduced in magnitude by k_*, reflecting the loss of energy to the product ion sound wave, with $\omega(\mathbf{k}_{L'})=\omega(\mathbf{k})-\Omega$, and where Ω and $\mathbf{K}$ satisfy the dispersion relation (2.3).

In Region I of Fig. 3, the denominator of the second term in the square brackets in Eq. (3.4) is very small for the unstable waves, implying that the three waves in Fig. 4 satisfy energy conservation. Near vanishing of the denominator of the first term in the square brackets corresponds to coalescence between the parent wave and an ion sound wave, but is not relevant here.

Figure 5 shows a plot of the Langmuir wave-number spectrum from a two-dimensional simulation of turbulence governed by the Zakharov equations (Robinson and Newman, 1989). This shows that the product waves L' are spread over a broad arc in k space toward the left of the figure, consistent with energy and momentum conservation at the quantum level. Moreover, subsequent decays carry the energy toward $k=0$ in a cascade, visible as a series of arcs, successively closer to the origin. This implies that energy initially injected at large k ends up in a condensate, seen as a peak near $k=0$. Waves with $k<k_*/2$ cannot undergo further decays. Note that the cascade could more precisely be termed an inverse cascade, because it transfers energy in the opposite direction to the more familiar Kolmogorov cascade in fluid turbulence. No sign of coalescence of sound waves with driven Langmuir waves is seen in Fig. 5 (i.e., no peak at higher k than the driver), although this does not preclude coalescence at a very low rate. In some cases of strong turbulence discussed later, the decay cascade does not extend all the way to $k=0$, owing to collisional damping or other effects (Hanssen *et al.*, 1992; Robinson, Newman, and Rubenchik, 1992; DuBois *et al.* 1993a, 1993b, 1995a).

Figure 6(a) shows contours of Γ vs $\mathbf{K}$ for a typical point in Region I of Fig. 3. The maximum growth rate is at the point given by Eq. (3.7), but the unstable waves

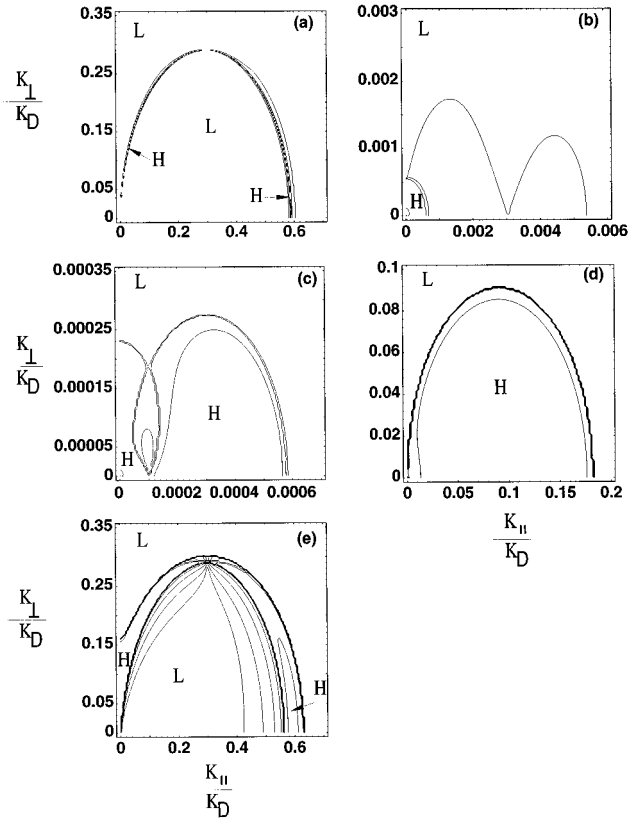

FIG. 6. Contour plots of $\Gamma_{\max}$ vs $\mathbf{K}$ for the density response in Eq. (3.4). The parent wave has $\mathbf{k}$ along the horizontal (parallel) axis. In all cases $T_e=100T_i$, contours are spaced logarithmically one decade apart, the lowest contour is at $10^{-9}\omega_p$, and the maximum Γ occurs at a point on the parallel axis. The letters H and L mark highs and lows, respectively, for clarity. (a) Region I, electrostatic decay instability for $k=0.3k_D$ and $W=10^{-6}$; (b) Region II, modulational instability for $k=0.003k_D$ and $W=10^{-6}$; (c) Region III, subsonic modulational instability for $k=10^{-4}k_D$ and $W=10^{-6}$; (d) Region IV, supersonic modulational instability for $k=10^{-4}k_D$ and $W=0.1$; (e) Region V, modified decay instability for $k=0.3k_D$ and $W=0.1$.

follow a thin arc of broad angular extent, along which energy and momentum conservation are satisfied. This arc is so thin as to be incompletely resolved in Fig. 6(a). Note that in all frames of Fig. 6 a good approximation to the full Green function from kinetic theory was substituted into Eq. (3.4) to obtain the numerical results shown.

2. Modulational instability

In Region II of Fig. 3 the instability with the largest growth rate is a modulational instability, which causes an initially uniform plane wave to become modulated, breaking up into wave packets with a scale $\sim K^{-1}$ (Vedenov and Rudakov, 1964). In terms of a Hamiltonian such as Eq. (2.29), development of modulation increases the magnitude of the negative $|\mathbf{E}|^4$ term faster than that of the first term $|\nabla\cdot\mathbf{E}|^2$. The modulated wave train thus has a lower energy than the original plane

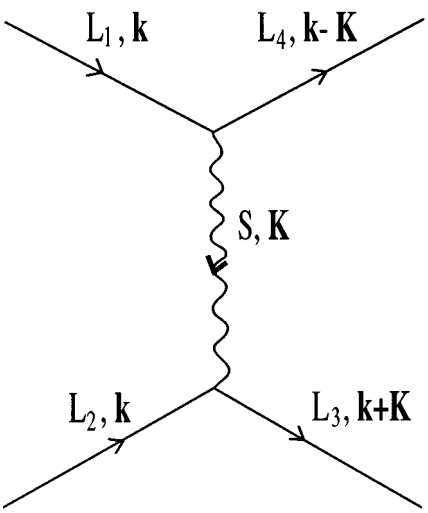

FIG. 7. Quantum view of a modulational instability. Two Langmuir quanta, L_1 and L_2, scatter into the states L_3 and L_4 via the exchange of an ion sound quantum of momentum $\mathbf{K}$, which can correspond either to a freely propagating ion sound wave or a strongly damped quasimode (a virtual quantum).

wave. For historical reasons, some modulational instabilities have been termed *oscillating two-stream instabilities* (OTSI) in much of the older literature, and even in some recent work. This terminology has proved to be highly confusing and should be rigorously avoided.

For $T_i \ll T_e$, this instability has (Zakharov *et al.*, 1985)

$$\Gamma_{\max} \approx \omega_p \frac{W}{4}, \tag{3.8}$$

$$\mathbf{K}(\Gamma_{\max}) \approx \left(\frac{W}{6}\right)^{1/2} k_D \hat{\mathbf{k}}, \tag{3.9}$$

with $K(\Gamma_{\max}) \ll k$ and $\Gamma_{\max} < \Omega$. The maximum growth rate occurs parallel to $\mathbf{k}$, but strong growth is also found along a broad arc extending around to the perpendicular direction, as seen at the bottom left of Fig. 6(b). The dependence of $\Gamma_{\max}$ and $\mathbf{K}(\Gamma_{\max})$ on T_i/T_e is only weak (Zakharov *et al.*, 1985).

At the quantum level, the modulational instability corresponds to the four-wave process shown in Fig. 7, in which two Langmuir quanta exchange an ion sound quantum. The latter quantum can correspond either to an ion sound wave that approximately satisfies the dispersion relation (2.3) or to a rapidly damped (or growing) nonresonant quasimode, i.e., a virtual quantum in field-theoretic terms. This instability broadens the initial Langmuir spectrum in k space, transferring quanta to both slightly higher and slightly lower k, since $K \ll k$ for the fastest-growing perturbations.

3. Subsonic modulational instability

This instability, which dominates in Region III of Fig. 3, is very closely related to the modulational instability considered above. However, $\Gamma_{\max}$ exceeds Ω, so we are dealing with an ion quasimode in Fig. 7, rather than an ion sound wave that satisfies the dispersion relation (2.3). In this case Eqs. (3.8) and (3.9) remain valid, but $\Gamma_{\max} > \Omega$ and $K(\Gamma_{\max}) \gg k$ (Zakharov *et al.*, 1985). This instability transfers Langmuir quanta to larger k, while increasing W in the modulated packets. Figure 6(c) shows that the region of near-maximal growth is very broad in this case, so the density response has a significant component perpendicular to $\mathbf{k}$. The highest growth occurs on the parallel axis for $K_\parallel \approx 0.003 k_D$, and the edges of the growth region are seen to be fairly sharp.

4. Supersonic modulational instability

Once W becomes sufficiently large, as in Region IV of Fig. 3, the phase velocity of the Langmuir perturbations exceeds the sound velocity and the modulational instability is termed *supersonic*. In this regime, the density response is weakened because ion inertia makes it hard for the ions to "keep up" with the changing Langmuir envelope as the perturbation evolves. Here (Zakharov *et al.*, 1985)

$$\Gamma_{\max} \approx \omega_p \left(\frac{m_e W}{3 m_i}\right)^{1/2}, \tag{3.10}$$

$$\mathbf{K}(\Gamma_{\max}) \approx W^{1/2} k_D \hat{\mathbf{k}}, \tag{3.11}$$

with $K(\Gamma_{\max}) \gg k$ [the factor of 3 in the denominator in Eq. (3.10) is from an unpublished calculation by I. H. Cairns]. This instability is similar to the subsonic modulational instability in that it carries energy to higher k. The weakened density response is seen in the scaling $\Gamma_{\max} \propto W^{1/2}$, which replaces $\Gamma_{\max} \propto W$ in the subsonic case. Figure 6(d) shows that, as for the subsonic modulational instability, the growth rate of this instability is large and nearly constant over a broad region with large perpendicular extent and quite sharp edges. This region satisfies $K^2 \lambda_D^2 < W \cos^2\theta$, with $\cos\theta = \hat{\mathbf{K}} \cdot \hat{\mathbf{k}}$.

5. Modified decay instability

The final instability regime discussed by Zakharov *et al.* (1985) was that of the modified decay instability, Region V of Fig. 3. The dominant instability in this region combines features of both the supersonic modulational instability and the decay instability because $\Gamma_{\max}$ exceeds Ω and the two branches of the nonlinear dispersion relation overlap due to the large uncertainty in the wave frequencies induced by the high growth rate. The sound quantum in Figs. 4 and 6 is thus a virtual quantum in a quasimode. It has (Nishikawa, 1968b; Zakharov *et al.*, 1985)

$$\Gamma_{\max} \approx \omega_p \left(\frac{m_e W k^2 \lambda_D^2}{m_i}\right)^{1/3} > \Omega, \tag{3.12}$$

$$\mathbf{K}(\Gamma_{\max}) \approx 2\mathbf{k}. \tag{3.13}$$

This instability carries Langmuir energy to smaller k, but is of little importance to us because it only occurs when k and W are both high, whereas Langmuir collapse most often begins at small k and/or W (see Secs.

IV–VI below). We do not consider this instability further in later sections. Figure 6(e) shows that regions of high growth follow a broadened arc, centered on the one shown in Fig. 6(a). The bandwidth of the broadened arc is $\sim\Gamma$, representing the intrinsic uncertainty in the frequency of a growing mode.

B. Weak turbulence

If an ensemble of Langmuir waves has a large enough bandwidth, phase information can become irrelevant due to the strong tendency of the waves to decohere. Characteristically, this occurs when the decoherence (i.e., phase-mixing) rate is greater than the competing nonlinear rates. In the case where the waves have random phases, one can average over phase to obtain a so-called *weak-turbulence* description of Langmuir interactions in terms of wave intensities. The adjective "weak" refers to the fact that nonlinear rates increase with W, so this description is restricted to weak fields for any given bandwidth (see Sec. III.C below).

In a weak-turbulence description, we introduce an *occupation number* $n(\mathbf{k})$, which represents the density of quanta in k space. The total energy in the waves is obtained by integrating $n(\mathbf{k})$ over all $\mathbf{k}$, weighted by $\hbar\omega(\mathbf{k})$, the energy per quantum. The occupation number is defined in terms of the second-order correlation function of the complex amplitude $a(\mathbf{k})$ of the waves [analogous to $\mathbf{E}$ in Eq. (2.9)], giving

$$\langle a(\mathbf{k})a(\mathbf{k}')^*\rangle = n(\mathbf{k})\,\delta^D(\mathbf{k}-\mathbf{k}'), \tag{3.14}$$

in a D-dimensional system, given suitable normalization. Equations for $n(\mathbf{k})$ can then be derived from those for the complex field amplitudes. Closure of the equations is achieved by making the assumption that the fields are Gaussian and stochastic when calculating fourth- and higher-order correlation functions. All correlation functions can then be expressed in terms of products of the $n(\mathbf{k})$ (Tystovich, 1977, 1995; Zakharov *et al.*, 1985; Melrose, 1986a). All odd-order correlation functions, except the third-order one, are zero.

Weak-turbulence descriptions of both three- and four-wave interactions have been reported in the literature (Tsytovich, 1977, 1995; Zakharov *et al.*, 1985; Melrose, 1986a; Musher *et al.*, 1995). For our purposes, only three-wave decay $L\rightarrow L'+S$ is relevant, because modulational instabilities are stabilized in the weak-turbulence regime (DuBois and Rose, 1981; Zakharov *et al.*, 1985; Melrose, 1986a; see also Sec. III.C below). In this case, we have (Melrose, 1986a)

$$\begin{aligned}\frac{dn_L(\mathbf{k})}{dt} = &-2n_L(\mathbf{k})\,\gamma(\mathbf{k}) \\ &-\int d^D\mathbf{k}_{L'}\int d^D\mathbf{k}_S w_{LL'S}\,\delta(\omega_L-\omega_{L'}-\omega_S) \\ &\times\delta^D(\mathbf{k}_L-\mathbf{k}_{L'}-\mathbf{k}_S)[n_L(\mathbf{k})n_{L'}(\mathbf{k}_{L'}) \\ &+n_L(\mathbf{k}_L)n_S(\mathbf{k}_S)-n_{L'}(\mathbf{k}_{L'})n_S(\mathbf{k}_S)],\end{aligned} \tag{3.15}$$

in dimensional units, where $w_{LL'S}$ is a weak function of the wave vectors of the three waves. The delta functions in Eq. (3.15) impose energy and momentum conservation in the three-wave process. The term $n_{L'}n_S$ has the opposite sign to the other two nonlinear terms because high levels of product waves tend to reverse the net interaction, resulting in coalescence $L'+S\rightarrow L$, which is implicitly included in Eq. (3.15). Equations analogous to Eq. (3.15) also exist for $n_{L'}$ and n_S. Even in the random-phase case, a decay instability can occur if n_L is large enough and $n_{L'}$ and n_S are not so big as to saturate it. In this case $\Gamma\propto W$ applies, rather than $\Gamma\propto W^{1/2}$.

Except in the case of high ion-sound-wave occupation numbers (a situation that requires low ion-sound-wave damping), three-wave interactions always cause n_L to decrease, carrying energy to lower k. In the case of strong ion-sound-wave damping, Zakharov *et al.* (1975) also showed rigorously that the Langmuir energy decreases monotonically. Hence weakly turbulent Langmuir waves accumulate in a condensate at very small k where further decays are no longer possible. This situation is seen in Fig. 5, where a central condensate peak is visible in the wave-number spectrum. It should also be noted that stimulated scattering of Langmuir waves off ions can also lead to condensation of energy to lower k and can be more important than electrostatic decay under some circumstances. The reader is referred to the book by Tsytovich (1995) for a detailed discussion of stimulated scattering processes, including this one.

C. Weak versus strong turbulence

In the previous subsections, it was noted that (strong-turbulence) phase-coherent interactions give way to weak-turbulence phase-incoherent interactions in the limit of large bandwidth. We now turn to two important issues that have generated much confusion in the literature: the transition from strong to weak turbulence and the possible coexistence of both types of turbulence in a single system. Musher *et al.*'s (1995) review and the books by Tsytovich (1977, 1995) and Vladimirov *et al.* (1995) discuss these issues in detail.

1. Criteria for validity of a weak-turbulence description

The transition from phase coherence to incoherence occurs at a characteristic bandwidth

$$\Delta\omega\approx\Gamma, \tag{3.16}$$

where Γ is the nonlinear growth rate; i.e., where the phase-mixing rate equals the growth rate. This transition can be gradual (Winglee, 1983; Zakharov *et al.*, 1985; Melrose, 1986b, 1987a, 1987b; Kruer, 1988; Vladimirov and Popel, 1995) or, in some cases of cyclic three-wave interactions, sudden (Robinson and Drysdale, 1996).

For Langmuir waves with the dispersion relation (2.1), there are two regimes,

$$\Delta\omega\approx 3k\Delta k\lambda_D^2\omega_p, \quad \Delta k\ll k, \tag{3.17}$$

$$\Delta\omega\approx 3k^2\lambda_D^2\omega_p/2, \quad \Delta k\approx k, \tag{3.18}$$

which we term the narrow-spectrum and broad-spectrum regimes, respectively. Substitution of Eq. (3.17) and the decay instability growth rate of Eq. (3.6) into the crossover criterion (3.16) gives the requirement

$$W \ll 36 \min(k\lambda_D)\left(\frac{m_i}{\gamma m_e}\right)^{1/2}(\Delta k\lambda_D)^2 = 12(\Delta k\lambda_D)^2, \tag{3.19}$$

for a weak-turbulence description of decay to be valid for a narrow spectral peak. The function $\min(k\lambda_D)$ is required to account for the whole of Region I in Fig. 3 by taking the minimum of its argument over this region; it can be omitted for specific values of k, leaving just a factor $k\lambda_D$. The corresponding criterion for a broad spectrum is

$$W \ll 9\left(\frac{m_i}{\gamma m_e}\right)^{1/2}\min(k\lambda_D)^3 = \frac{\gamma m_e}{3m_i}, \tag{3.20}$$

where the minimum function again accounts for the whole region. Since $\Delta k\lambda_D \leqslant k\lambda_D$ and $k\lambda_D \ll 1$ for weakly damped Langmuir waves to exist, Eqs. (3.19) and (3.20) impose very small upper bounds on W for weak-turbulence theory to be valid. Nonetheless, experimental conditions exist in which these bounds are satisfied.

If the crossover criterion [Eq. (3.16)] is combined with the modulational instability (or subsonic modulational instability) growth rate given by Eq. (3.8), one finds the following criteria for a weak-turbulence description to apply

$$W \ll 12k\Delta k\lambda_D^2, \tag{3.21}$$

$$W \ll 6k^2\lambda_D^2, \tag{3.22}$$

for narrow and broad spectra, respectively. However, DuBois and Rose (1981), Zakharov *et al.* (1985), Popel *et al.* (1994), Vladimirov and Popel (1995), and Vladimirov *et al.* (1995) have showed that if these criteria are satisfied, (subsonic) modulational interactions are stable. In other words, the (subsonic) modulational instability is either a phase-coherent instability or does not exist, at least in a Maxwellian plasma. Since $k \leqslant k_*/2 = (\gamma m_e/9m_i)^{1/2}$ for these modulational instabilities to dominate over decay, Eqs. (3.21) and (3.22) impose very strict conditions on a weak-turbulence description and, ultimately, such a description will break down due to accumulation of energy via a cascade, or through narrowing of the spectrum (Zakharov, 1984; Musher *et al.*, 1995) unless other physical effects intervene to prevent this.

For the supersonic modulational instability, Eqs. (3.10) and (3.16) give

$$W \ll \frac{27m_i}{m_e}(k\lambda_D)^2(\Delta k\lambda_D)^2, \tag{3.23}$$

$$W \ll \frac{27m_i}{4m_e}(k\lambda_D)^4, \tag{3.24}$$

for weak turbulence with narrow spectra and broad spectra, respectively. Equations (3.23) and (3.24) are not consistent with the right boundary of Region IV in Fig. 3 for $k > k_*/2$, nor with the lower boundary of the region in the opposite case. Hence weak-turbulence theory is irrelevant to description of the supersonic modulational instability.

In the case of the modified decay instability, Eqs. (3.12) and (3.16) yield

$$W \ll 27\frac{m_i}{m_e}(k\lambda_D)(\Delta k\lambda_D)^3, \tag{3.25}$$

$$W \ll \frac{27m_i}{8m_e}(k\lambda_D)^4, \tag{3.26}$$

as the conditions for a weak-turbulence description to apply to narrow and broad spectra, respectively. These conditions can only be consistent with the bounds of Region V in Fig. 3 for $k \geqslant \Delta k \gg k_*/2$ and $k \gg k_*/2$, respectively.

2. Coexistence of weak and strong turbulence

It is possible for the criteria for a weak-turbulence description to be satisfied for some waves in a system, but not for others. For example, in a cascade spectrum maintained by input of energy at high k (see Fig. 5), the waves at high k may satisfy Eq. (3.20) if their energy density is low enough (energy densities in the crossover criteria above refer to the relevant part of the spectrum, not the spectrum as a whole). At the same time, energy accumulation in the condensate, which has $\Delta k \approx k$, will eventually cause Eq. (3.22) to be violated, leading to a phase-coherent modulational instability. Thus it is possible for weak and strong turbulence to coexist in the same system. Such a situation was studied by Robinson, Newman, and Rubenchik (1992), who showed that a weak-turbulence description gave a good account of the waves in the cascade shown in Fig. 5, while the condensate waves underwent phase-coherent processes, including wave collapse. Rubenchik and Shapiro (1991), DuBois *et al.* (1991, 1993a, 1993b), Hanssen *et al.* (1992), and Musher *et al.* (1995) have also discussed the coexistence of weak and strong turbulence in various situations.

IV. OVERVIEW OF WAVE COLLAPSE AND STRONG TURBULENCE

Sections V and VI address the phenomena of wave collapse and strong turbulence in detail. The purpose of this section is to give a brief overview of the phenomena involved in wave collapse and the way in which collapse relates to strong turbulence when many collapsing, coherent, nonlinear wave packets are present simultaneously, amid lower-level incoherent waves (the wave packets do not satisfy the linear dispersion relation). This provides a compact summary of the main ideas and serves to orient the reader prior to the more detailed discussions in Secs. V and VI. In brief, Sec. IV.A considers the formation of solitons in one-dimensional systems, self-focusing, and wave collapse, Sec. IV.B discusses weak turbulence, and Sec. IV.C is concerned with the transition between weak and strong turbulence.

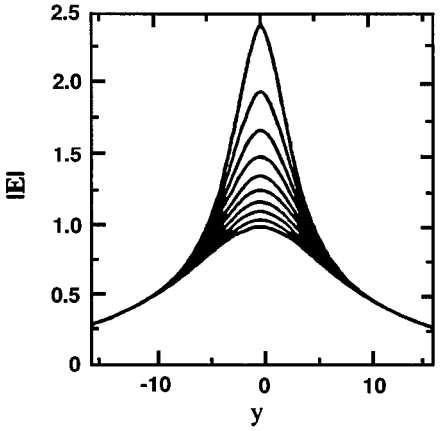

FIG. 8. Profiles of electric field, taken through a three-dimensional collapsing wave packet, calculated numerically using the nonlinear Schrödinger equation by Newman *et al.* (1989). Curves are plotted at several instants during collapse, with time increasing toward the top. The units on both axes are arbitrary and y denotes a spatial coordinate.

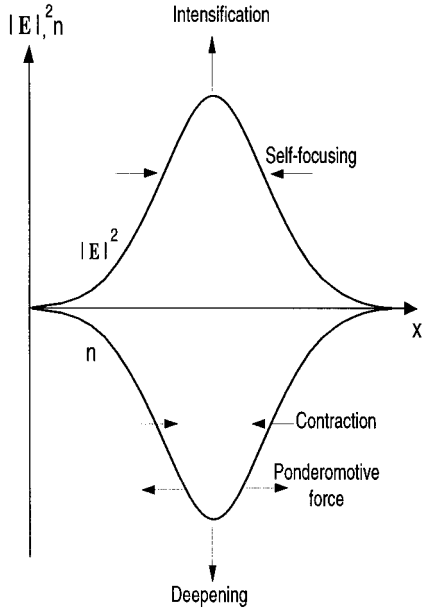

FIG. 9. Schematic of a collapsing Langmuir wave packet and its associated density well, indicating the self-focusing and intensification of the packet and the deepening and contraction of the density well caused by the ponderomotive force.

A. Wave collapse and self-focusing

As was seen in Figs. 2(a) and 2(b), intense localized wave packets form spontaneously amid Langmuir turbulence. We also saw in Sec. III that even initially uniform wave trains can break up into localized packets due to modulational instabilities, although only a linear stability analysis was outlined. Figure 8 shows cross sections through an intense Langmuir wave packet governed by the undamped nonlinear Schrödinger equation (2.20), as calculated by Newman *et al.* (1989); early stages of Zakharov simulations with dissipation are similar. As time progresses, the initial wave packet narrows and becomes more intense, i.e., it collapses. The corresponding density well also deepens and narrows as the ponderomotive force becomes stronger, as shown schematically in Fig. 9. The combined multidimensional entity, consisting of a nonlinear collapsing wave packet and its associated density well, has been called a *soliton*, a *cavern*, a *caviton*, and a *collapson* in the literature. However, each term has its drawbacks: (i) The packet is not a true soliton, because it is unstable and subject to short-scale dissipation. Moreover, packets do not pass through each other subject only to a phase shift (part of the standard definition of a soliton). (ii) The terms "cavern" and "caviton" put undue emphasis on the density well and, in the case of some magnetized plasma waves (see Sec. IX), give the wrong impression that the density perturbation is always negative. (iii) "Collapson" has been used in only a few publications. For these reasons, we stick to descriptions in terms of the nonlinear wave packet and its associated density perturbation (or density well, if it is actually a negative perturbation).

1. One-dimensional solitons

The physics underlying the modulational instability of a uniform wave train has been mentioned: modulations can increase the size of the negative (self-focusing) term in a Hamiltonian, such as (2.29), faster than the positive one that corresponds to dispersion. However, in the one-dimensional case, dispersion can ultimately balance nonlinear self-focusing to yield stable soliton solutions of the nonlinear Schrödinger or Zakharov equations. Such a solution of the nonlinear Schrödinger equation (2.20) is

$$E(t,x)=E_0\mathrm{sech}[E_0(x-vt)/\sqrt{2}] \times\exp i\left[\frac{1}{2}vx-\left(\frac{v^2}{4}-\frac{E_0^2}{2}\right)t\right], \tag{4.1}$$

where v is the propagation velocity of the sech envelope (Zakharov and Shabat, 1971; Bullough and Caudrey, 1980; Kuznetsov *et al.*, 1986; Vladimirov *et al.*, 1995). The contents of the first set of square brackets in Eq. (4.1) emphasize the inverse relationship between E_0 and spatial quantities. Similarly, the exponential factor shows that the characteristic evolution time T is of order E_0^{-2}. We thus have two important scalings for the nonlinear Schrödinger equation,

$$L\sim E^{-1}\sim W^{-1/2}, \tag{4.2}$$

$$T\sim E^{-2}\sim W^{-1}. \tag{4.3}$$

These scalings can also be obtained by requiring that all the terms in the nonlinear Schrödinger equation (2.20) be of the same order.

It is significant to note from Eqs. (3.8) and (3.9) that the scalings given by Eqs. (4.2) and (4.3) are obeyed by the modulational and subsonic modulational instabilities. Analyses of these instabilities implicitly assume that the growth rates are small enough that the density fluctuations adjust to be consistent with the ponderomotive

forces due to the developing Langmuir modulations. This corresponds precisely to the conditions for the nonlinear Schrödinger equation to be a good approximation to the Zakharov equations (see Sec. II.B). Hence, in one dimension, Eq. (4.1) can be viewed as a nonlinearly saturated state of an initial modulational instability that has not reached the supersonic regime. More generally, an initially uniform one-dimensional wave train of amplitude E will break up into $\sim E$ solitons per unit length in accord with Eq. (4.2). This point has been verified numerically by Shen and Nicholson (1987), for example. Solitons are thus essential building blocks of the theory of the one-dimensional nonlinear Schrödinger equation, augmenting the set of plane waves, which are the building blocks of linear theory.

A very important insight into the physics of solitons is obtained by noting that the soliton field is a *linear* eigenstate of the self-consistent potential $V=-|\mathbf{E}|^2$ within the standard Schrödinger equation $i\partial_t\mathbf{E}=(-\nabla^2+V)\mathbf{E}$ ($c_S=1$ here). This idea has also been widely used in nonlinear optics (for example, by Saleh and Teich, 1991). In the case of the Zakharov equations, where $V=n$, the application of this idea is (perhaps paradoxically) simpler than for the nonlinear Schrödinger equation because V is not directly dependent on $\mathbf{E}$. We shall use this insight later in studying the formation of multidimensional wave packets.

In the absence of damping, the Zakharov equations (2.17) and (2.18) have the solution (Gibbons *et al.*, 1977; Kuznetsov *et al.*, 1986)

$$E(t,x)=E_0\mathrm{sech}\left(\frac{E_0(x-vt)}{[2(1-v^2)]^{1/2}}\right)\times\exp i\left[\frac{1}{2}vx-\left(\frac{v^2}{4}-\frac{E_0^2}{2(1-v^2)}\right)t\right], \tag{4.4}$$

$$n=-\frac{|E|^2}{1-v^2}, \tag{4.5}$$

where $v<1$ is the soliton speed in units of the sound velocity. Equation (4.4) reproduces Eq. (4.1) for $v\ll 1$, and Eq. (4.5) shows that the density response strengthens as the soliton speed approaches the sound velocity, with a breakdown in this equation's validity as $v\to 1$. The appearance of this soliton depends on the ratio of v to E_0, as shown in Fig. 10. As in the case of the nonlinear Schrödinger equation, solutions to the initial-value problem for the 1D Zakharov equations can be decomposed into a collection of solitons plus plane waves.

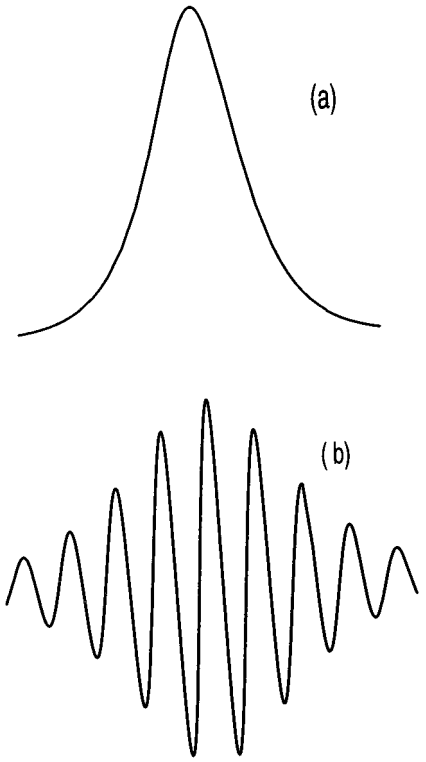

FIG. 10. Spatial soliton profiles vs velocity, from Eq. (4.4) with $v^2\ll 1$ and ReE plotted: (a) $v=0$; (b) $v=14E_0$.

2. Multidimensional wave collapse

In more than one dimension, there are no stable soliton solutions to the nonlinear Schrödinger equation or the Zakharov equations. In the case of the nonlinear Schrödinger equation, this can be straightforwardly proved from a Hamiltonian perspective if damping is neglected. Specifically, it is possible to show that the root-mean-square size Δr of a wave packet tends to zero with time if the initial intensity exceeds a threshold value (Kelley, 1965; Zakharov, 1972; Goldman and Nicholson, 1978; Goldman *et al.*, 1980; Kuznetsov *et al.*, 1986).

The first step in the Hamiltonian argument is to define the N-weighted mean of an arbitrary quantity f by

$$\langle f(t)\rangle_N=\frac{1}{N}\int f(t,\mathbf{r})|\mathbf{E}(t,\mathbf{r})|^2d^D\mathbf{r}, \tag{4.6}$$

with N given by Eq. (2.30). Using the nonlinear Schrödinger equation (2.20) with $\hat{\gamma}_L=0$ and $c_S=1$, one then finds

$$\partial_t\langle x_j\rangle_N=2P_j/N, \tag{4.7}$$

$$\partial_t^2(\Delta r)^2=\partial_t^2\langle(\mathbf{r}-\langle\mathbf{r}\rangle_N)^2\rangle_N, \tag{4.8}$$

$$=A+2(2-D)\langle|\mathbf{E}|^2\rangle_N, \tag{4.9}$$

$$A=8\left(\frac{H}{N}-\frac{P^2}{N^2}\right), \tag{4.10}$$

where H and P are given by Eqs. (2.27) and (2.31), respectively. Equation (4.9) is termed a *virial theorem*.

Equation (4.9) implies that Δr will decrease monotonically for $D\geq 2$, provided $A<0$; in the opposite case, the packet will disperse. For a wave packet at rest ($P=0$), the latter requirement reduces to $H<0$, which is achieved for characteristic fields and scales satisfying $E\gg L^{-1}$. In such circumstances, the packet will contract to a point in the absence of other effects such as damping. This contraction occurs in a finite amount of time, as

can be seen from the upper bound

$$(\Delta r)^2 \leqslant At^2 + Bt + C, \tag{4.11}$$

with $B = \partial_t (\Delta r)^2$ and $C = (\Delta r)^2$ at $t = 0$. Hence the collapse time t_c satisfies

$$t_c \leqslant [-B + (B^2 + 4|A|C)^{1/2}]/(2|A|), \tag{4.12}$$

with equality in Eq. (4.12) for $D = 2$. The Hamiltonian description has been used to obtain improved estimates of the collapse time for specific three-dimensional packet structures by approximating the final term on the right of Eq. (4.9) (Goldman and Nicholson, 1978; Goldman *et al.*, 1980).

Arguments similar to the above can be made for waves governed by the Zakharov equations. Although no rigorous virial theorem exists in this case, it is argued that the early stages of the evolution of a wave packet are slow and can thus be approximated by the nonlinear Schrödinger equation. Hence the nonlinear Schrödinger virial theorem should give a good estimate of the collapse threshold. This argument has been confirmed by numerical simulations in a number of cases and it is found that the collapse threshold obtained via the nonlinear Schrödinger equation gives a good estimate of the corresponding threshold for waves governed by the Zakharov equations (Newman *et al.*, 1990).

In multidimensional systems, it is thus found that the fundamental Langmuir wave structures are plane waves and collapsing wave packets, rather than the plane waves and solitons of the one-dimensional case. We consider these components further below and in Secs. V and VI.

B. The wave-packet cycle

In a large steadily driven system many collapsing Langmuir wave packets will be simultaneously present, along with a background of plane waves, as in Figs. 2(a) and 2(b). Since they are not stable, these packets will form, collapse, dissipate, then reform, drawing energy ultimately from the driver. This section briefly summarizes the main stages in this *wave-packet cycle*, to which we return in detail in Sec. V.

Localized wave packets can form via modulational instability of a monochromatic plane wave, or an ensemble of plane waves, as discussed in Sec. III. This mechanism was confirmed by early numerical simulations (Goldman and Nicholson, 1978; Nicholson and Goldman, 1978; Nicholson *et al.*, 1978) and can be relevant in turbulence if the instability time scale is short enough. However, the alternative *nucleation mechanism* is more relevant in many turbulent systems. This mechanism depends on the fact that, in the presence of density fluctuations, localized Langmuir eigenstates exist in addition to the plane-wave ones (Doolen *et al.*, 1985; Russell *et al.*, 1988). These states are trapped as standing waves in density depressions where the refractive index is higher than average [see Eq. (2.8)]. These states are then free to accumulate energy from the background turbulence, via three-wave decays or directly from a driver tuned to the eigenstate frequency (Doolen *et al.*, 1985; Russell *et al.*, 1988; DuBois *et al.*, 1990, 1993b; Robinson and Newman, 1990a; DuBois and Rose, 1991; Robinson, Wouters, and Broderick, 1996). This mechanism is particularly favored because suitable density depressions are left over after wave packets collapse and dissipate. Indeed, Doolen *et al.* (1985) and Russell *et al.* (1988) observed packets renucleating repeatedly in the density wells generated by the ponderomotive force of previous collapsing wave packets that had since dissipated, a phenomenon some signs of which had been seen in 1D simulations by Doolen *et al.* (1983). Subsequent statistical analysis confirmed this tendency quantitatively (Robinson *et al.*, 1988). Nucleation is particularly effective for shallow wells with $n \sim -\langle |\mathbf{E}|^2 \rangle$ (see Sec. V).

If the intensity of a nucleating state increases to the point that the collapse threshold $A = 0$ is passed, collapse will commence. After this point, the wave packet narrows and becomes more intense (see Figs. 1 and 8). During this collapse phase of the wave-packet cycle, Langmuir ponderomotive forces push aside the plasma to produce a density well that helps to confine the waves (see Fig. 9).

Ultimately, other physical processes must cut into arrest collapse and prevent a singularity from being reached. This is usually accomplished by dissipation—often called burnout—of a large fraction of the Langmuir energy at short scales (Zakharov, 1972; Zakharov, 1984; Robinson, 1991), although in principle the advent of higher-order nonlinearities can also arrest collapse.

Once a large part of the Langmuir energy in a packet has been dissipated, its ponderomotive force is no longer sufficient to support the deep density well formed in the collapse phase. In the relaxation phase, this well gradually relaxes, spreading and decreasing in magnitude until it is shallow enough to nucleate further waves effectively. At this point, a large fraction of wells renucleate further waves to the point that the collapse threshold is again exceeded. Robinson *et al.* (1988) found that roughly 80% of collapse sites renucleate further collapses, consistent with earlier work by Doolen *et al.* (1985) and Russell *et al.* (1988). Figure 11 shows the main stages in the wave-packet cycle schematically.

C. Strong turbulence

The main features of strong Langmuir turbulence are evident in Figs. 2(a) and 2(b). There are two clearly distinguishable components to the turbulence: (i) localized, coherent wave packets, which have high fields and short scales (high wave numbers) and (ii) a background of incoherent waves that have low fields and longer scales (lower k); seen directly only in Fig. 2(a), this latter component also fills the spaces between the high-E clumps seen in Fig. 2(b). Under most circumstances, dissipation is concentrated in the coherent component, where it occurs primarily near the point of arrest of collapse. Energy input can be to the incoherent waves or, from a suitably tuned driver, directly to the localized packets.

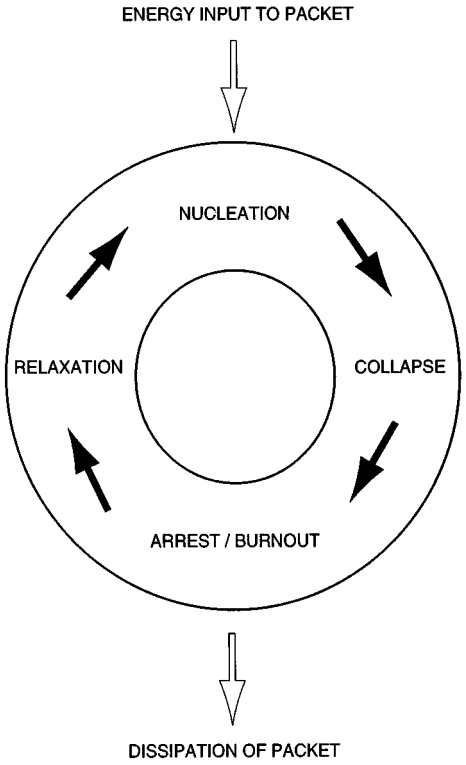

FIG. 11. The wave-packet cycle, showing nucleation, collapse, burnout, and relaxation, with energy input during nucleation and dissipation during burnout.

Energy exchange between the two components occurs during nucleation to balance dissipation in the steady state.

Figure 12 shows schematics of the localized and condensate components of strong Langmuir turbulence, plus a third, cascade component to account for cases in which energy enters the system at large k, then cascades

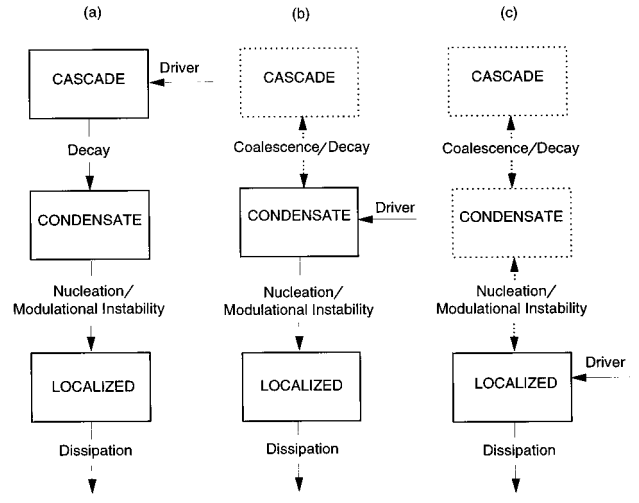

FIG. 12. Schematics of localized, condensate, and cascade components of Langmuir turbulence, and the interactions between them in three cases of pumping: (a) driven at high k; (b) condensate driven directly; (c) localized states driven directly.

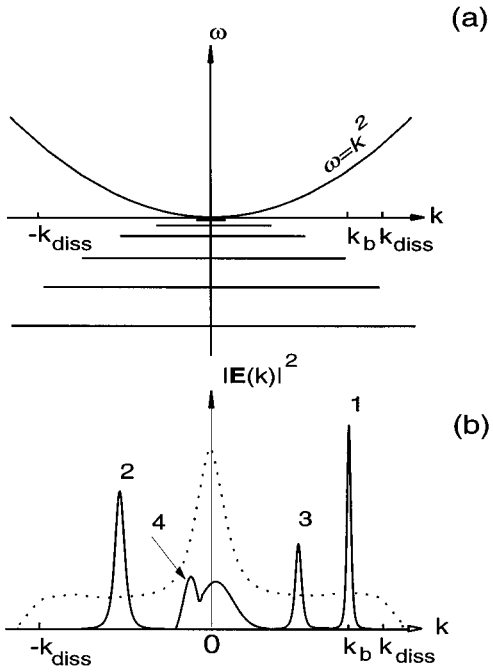

FIG. 13. Schematics of strong turbulence in Fourier space: (a) Langmuir dispersion relation, showing propagating modes at $\omega>0$ and localized eigenstates at $\omega<0$. The discrete structure seen for $\omega<0$ is smoothed out in observations if averaging over many packets occurs. (b) Corresponding wave-number spectrum resulting from beam-driven waves at k_b, showing the cascade (numbered peaks) and condensate components as solid curves and the localized component dashed. Dissipation increases rapidly for $k>k_{\rm diss}$.

down to the condensate through a series of electrostatic decays. The main energy flows between the components, and the processes involved are also shown in Fig. 12, with single-headed arrows indicating dominant flow in one direction and double-headed ones indicating a balance in the steady state. Column (a) of this figure corresponds to driving at high k, followed by cascade, then nucleation from (or, possibly, modulational instability of) the resulting condensate. Column (b) represents the case in which a driver at low k drives the condensate directly. Some weak-turbulence broadening to higher k is possible via electrostatic coalescence ($L+S\rightarrow L'$), as indicated by a dashed arrow, but this appears to be relatively unimportant under most circumstances. Column (c) corresponds to direct driving of localized states. Inverse nucleation processes (e.g., coalescence between a localized Langmuir wave and a propagating ion-sound wave to produce a propagating Langmuir wave), and radiation of Langmuir waves from collapsing wave packets (see Sec. V.E) transfer some energy into the low-k condensate in this case. Note that, in some cases, driven by a strong pump tuned well above the local plasma frequency, the cascade is truncated before reaching $k=0$ (see Secs. V.C, VI.A, and VIII.F). In such cases coupling mechanisms other than nucleation can have a role.

Figure 13(a) shows the dispersion relation of Langmuir eigenstates in a turbulent plasma. At the top is the

(dimensionless) dispersion curve $\omega=k^2$ for plane Langmuir waves ($\omega_p=0$ in these units). Localized eigenstates are seen at $\omega<0$, each of which corresponds to a range of k values, since it is not a plane wave. This range broadens as ω decreases, corresponding to a deepening and narrowing of the confining density well. The typical density of states also decreases, because collapse accelerates at short scales (indicated schematically by the increasing separation between the discrete eigenvalues in Fig. 13). Energy flows to localized eigenstates near $\omega=0$ directly or from the low-k condensate, possibly after undergoing a cascade from high k. Collapse then carries it to higher k where it eventually dissipates at $k\approx k_{\rm diss}$. Figure 13(b) is a schematic of the corresponding wave-number spectrum for a case in which energy enters at high k ($k=k_b$), then cascades to low k via the four numbered spectral peaks, corresponding to successive electrostatic decays. Eventually energy reaches the central condensate peak, shown at $k=0$. The dashed curve shows the spectrum associated with localized states. It peaks at $k=0$, where nucleation is taking place, then declines rapidly toward higher k, corresponding to collapsing packets. For $k\gtrsim k_{\rm diss}$ the falloff is even steeper, as packets are arrested and dissipated at a characteristic scale $\sim k_{\rm diss}^{-1}$. Recent numerical work by Goldman *et al.* (1996) shows evidence of structure similar to that in Fig. 13, although the discrete structure at $\omega<0$ is smeared out by time averaging.

Starting from a two- or three-component picture, it has been possible to construct a simplified picture of strong Langmuir turbulence by accounting for the dynamics of both components and the interaction between them (Robinson and Newman, 1990a, 1990b, 1990c; Robinson, 1996a). Treatment of the interaction between the components is rendered tractable by the dominance of nucleation under a wide variety of circumstances. The features and predictions of this model are discussed in detail in Sec. VI, along with their verification against numerical simulations.

V. WAVE COLLAPSE

Since the work of Zakharov (1972), it has been known that localized multidimensional Langmuir wave packets can undergo wave collapse, attaining short scales and high intensities, before dissipating. This section discusses the main stages of the wave-packet cycle: packet formation and structure, power input to the forming packet, the collapse threshold, collapse, arrest of collapse, and relaxation. The insights obtained are used in the model of strong turbulence discussed in Sec. VI and in some of the applications in Secs. VIII and IX.

A. Wave-packet formation

Early work concentrated on modulational instability of monochromatic plane waves as the mechanism for producing an initial localized wave packet that would later collapse (e.g., Papadopoulos *et al.*, 1974; Rowland and Papadopoulos, 1977; Rowland, 1980; Rowland *et al.*, 1981). Some early numerical simulations also confirmed the viability of this mechanism and the subsequent collapse of wave packets formed at either high or low wave numbers (Nicholson and Goldman, 1978; Nicholson *et al.*, 1978).

One problem with the modulational-instability route to collapse is that, in fully developed turbulence, the turbulent spectrum is usually so broad that it is modulationally stable (Sec. III.C; Russell *et al.*, 1988). A second problem is that analysis of modulational instabilities usually assumes that all Langmuir waves have the dispersion relation given by Eq. (2.1). In reality, in a turbulent plasma, localized eigenstates exist in which Langmuir waves are trapped as standing waves in density depressions (in geometric-optics terms, regions of low density and high refractive index trap Langmuir waves by total internal reflection). The dispersion diagram shown in Fig. 13(a) thus contains discrete eigenfrequencies as well as those given by Eq. (2.1); these discrete states cannot be ignored.

The existence of localized Langmuir states has two main consequences: (i) These states can accumulate energy from background turbulence via nonlinear couplings. For example, the existence of such states (lower in energy than the lowest plane-wave state) permits additional steps in the decay cascade, whose energy is then concentrated in the localized states (Robinson, Wouters, and Broderick, 1996). Alternatively, an external field tuned to a frequency just below the unperturbed plasma frequency ω_p can couple directly to these states (Doolen *et al.*, 1985; Russell *et al.*, 1988; DuBois *et al.*, 1990, 1993b), with three-wave interactions transferring some energy to plane-wave states. (ii) These states are relatively long lived, evolving only on the slow time scale of density fluctuations. Near the threshold of collapse, this rate of change is expected to become even slower as Langmuir ponderomotive force increasingly supports the well against relaxation (see below). Hence modulational instability of these localized states is favored relative to the plane-wave case, since the bandwidth of these waves is small.

Doolen *et al.* (1985) were the first to recognize the importance of localized states in strong Langmuir turbulence. They also noted the critical point that these states, which can nucleate energy to seed collapse, are likely to be localized in density depressions excavated by the ponderomotive forces of collapsing wave packets themselves. Once the collapsing packets dissipate, these remnant density wells relax, unsupported by ponderomotive forces, until they reach a depth and scale that can once again efficiently nucleate energy from the source (see Sec. V.C). This closes a loop that leads to the dominance of nucleation under a wide variety of situations—density wells not only favor wave collapses, but are produced by them.

B. Wave-packet structure

The next question to which we must turn is that of the structure of the nucleating wave packets. Numerical

simulations show that collapsing wave packets are predominantly roughly oblate with typical axial ratios of around 1.5:1.5:1 to 2:2:1 in three dimensions, with a single central peak of electric-field strength (Robinson, Newman, and Goldman, 1988; Newman, Robinson, and Goldman, 1989, 1991; and references therein). Furthermore, collapsing packets are found to move with group velocities that are zero, or at most a very small fraction of the sound velocity. These features differ from those of the one-dimensional form given by Eqs. (4.4) and (4.5), which represents a moving packet with multiple field maximums in general (see Fig. 10).

Although multiply peaked (often called quasiclassical) wave packets can collapse (Zakharov *et al.*, 1984; Zakharov and Kuznetsov, 1986; Kuznetsov and Turitsyn, 1990; Shapiro *et al.*, 1995), it has recently been argued by Robinson (1996a), Robinson, Melatos, and Rozmus (1996a), and Robinson, Wouters, Broderick (1996), that collapse of multiply peaked wave packets is not likely to dominate that of singly peaked ones (see also Sec. V.D below). Zakharov and Kuznetsov (1986) also found that quasiclassical packets are unstable to breakup into shorter-scale, singly peaked ones, a scenario for which simulations of lower-hybrid waves have recently provided some support (Shapiro *et al.*, 1995). Robinson, Wouters, and Broderick (1996) showed that damping of ion fluctuations suppresses the ion response to moving packets, also making it impossible for moving packets to collapse above a very small critical damping level and velocities much smaller than the sound velocity. They also showed that power input to localized states is most effective for a singly peaked state (see Sec. V.C below). Thus, except where noted to the contrary, attention is henceforth restricted to singly peaked, stationary collapsing wave packets.

In the nucleation scenario, most collapsing wave packets form initially in density wells remaining after the collapse of a previous packet. Such wells are approximately isotropic, having been made so during their relaxation (see Sec. V.G below). The wells are also essentially unsupported by ponderomotive forces during relaxation, because their trapped Langmuir fields largely dissipated during burnout. This means that the Langmuir fields can be considered to be linear eigenstates of a spherically symmetric well whose form results from linear processes.

Under the electrostatic Zakharov equations (2.17) and (2.18) the electric field can be represented in terms of the potential Φ, with $\mathbf{E}=-\nabla\Phi$. At fixed t, this potential can be decomposed in spherical harmonics, centered on the center of the density well (Newman *et al.*, 1989), giving

$$\Phi(r,\theta,\phi)=\sum_{l=0}^{\infty}\sum_{m=-l}^{l} h_{lm}(r)Y_{lm}(\theta,\phi), \tag{5.1}$$

$$=\sum_{l,m}\Phi_{lm}(r,\theta,\phi), \tag{5.2}$$

where the radial functions h_{lm} are complex, the Y_{lm} are standard spherical harmonics, and r, θ, and ϕ are the usual spherical polar coordinates. Angle-averaged partial energies $W_{lm}(r)=(4\pi)^{-1}\int|\nabla\Phi_{lm}|^2\sin\theta d\theta d\phi$ can be defined in terms of Eq. (5.2).

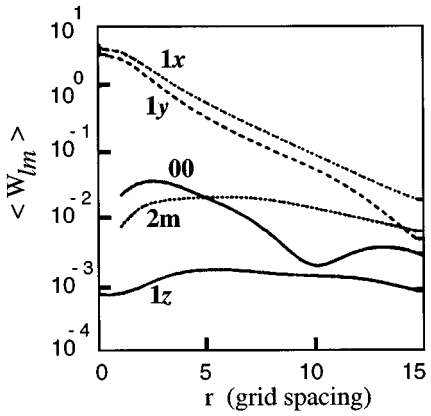

FIG. 14. Relative angle-averaged energy densities W_{lm} [see the discussion following Eq. (5.2) for the precise definition] in the various components of a spherical-harmonic decomposition of the field of a spontaneously formed wave packet from a simulation of strong Langmuir turbulence (Newman *et al.*, 1989). The curves show the energy densities corresponding to the various harmonics lm, as labeled. Note that the units of r and W_{lm} are arbitrary.

The radial functions in Eq. (5.1) satisfy $\partial_r h_{lm}\sim r^{|l|-1}$ for $|l|\geqslant 1$ and small r, and $\partial_r h_{0m}=0$ at $r=0$. Hence the $l=\pm 1$ components dominate in determining the field at small r in a packet with a peak of electric field at $r=0$ (Newman *et al.*, 1989). It is possible to rotate coordinates so that the general wave packet in Eq. (5.1) is in *standard orientation* with the polarization ellipse of the high-frequency electric field $\boldsymbol{\mathcal{E}}$ [cf. Eq. (2.9)] in the x-y plane and the major and minor axes of this ellipse pointing in the x and y directions, respectively. The dominant terms in Eq. (5.1) can be written as

$$\Phi(r,\theta,\phi)=E_0\left(a_{00}h_0(r)+\frac{a_{1x}x+a_{1y}y+a_{1z}z}{r}h_1(r)\right), \tag{5.3}$$

$$=E_0\left(a_{00}h_0(r)+\frac{\alpha x+i\beta y}{r}h_1(r)e^{i\delta}\right), \tag{5.4}$$

in general orientation and standard orientation, respectively. Here E_0 is the central-field strength, h_0 and h_1 are real functions that apply to the $l=0$ and $l=1$ components, respectively, the a_{lm} are constants that satisfy $\Sigma_{lm}|a_{lm}|^2=1$, α and β are real constants that satisfy $|a_{00}|^2+\alpha^2+\beta^2=1$ and $\alpha^2\geqslant\beta^2$, and δ is a real phase constant. When restricted to the x-y plane, this potential is also the one relevant to two-dimensional wave-packet structures.

Figure 14 shows the dominance of the $l=1$ components of Φ near the center of a representative wave packet that formed spontaneously in numerical simulations of strong Langmuir turbulence (Newman *et al.*, 1989). The $l=0$ and $l=2$ components are much smaller, as is the $zh_1(r)/r$ part, because the packet has been brought into standard orientation. Newman *et al.* (1989)

found that this dominance persists throughout collapse. Note that the packet in Fig. 14 is approximately circularly polarized near $r=0$, consistent with the comparable levels of the $1x$ and $1y$ components there. This is contrary to the original figure in Newman *et al.*'s (1989) paper, whose two frames were accidentally reversed.

The potential (5.4) has a dipole structure, giving a central peak of $|\mathbf{E}|$. Dipole potentials have long been used to model initial wave packets in numerical studies of Langmuir wave collapse (e.g., Degtyarev *et al.*, 1975, 1976). For $a_{00}=0$ the constants α and β describe the polarization of the high-frequency field $\boldsymbol{\mathcal{E}}$ at the center of the packet: (i) for $\alpha=1$ the packet is linearly polarized along the x axis, (ii) for $|\alpha|^2=|\beta|^2=1/2$ the polarization is circular, with the handedness depending on the relative signs of α and β, and (iii) in other cases the central polarization is elliptical. Being electrostatic, plane Langmuir waves are always longitudinally polarized. Elliptical polarization arises because the localized packet comprises two degenerate eigenstates with the same frequency, different directions of $\boldsymbol{\mathcal{E}}$, and a relative phase controlled by α and β.

Near $r=0$, the energy density $|\mathbf{E}|^2$ for the potential in Eq. (5.4) with $a_{00}=0$ is given by (Newman *et al.*, 1991)

$$W=\frac{h_1^2}{r^2}+\left(\frac{\alpha^2x^2+\beta^2y^2}{r^2}\right)\left[\left(\frac{dh_1}{dr}\right)^2-\frac{h^2}{r^2}\right]. \tag{5.5}$$

One consequence of this result is that the three-dimensional energy density cannot be spherically symmetric, even where the state is trapped within a spherically symmetric density depression. If W has a quadratic maximum at $r=0$, nearby surfaces of constant W are ellipsoids with principal axes in the x, y, and z directions having lengths in the ratio (Newman *et al.*, 1989, 1991)

$$1:\left(\frac{3+R}{1+3R}\right)^{1/2}:\left(\frac{3+R}{1+R}\right)^{1/2}, \tag{5.6}$$

with $0\leqslant R=\beta^2/\alpha^2\leqslant 1$. These axes cannot all be equal in three dimensions. In two dimensions only the first ratio in Eq. (5.6) is relevant and is unity only for $R=1$; i.e., for circular polarization.

The preponderance of pancake-shaped wave packets (i.e., packets in which the surfaces of constant W are roughly oblate spheroids near $r=0$) seen in simulations of turbulence, such as in Fig. 2, can be explained in terms of the potential (5.3) with $a_{00}=0$; other terms do not affect the shape near $r=0$, where the field is strong. If the nucleating density wells have no preferred directions, individually or statistically, the three coefficients a_{1m} will be identically and independently distributed, subject to $\Sigma_{m=1}^{3}|a_{1m}|^2=1$. This corresponds to the complex vector $\mathbf{a}=(a_{1x},a_{1y},a_{1z})$ being uniformly distributed on the surface of a six-dimensional unit sphere (the real and imaginary parts of the three coefficients a_{1m} correspond to the six axes). The resulting probability distribution of R, denoted $P(R)$, is (Newman *et al.*, 1989)

$$P(R)=\frac{1-R}{(1+R)^3}K\left[\left(\frac{1-R}{1+R}\right)^2\right], \tag{5.7}$$

where K is the complete elliptic integral of the first kind (Abramowitz and Stegun, 1970, p. 569). This distribution strongly favors small values of R, with $\langle R\rangle=4G-1-\pi^2/4\approx 0.196$, where $G\approx 0.9156$ is Catalan's constant (Abramowitz and Stegun, 1970, p. 807). For $R=\langle R\rangle$, the packet is triaxial, with principal axes in the approximate ratio 1:1.4:1.6. In the limiting cases $R=0$ and $R=1$ the packet is oblate and prolate, respectively, with corresponding axial ratios of $1:\sqrt{3}:\sqrt{3}$ and $1:1:\sqrt{2}$. The strong bias toward small R means that a linearly polarized packet, with $R=0$, is a good approximation for many purposes.

The above arguments explain the observed statistical preponderance of approximately oblate wave packets without resort to dynamic mechanisms by which packets might flatten during collapse. Such effects had previously been thought to be necessary and their plausibility was established via analysis of scalar-field Zakharov equations (Pelletier, 1987) where such flattening indeed occurs. However, vector wave packets do not appear to flatten further during collapse (Degtyarev *et al.*, 1976; Robinson *et al.*, 1988; Robinson and Newman, 1990a) and the present mechanism is adequate to account for the observed shape distribution. (A further argument is actually required, to the effect that the collapse threshold is nearly polarization independent; it is summarized in Sec. V.D.)

Two-dimensional systems are relevant, for example, to self-focusing of laser beams in the two directions transverse to their propagation. In such systems circularly symmetric wave packets are possible for $R=1$, but the probability distribution (Newman *et al.*, 1991)

$$P(R)=\frac{1-R}{R^{1/2}(1+R)^2} \tag{5.8}$$

favors anisotropic profiles even more strongly than Eq. (5.7), with $\langle R\rangle=\pi-3$ corresponding to an axial ratio of approximately 1:1.5. The maximum axial ratio in this case is $1:\sqrt{3}$, which occurs for $R=0$.

Newman *et al.* (1991) showed that the functions

$$h_0(r)=\frac{a^2}{a^2+r^2}, \tag{5.9}$$

$$h_1(r)=\frac{ar}{a^2+r^2} \tag{5.10}$$

are eigenfunctions of the Zakharov equation (2.17) with $\hat{\gamma}_L=0$ for almost identical three-dimensional density wells of characteristic width a, as shown in Fig. 15. These functions are thus very close to being simultaneous eigenfunctions of the same well and hence are suitable model eigenfunctions for studying properties of localized wave packets. The central density depressions corresponding to Eqs. (5.9) and (5.10) are $n_0(0)=-20/a^2$ and $n_1(0)=(4\log 2-22)/a^2\approx -19.2/a^2$, only a 4% discrepancy. Hence the well corresponding to h_0

$$n_0(r)=-\frac{4(5a^2-r^2)}{(a^2+r^2)^2}, \tag{5.11}$$

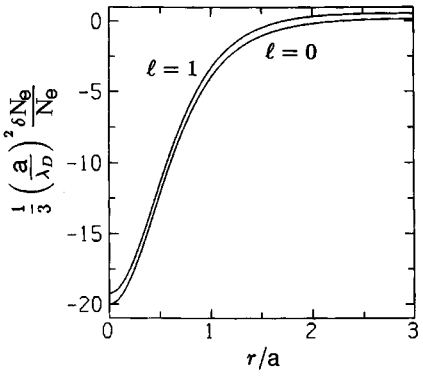

FIG. 15. Density wells for which $h_0(r)$ $(l=0)$ and $h_1(r)$ $(l=1)$ are eigenfunctions in three dimensions (Newman *et al.*, 1991).

is a reasonable approximation to the density well that corresponds to both eigenfunctions. In physical units

$$\frac{\delta N_e}{N_e} = \frac{3\lambda_D^2}{a^2} n. \tag{5.12}$$

Note that the Lorentzian factors $(a^2+r^2)^{-1}$ in Eqs. (5.9) and (5.10) could be replaced by Gaussian ones, for example, while preserving the main features of the field structure.

Before leaving the question of wave-packet structure, a few words about the role of the constant a_{00} are warranted. This constant enters the angular momentum density in Eq. (2.32) through the term $i\mathbf{E}\times\mathbf{E}^*$. Newman *et al.* (1991) showed that $i\mathbf{E}\times\mathbf{E}^*$ can have a dipole or ringlike structure, depending on the relative values of α, β, and a_{00} in Eq. (5.4). Figure 16 shows three examples: in frame (a) one has $a_{00}=0$ and the field $i\mathbf{E}\times\mathbf{E}^*$ has a dipole form; in frame (c), where a_{00} is

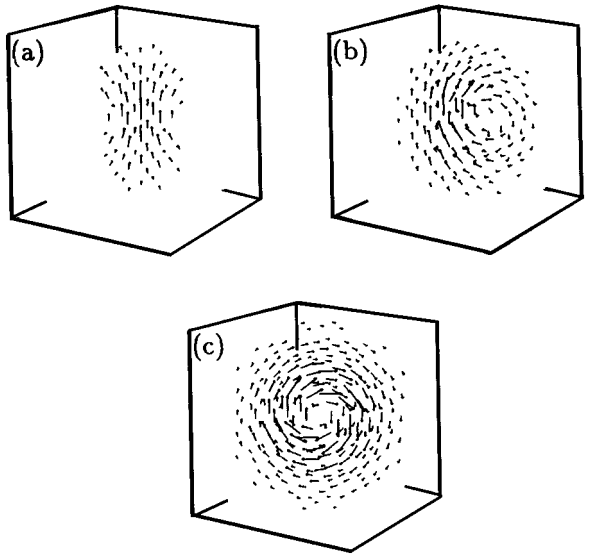

FIG. 16. Vector plots of $i\mathbf{E}\times\mathbf{E}^*$ for the model potential given in Eq. (5.4) with (a) $\beta/\alpha=0.6$, $a_{00}/\alpha=0$; (b) $\beta/\alpha=0.5$, $a_{00}/\alpha=0.5+0.5i$; (c) $\beta/\alpha=0$, $a_{00}/\alpha=0.5i$ (Newman *et al.*, 1991).

purely imaginary, it forms a ring, while case (b), where a_{00} is complex, is intermediate between these two limits.

There is substantial numerical evidence that only a single eigenstate is relevant to nucleation and that this state is the one with a single central peak of $|\mathbf{E}|$, rather than a more complicated structure. Robinson, Wouters, and Broderick (1996) investigated this problem, calculating the approximate eigenfrequency of a state j trapped in a D-dimensional well of a given depth and length scale a. They found

$$\frac{\omega_j-\omega_p}{\omega_p} \approx \frac{\Delta N_e}{2N_e} + \frac{3\pi^2 m^2}{2}\frac{\lambda_D^2}{a^2}, \tag{5.13}$$

in dimensional units, where ω_p is the unperturbed plasma frequency, ΔN_e is the characteristic depth of the well, and m^2 is the sum of the squares of the quantum numbers m_i along D orthogonal axes, with $m_i=1,2,\ldots,$ giving $m^2 \geqslant D$. The requirement $\omega_j \lesssim \omega_p$ for the state to be localized then implies

$$D \leqslant m^2 \lesssim \frac{1}{3\pi^2}\left|\frac{\Delta N_e}{N_e}\right|\frac{a^2}{\lambda_D^2}. \tag{5.14}$$

Conservation of mass during relaxation of an unsupported density well (see Sec. V.G) can then be used to relate the quantities in Eq. (5.14) to those at the arrest scale a_f, giving

$$D \leqslant m^2 \lesssim \frac{1}{3\pi^2}\left|\frac{\Delta N_f}{N_e}\right|\frac{a_f^2}{\lambda_D^2}\left(\frac{a_f}{a}\right)^{D-2}, \tag{5.15}$$

where ΔN_f is the density perturbation at arrest (Robinson, Wouters, and Broderick, 1996). Because $\Delta N_f \leqslant N_e$ and the nucleation scale of the packet must be greater than its arrest scale $a_f \approx 20\lambda_D$ (see Sec. V.F), this relationship implies $D \leqslant m^2 \lesssim 12$ and, hence, $1 \leqslant m_i \lesssim 3$. For an isotropic situation with equal values of m_i for all i, one finds $1 \leqslant m_i \lesssim 2$. Robinson, Wouters, and Broderick (1996) took this argument further, incorporating the effects of well relaxation and the estimated nucleation scale (see Sec. VI.A) to obtain the bound

$$D \leqslant m^2 \lesssim 2 \tag{5.16}$$

at nucleation. This implies that m^2 is minimal at the point of renucleation; i.e., the state has the fewest possible nodes and is the ground state of the well.

C. Power input to packets

Wave packets in slowly relaxing density wells can accumulate energy directly from a driver or via nonlinear interactions with propagating waves. Such energy accumulation can be studied by adding source terms $\nabla\cdot\mathbf{S}_E$ and $\nabla^2 S_n$ to the right sides of the Zakharov equations (2.17) and (2.18), respectively (DuBois and Rose, 1991). The first of these sources,

$$\mathbf{S}_E = n\mathbf{E}_C e^{-i\omega_C t}, \tag{5.17}$$

takes into account a spatially uniform pump field $\mathbf{E}_C$ oscillating at a frequency ω_C. Such a pump is called a "clamp" field if its amplitude is fixed. It can either be

added to the auxiliary $k=0$ component of the first Zakharov equation [see the discussion following Eq. (2.10)] or it can replace it, the latter being the more common procedure in the clamp-drive literature to date. The second source,

$$S_n=\mathbf{E}\cdot\mathbf{E}_C^*e^{i\omega_C t}+\mathbf{E}^*\cdot\mathbf{E}_C e^{-i\omega_C t}+n_a\xi(x,t), \tag{5.18}$$

incorporates beats between the packet field and a clamp driver in the ponderomotive force, as well as stochastic driving by other processes [the final term in Eq. (5.18)], to account for ambient density fluctuations that are unrelated to Langmuir waves. In principle, these sources can also account for particle noise associated with the damping terms $\hat{\gamma}_L$ and $\hat{\gamma}_S$ (DuBois and Rose, 1991). Note that the stochastic term $n_a\xi(x,t)$ is defined to have zero mean and a variance n_a^2, averaged over space, time, or both; subject to these conditions, spatial and temporal correlations of this term may exist.

The Langmuir field can be expanded in terms of instantaneous vector eigenstates $|m\rangle$ of the source-free Zakharov equation (2.17) in the unperturbed density profile n, where we use standard Dirac bracket notation (Schiff, 1968)

$$\mathbf{E}=\sum_m a_m|m\rangle\exp(-i\omega_m t), \tag{5.19}$$

where the coefficients a_m vary slowly in time and ω_m is the eigenfrequency of the state $|m\rangle$. Zakharov and Shur (1981), Doolen *et al.* (1985), DuBois *et al.* (1988, 1990), Newman *et al.* (1989), Robinson and Newman (1991b), Robinson (1996a), and Robinson, Wouters, and Broderick (1996) have all argued that the trapped state is dominated by a single eigenfunction, which is the ground state. More generally, the sum in Eq. (5.19) can be split into a sum over localized eigenstates and a sum over freely propagating states, which can be approximated as plane waves.

During nucleation, $\mathbf{E}$ can be considered to evolve within a linearly determined density well n in the absence of damping, which is only significant near the end of collapse (see Sec. V.F). If the source (5.17) is added to Eq. (2.17) in this regime and the expansion (5.19) is made, one finds (Doolen *et al.*, 1985; DuBois *et al.*, 1988, 1991; DuBois and Rose, 1991; Robinson and Newman, 1991b; Robinson, Wouters, and Broderick, 1996)

$$i\frac{da_j}{dt}=\sum_m \langle j|\delta n|m\rangle e^{i(\omega_j-\omega_m)t}+\langle j|n|C\rangle e^{i(\omega_j-\omega_C)t}, \tag{5.20}$$

where $|C\rangle$ corresponds to $\mathbf{E}_C$, $\delta n\sim n_a$ is the part of n due to stochastic driving, and products of source terms have been neglected. In general, terms involving derivatives of the states $|m\rangle$ and their eigenfrequencies should also appear on the right of Eq. (5.20). However, as we shall see shortly, nucleation is most effective when the packet is near the threshold for collapse and these derivatives are zero. Equation (5.20) can be expanded as a perturbation series, as in standard quantum-mechanical time-dependent perturbation theory (Schiff, 1968), and the resulting equations can then be integrated successively to obtain a_j to arbitrary order in the expansion.

In the lowest nontrivial order of the perturbation expansion, the two terms on the right of Eq. (5.20) represent two different mechanisms by which energy can be transferred to a nucleating state $|j\rangle$:

(i) The first term in Eq. (5.20) represents scattering of energy from continuum states with $\omega_m>0$, off density fluctuations imposed by the stochastic source in Eq. (5.18), into the state $|j\rangle$. This is analogous to the electrostatic decay of a plane Langmuir wave L into a product Langmuir wave L' and an ion sound wave S, $L\rightarrow L'+S$ (see Secs. III.A and III.B). However, in the present case, the state L' is a localized Langmuir state. When this term dominates in Eq. (5.20), Fermi's Golden Rule (Schiff, 1968) implies that the energy-transfer rate peaks for $\omega_j=\omega_m-\omega_q$, where q labels a set of eigenfunctions into which δn is decomposed (e.g., plane waves). Since $\omega_m>0$ for plane waves and ω_q is small compared to the plasma frequency ω_p, the strongest coupling occurs for states with small $|\omega_j|$. The overlap integrals (S-matrix elements, in quantum terminology) in Eq. (5.20) are also likely to be dominated by states m whose wavelength is of the same order as the length scale of the localized state j. Essentially, the localized states enable the decay cascade to be extended relative to the plane-wave case, with energy cascading into eigenstates with $\omega_j<0$ [see Fig. 13(a)]. The term $\langle j|\delta n|m\rangle$ also contains an implicit dot product between the vector parts of the states $\langle j|$ and $|m\rangle$. Hence the strongest coupling is to continuum states with polarizations similar to that of the localized state. However, the field of the localized state is not unidirectional, so there is some coupling to all continuum-state polarizations. The longest characteristic period available for nucleation occurs approximately at the point at which the lowest-lying eigenstate is about to detrap due to relaxation of the well.

(ii) The second term in Eq. (5.20) represents direct coupling from the source to the localized state. The strongest coupling occurs where $\omega_j=\omega_C$ (DuBois *et al.*, 1988, 1990; DuBois and Rose, 1991). For effective coupling to occur, the source must thus be tuned near or below the plasma frequency. Again, the strongest coupling occurs when the driver polarization is similar to that of the state $|j\rangle$.

For both the background-turbulence source and the direct-drive source above, the strongest coupling to a nucleating state involves frequencies (of the background waves or clamp, respectively) that are close to the frequency of the trapped state. In the case of energy input from background turbulence, nucleation will be ineffective unless the trapped eigenfrequency is close to the unperturbed plasma frequency ω_p (the lowest frequency of propagating waves). If the energy enters the background turbulence at high frequencies, it will undergo a cascade to lower k before it can couple effectively to nucleating states. A similar cascade must also occur if a clamp drive is applied with a frequency well above ω_p (DuBois *et al.*, 1990, 1993a, 1993b; Hanssen *et al.*, 1992). Reasonable criteria for the occurrence of a cascade are

that (i) $k > k_*/2$, as in Fig. 3 and (ii) the decay instability rate exceeds that of the modulational instability of the trapped waves (Hanssen *et al.* 1992; DuBois *et al.*, 1993a, 1993b). The latter criterion is discussed further in Sec. VI.A, where it is noted that if (ii) is not satisfied the cascade can be truncated before reaching $k=0$.

D. Collapse thresholds

Once a nucleating wave packet has accumulated sufficient energy, it will begin to collapse. A necessary condition for wave collapse is that the Hamiltonian be unbounded from below as the packet contracts, thereby making collapse to a singularity an energetically allowed process (Zakharov, 1972, 1984; Kuznetsov *et al.*, 1986). A sufficient condition for collapse of packets governed by the nonlinear Schrödinger equation is $A<0$, where A is given by Eq. (4.10), as discussed in Sec. IV.A.

In the vicinity of the collapse threshold, ponderomotive forces due to the localized packet are close to the value needed to support the density well and prevent it from relaxing. Hence, in this phase, the packet is very slowly evolving and the nonlinear Schrödinger equation can be expected to provide a reasonable approximation. Hence it is argued that the criterion $A=0$ should give a reasonable estimate of the collapse threshold. This has been verified for stationary wave packets using particle-in-cell simulations (Newman *et al.*, 1990). Indeed, these simulations showed that the condition $A=0$ is actually a better estimate of the threshold than the condition that the full Hamiltonian of the Zakharov equations be zero. Collapse is actually possible for H slightly larger than zero in the Zakharov case (Zakharov, 1984; Kuznetsov *et al.*, 1986; Newman *et al.*, 1990).

The collapse threshold for the field given by Eqs. (5.4) and (5.10) with $a_{00}=0$ was calculated by Newman *et al.* (1990). Robinson, Wouters, and Broderick (1996) generalized their results to arbitrary polarizations using an ansatz field of the form

$$\Phi(\mathbf{r}) = E_0(\alpha x + i\beta y)e^{-r^2/a^2}, \tag{5.21}$$

which has the same characteristic features. Robinson, Wouters, and Broderick (1996) found that three-dimensional collapse of this field occurs when the quantity $a^2E_0^2$ exceeds a threshold Θ given by

$$\Theta(\alpha) = \frac{1792\sqrt{2}}{205-60\alpha^2(1-\alpha^2)}, \tag{5.22}$$

for $c_S=1$. The quantity Θ is dimensionless and, in terms of dimensional units, is the threshold value of the quantity Wa^2/λ_D^2 above which collapse occurs, where W is given by Eq. (2.21). This form of the threshold implies that there is no energy threshold for 3D collapse, because the characteristic energy is proportional to $Wa^3 \propto \Theta a$ in this case. However, once damping is incorporated, a must be greater than the arrest scale, which imposes an effective minimum initial energy for collapse. In Sec. VI we also note that, for collapse amid turbulence, W must exceed the mean turbulent energy density.

The α dependence of the threshold in Eq. (5.22) is weak, with only an 8% difference between the highest ($\alpha^2=1/2$) and lowest ($\alpha=1$) thresholds. This implies that the polarization of the wave packets does not strongly affect the threshold and hence that the distribution of polarizations of collapsing packets is nearly the same as that of nucleating packets, at least at the start of collapse. Newman *et al.* (1989, 1991) found that the polarization does not change substantially during collapse. These points complete the argument of Sec. V.B that leads to the predicted shape distribution of collapsing wave packets.

The collapse threshold is somewhat higher for packets with Lorentzian profiles than for Gaussian ones, because more of the energy is in the low-field tail, thereby enhancing the $|\nabla\cdot\mathbf{E}|^2$ term relative to the $|\mathbf{E}|^4$ term in the Hamiltonian (2.29). Newman *et al.* (1990) calculated $\Theta\approx 50$ for a 2D linearly polarized Lorentzian dipole field with $c_S=1$ and $\alpha=1$. They found that this estimate was in good accord with the numerically determined collapse threshold for a single wave packet governed by the Zakharov equations and for an equivalent packet simulated by particle-in-cell methods. Robinson and Newman (1990a, 1990c) estimated the collapse threshold from the rate of energy dissipation in strong turbulence. In the limit of low mean Langmuir energy density, their results imply $\Theta\approx 150$ in two dimensions and $\Theta\approx 260$ in three dimensions, both for $c_S^2=1.6$. These values are likely to be higher than the true minimum threshold because they include cases in which packets exceed the threshold by a factor of order unity.

Robinson, Wouters, and Broderick (1996) estimated the collapse threshold from the requirement that the ground state of a nucleating well have $\omega_j=0$. From Eq. (5.13), with $m^2=D$, this yields

$$\Theta \approx 3\pi^2 D c_S^2, \tag{5.23}$$

which exhibits the dependence of Θ on c_S. Equation (5.23) is in semiquantitative agreement with the 2D and 3D numerical results cited above and also corresponds semiquantitatively to the condition $H=0$, since $\hbar\omega_j$ is an energy eigenvalue for a Langmuir quantum with Hamiltonian H. It is important to note that the characteristic value of Θ is several tens, rather than order unity, as would be found from naive balancing of dispersion and self-focusing terms in the Hamiltonian (2.29).

E. Collapse

Once the collapse threshold is exceeded, the virial theorem (4.9) implies that the root-mean-square size of the packet decreases monotonically in systems of dimensionality $D\geq 2$; i.e., the packet collapses and decouples from the driver as the density well deepens and the packet eigenfrequency decreases as a result. Zakharov (1972) showed that the potential of the collapsing field approaches the self-similar form

$$\Phi(t,\mathbf{r})=\frac{e^{i\omega_j t_c \tau}}{\tau^{\delta}}\tilde{\Phi}\left(\frac{\mathbf{r}}{\tau^{\chi}}\right), \tag{5.24}$$

$$\tau=1-t/t_c, \tag{5.25}$$

where the collapse is assumed to start at $t=0$, t_c is the time at which a singularity would be reached in the absence of any additional physics, $\tilde{\Phi}$ has a constant functional form, and δ and χ are constants. This form is termed self-similar because temporal evolution is embodied in the change of scale and amplitude, within a constant functional form $\tilde{\Phi}$. The length scale a of the field decreases as τ^{χ}, while the characteristic electric-field strength increases as $\tau^{-\delta-\chi}$. Collapse thus corresponds to the nonlinear stage of a modulational instability of localized (rather than plane) waves. The form of Eq. (5.24) only applies for the so-called *inertial range* between the nucleation and dissipation scales, where the packet undergoes free collapse, without appreciable driving or damping.

A number of different regimes of self-similar wave collapse exist. The first subdivision is into cases of weak and strong collapse. In weak collapse, energy is not conserved during collapse, with $|\mathbf{E}|^2 a^D \sim \tau^{-\mu}$ and

$$\mu=2\delta+(2-D)\chi<0, \tag{5.26}$$

implying that Langmuir waves are radiated from the packet. In strong collapse, the inequality in Eq. (5.26) becomes an equality. Kuznetsov and Skorić (1988a, 1988b) showed that radiation from a collapsing packet can speed collapse by increasing the ratio $|H|/N$, implying that weak-collapse scalings dominate over strong ones even when self-similarity is not imposed from the start. Their work dealt with magnetized-plasma waves in the adiabatic limit, but this result carries over to the unmagnetized case.

The second subdivision of collapse regimes depends on which terms dominate in Eqs. (2.17) and (2.18). In the subsonic case collapse is adiabatic and the time derivatives can be neglected in Eq. (2.18). Ignoring damping and requiring that the terms in Eq. (2.17) all be of the same order then yields $\omega_j \propto n \propto -|\mathbf{E}|^2$,

$$\delta=0, \quad \chi=1/2. \tag{5.27}$$

Subsonic collapse is strong for $D=2$ and weak for $D=3$. In the supersonic case, the temporal derivatives in Eq. (2.18) dominate over the spatial derivatives, and ion inertia is so great that the density cannot keep pace with the changing ponderomotive force of the collapsing fields. In this case $\partial^2 n/\partial t^2 \sim \nabla^2 |\mathbf{E}|^2$ holds. If we require in addition that energy be conserved, we find in three dimensions

$$\delta=1/3, \quad \chi=2/3, \tag{5.28}$$

and

$$N=\frac{1}{\tau^{4/3}}\tilde{N}\left(\frac{\mathbf{r}}{\tau^{\chi}}\right), \tag{5.29}$$

where the function $\tilde{N}$ gives the self-similar density profile. Supersonic collapse of this type is always strong, by construction. Any crossover from subsonic to supersonic collapse occurs when the time derivative in Eq. (2.18) exceeds the spatial one; i.e., where $\dot{a} \approx v_S$ in dimensional units. If the collapse is not arrested first (see Sec. V.F), this crossover point will always be reached, because $\dot{a} \propto \tau^{-1/2}$ for self-similar subsonic collapse. The characteristic dimensionless crossover condition $a/t_c=1$ implies $W \sim m_e/m_i$ after conversion back to dimensional units. This criterion is also the one that defines the boundary between subsonic and supersonic plane-wave instabilities (see Fig. 3). An improved estimate, applicable to collapse amid background turbulence, is discussed in Sec. VI.C.

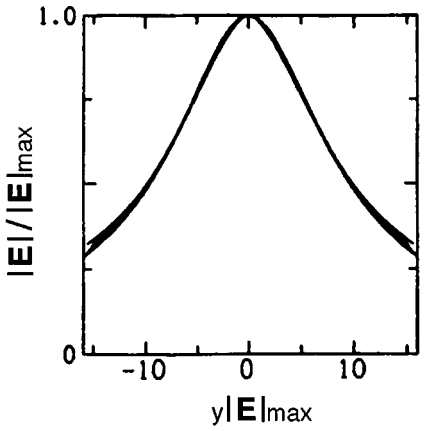

FIG. 17. Profiles through a collapsing wave packet, as in Fig. 8, but rescaled according to the subsonic scalings of Eq. (5.27); $|\mathbf{E}|/|\mathbf{E}_{\max}|$ is plotted against $y|\mathbf{E}|_{\max}$, where y is a spatial coordinate.

The existence of wave collapse has been verified numerically by many authors, and several have verified specific self-similar forms. Figure 8 shows a series of field profiles taken through a collapsing solution of Eq. (2.20) in the absence of damping. Figure 17 shows the same profiles plotted using variables rescaled according to the subsonic scalings given by Eq. (5.27). The curves in Fig. 8 collapse very nearly into a single curve in Fig. 17, demonstrating the subsonic scaling of the wave collapse. In simulations of the Zakharov equations Degtyarev *et al.* (1976) and Budneva *et al.* (1975) found reasonable agreement of simulations with the supersonic collapse scalings in Eqs. (5.28) and (5.29) at high wave intensities. However, it appears that the crossover point is substantially higher than $W=m_e/m_i$. For example, Robinson and Newman (1990a) also showed that the statistical properties of strong turbulence are consistent with Eq. (5.27) rather than Eq. (5.28), at least for $W \ll 1$, rather than $W \ll m_e/m_i$ (see Sec. VI for more details).

F. Arrest of collapse

The self-similar solution (5.24) implies the formation of a field singularity at $t=t_c$ ($\tau=0$). In reality, effects neglected in the dissipation-free Zakharov equations

must intervene to prevent such an unphysical occurrence. Mechanisms that could, in principle, arrest wave collapse include linear Landau damping given by Eq. (2.2), transit-time damping due to enhanced interactions between electrons and localized coherent waves (Morales and Lee, 1974; Valeo and Kruer, 1974; DeNeef and DeGroot, 1977; Rozanov and Shumskiĭ, 1986, 1987; Robinson, 1989, 1991; Melatos and Robinson, 1993a, 1993b, 1995), wave breaking (Dawson, 1959; Kruer, 1988), onset of higher-order nonlinearities (Škorić and ter Haar, 1980; Malkin, 1986; Newman *et al.*, 1990), or breakdown of quasineutrality due to ion inertia (Newman *et al.*, 1990). Of these, recent work strongly favors the mechanism of transit-time damping, which we discuss next, before briefly addressing why the other alternatives appear less favorable.

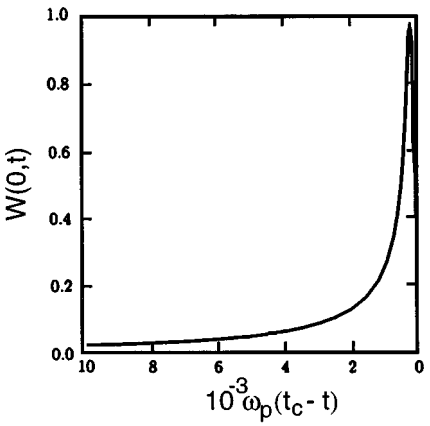

FIG. 18. Central energy density vs time during collapse, calculated from the transit-time damping expression [Eq. (5.35)] for the wave packet in Eq. (5.30) with a Gaussian profile in three dimensions (Robinson, 1991).

1. Arrest by transit-time damping

For damping to arrest collapse, wave-packet fields must be dissipated as fast as they build up due to collapse. Zakharov and Shur (1981) and Russell *et al.* (1986) have showed that linear damping must increase at least as fast as $k^{D/2}$ at large k to arrest collapse in a D-dimensional system. This requirement is not satisfied by the Landau damping operator (2.2), so random-phase linear damping of Langmuir waves in a thermal plasma cannot halt collapse unless it does so at small k where Eq. (2.2) *is* steeply increasing. The presence of a high level of superthermal electrons may change this conclusion by increasing the high-k damping, as may improved calculation of the thermal Landau damping operator, since Eq. (2.2) is only valid for $(k\lambda_D)^2 \ll 1$. However, high levels of superthermal electrons will increase transit-time interactions even more.

The damping operator (2.2) applies to interactions between plane waves and a thermal plasma. If, however, the waves are coherent and localized, it is possible to lose energy to particles much more rapidly via *transit-time damping*. Transit-time interactions occur when particles cross a localized, coherent, oscillating field in a time comparable to, or shorter than, the period of oscillation. To first order, very fast particles see a dc field during their passage and exchange an amount of energy of order $q|\mathbf{E}|a$, where q is their charge. For an isotropic distribution of particles, positive and negative contributions cancel exactly to this order. However, to order $|\mathbf{E}|^2$, the net energy exchange is nonzero.

Robinson (1991) calculated the local power exchange between a particle of initial velocity v_0 and a field

$$\mathcal{E}(t,\mathbf{r}) = \mathbf{E}(\mathbf{r})\cos(\omega_p t + \phi), \tag{5.30}$$

where ϕ is a phase constant and $\mathbf{E}(\mathbf{r})$ is an arbitrary spatial profile. He used a perturbation expansion in which the trajectory of the particle is expanded about the unperturbed one in powers of the perturbing field, and the phase ϕ is averaged over to account for random arrival times of individual particles. For a unidirectional Gaussian field $\mathbf{E}(\mathbf{r}) = \mathbf{E}_0 e^{-r^2/a^2}$, and after integration over a Maxwellian distribution, this yielded a mean rate of power dissipation per unit volume $P(0)$ given by

$$\gamma_{\rm eff} = \frac{P(0)}{\frac{1}{2}\epsilon_0 E_0^2} = \frac{\pi\omega_p}{D\Gamma(D/2)2^{D/2}} z^{D/2} e^{-z}(z + D - 1), \tag{5.31}$$

at the center of the wave packet in Eq. (5.30), where dimensional units have been used, $z = a/(\lambda_D\sqrt{2})$, D is the dimensionality, and Γ denotes a gamma function. The notation $\gamma_{\rm eff}$ indicates that this quantity is the effective damping rate for the central energy density.

The effective growth rate of the central energy density $W(t,0) = |E(t,0)|^2$ in a collapsing wave packet is

$$\Gamma_{\rm eff} = \frac{1}{|E(t,0)|^2}\frac{d}{dt}|E(t,0)|^2 = \frac{2(\delta+\chi)}{\omega_p t_c}\left(\frac{a_i}{a}\right)^{1/\chi}, \tag{5.32}$$

where a_i is the initial scale of the packet. Robinson and Newman (1990a) found $\delta = \chi = 1/2$ during the bulk of collapse and $\omega_p t_c \approx (a_i/\lambda_D)^2$ (see Sec. VI.C). These results yield

$$\Gamma_{\rm eff} \approx \omega_p \lambda_D / a^2. \tag{5.33}$$

Combining Eqs. (5.31) and (5.32) yields the evolution equation

$$\frac{d}{dz}W(t,0) = -\frac{4z}{\omega_p}[\Gamma_{\rm eff}(z) - \gamma_{\rm eff}(z)]W(t,0), \tag{5.34}$$

which can be integrated by steepest descents to give

$$\frac{W(0,t)}{W(0,0)} \approx \frac{z_i^2}{z^2}\exp\left[-\frac{4z\,\gamma_{\rm eff}(z)}{\omega_p}\right], \tag{5.35}$$

where $W(0,0)$ is the initial central field and z_i the initial scale parameter. Figure 18 shows that $W(0,t)$ increases at an accelerating rate early in collapse, peaks sharply at a value of order unity, then falls rapidly during burnout, just as was seen in simulations that use the Zakharov equations or particle-in-cell methods (e.g., D'yachenko *et al.*, 1988; Zakharov, Pushkarev, Rubenchik, Sagdeev,

and Shvets, 1988, 1989; Zakharov, Pushkarev, Sagdeev, Solov'ev, Shapiro, Shvets, and Shevchenko, 1989; Newman *et al.*, 1990).

Two essentially equivalent estimates of the arrest scale can be made from Eq. (5.35). First, the condition $\Gamma_{\rm eff}=\gamma_{\rm eff}$ gives $a_f=13.6\lambda_D$ and $15.0\lambda_D$ for $D=2$ and $D=3$, respectively. At this point, approximately 30–40% of the energy has been dissipated, in excellent agreement with the results of two-dimensional particle-in-cell simulations. Second, the point at which the exponent in Eq. (5.35) is -1 (i.e., where the central energy density has been reduced by a factor of e relative to the free-collapse value) occurs at $11.8\lambda_D$ and $13.2\lambda_D$, respectively.

The arrest scales obtained from Eq. (5.35) are only weakly dependent on the collapse exponents δ and χ because of the exponential dependence in Eq. (5.31). What is more significant is that the arrest scales in three dimensions are greater than those in two. This result had been seen in particle-in-cell simulations (D'yachenko *et al.*, 1988; Zakharov, Pushkarev, Rubenchik, Sagdeev, and Shvets, 1988, 1989; Zakharov, Pushkarev, Sagdeev, Solov'ev, Shapiro, Shvets, and Shevchenko, 1988) prior to Robinson's (1991) work, but had been considered paradoxical because nonlinear self-focusing becomes stronger as D increases. Hence, it was reasoned, collapse should proceed to shorter scales before arrest. The theory of transit-time damping makes it clear that the contrary trend occurs because the fraction of high-velocity particles in a 3D distribution is higher than that in a 2D distribution and hence transit-time damping is stronger.

Robinson (1991) also calculated the arrest scales for the packet derived from the dipole potential (5.4), with Eq. (5.10), $a_{00}=0$ and $\alpha=1$, which is a more realistic representation of the potential of a collapsing packet. He obtained

$$\frac{W(0,t)}{W(0,0)}\approx\frac{z_i^2}{z^2}\exp\left(-\frac{2w^2\gamma_{\rm eff}(w)}{\omega_p}\right), \tag{5.36}$$

$$\gamma_{\rm eff}(w)=\left(\frac{2\pi}{3}\right)^{1/2}\frac{\pi\omega_p}{D\Gamma(D/2)2^{D/2}}w^{(D+1)/2} \times(w^2-w+D-1)e^{-3w/2}, \tag{5.37}$$

$$w=(a/\lambda_D)^{2/3}. \tag{5.38}$$

These expressions yield estimates $a_f=23\lambda_D$ and $a_f=26\lambda_D$ in two and three dimensions, respectively, based on the point at which the central energy density has decreased by a factor of e. Corresponding peak values of W are achieved at $32\lambda_D$ and $35\lambda_D$, respectively.

The above estimates of arrest scales are reasonably consistent with the value of $(11–15)\lambda_D$ found in two-dimensional particle-in-cell simulations and the range $(17–30)\lambda_D$ inferred from three-dimensional experiments and particle-in-cell simulations (Janssen, Bonnie, Granneman, Krementsov, and Hopman, 1984; Janssen, Granneman, and Hopman, 1984; Wong and Cheung, 1984; Levron *et al.*, 1987; D'yachenko *et al.*, 1988; Zakharov, Pushkarev, Rubenchik, Sagdeev, and Shvets, 1988, 1989; Zakharov, Pushkarev, Sagdeev, Solov'ev, Shapiro, Shvets, and Shevchenko, 1989; Newman *et al.*, 1990; Robinson and Newman, 1990c; see Sec. VIII for details of the experiments). It should be stressed that the length scale is much bigger than would be crudely estimated from the characteristic cut-in point of transit-time interactions, $V_e\approx a\omega_p$, which gives $a_f\approx\lambda_D$.

The peak values of $W(0,t)$ predicted by Robinson (1991) were 0.2–1, depending on the packet structure. These values are in good agreement with numerical results from Zakharov equation and particle-in-cell (PIC) simulations after allowing for the higher values of $W(0,0)$ used in PIC simulations for computational tractability (Newman *et al.*, 1990; Robinson, 1991).

Further evidence for arrest of collapse by means of transit-time damping was found in PIC simulations carried out by Zakharov, Pushkarev, Rubenchik, Sagdeev, and Shvets (1989) and Newman *et al.* (1990). Near arrest, coherent phase-space "jets" of fast particles were observed to be emitted from the collapsing packet. These jets are consistent with transit-time acceleration peaking when the field reaches its maximum each plasma period. They are not consistent with ordinary, random-phase Landau damping.

The sudden dissipation of Langmuir energy near arrest heats the plasma locally, leading to an increase in $\lambda_D=V_e/\omega_p$ and a corresponding rise in the arrest scale by tens of percent for $W_f\approx1$ (Zakharov, Pushkarev, Rubenchik, Sagdeev, and Shvets, 1989; Newman *et al.*, 1990; Robinson, 1991). It does not, however, change the main conclusions above.

2. Particle scattering by transit-time interactions

In many contexts the scattering of fast electrons involved in transit-time interactions is of greater interest than arrest itself. These electrons acquire an energy

$$W=q\int dt\mathbf{v}(t)\cdot\mathcal{E}(t,\mathbf{r}), \tag{5.39}$$

during their passage through the localized field given by Eq. (5.30) (Morales and Lee, 1974; Valeo and Kruer, 1974; DeNeef and DeGroot, 1977; Rozanov and Shumskiĭ, 1986, 1987; Robinson, 1989). Expansion of the position and velocity about their unperturbed values in powers of the electric-field strength yields a first-order energy exchange $W^{(1)}$. This is given by (Robinson, 1989; Melatos and Robinson, 1993a)

$$W^{(1)}=q\,{\rm Re}[e^{i\phi}\hat{\mathbf{v}}^{(0)}\cdot\tilde{\mathbf{E}}\,(k_0)]=q\,\hat{\mathbf{v}}^{(0)}\cdot\tilde{\mathbf{E}}\,(k_0)\cos\phi, \tag{5.40}$$

$$=\tilde{\mathbf{E}}\,(k_0)\int dl e^{ikl}\int\frac{d^3\mathbf{k}'}{(2\pi)^3}e^{i\mathbf{k}'\cdot\mathbf{r}^{(0)}(l)}\mathbf{E}(\mathbf{k}'), \tag{5.41}$$

where $\mathbf{E}(\mathbf{k})$ is the standard Fourier transform of $\mathbf{E}$, l is the distance along the unperturbed trajectory from the point of closest approach to $r=0$, $\mathbf{v}^{(0)}$ is the unperturbed velocity, $k_0=\omega_p/v^{(0)}$, the hat denotes a unit vector, and the second equality in Eq. (5.40) holds only if $\tilde{\mathbf{E}}\,(k_0)$ is

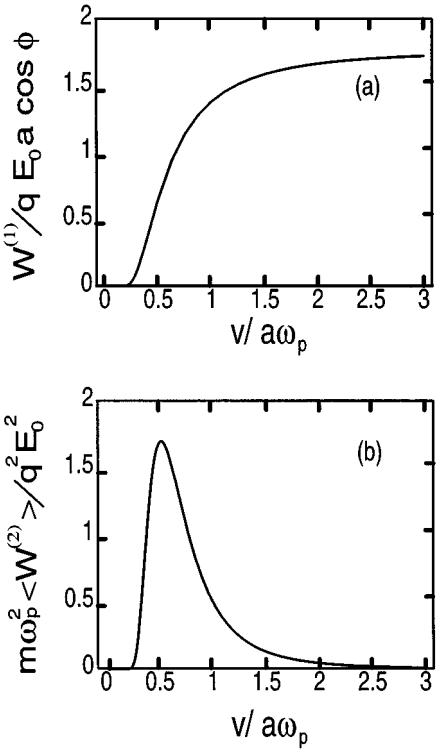

FIG. 19. First-order and mean second-order energy transfers vs velocity for the wave packet in Eq. (5.30) with a Gaussian profile in one dimension: (a) $W^{(1)}$; (b) $\langle W^{(2)}\rangle$.

real. In these terms, the unperturbed trajectory is $\mathbf{r}^{(0)}=\mathbf{b}_0+\hat{\mathbf{v}}^{(0)}l$, where $\mathbf{b}_0$ is the impact parameter at which $r^{(0)}$ is minimal.

The first-order interaction in Eq. (5.40) scatters particles in energy, but does not lead to any net energy transfer when averaged over the phase ϕ (which corresponds to averaging over random arrival times of the particles at the packet). The second-order energy exchange is nonzero, even when averaged over ϕ, because particles that are accelerated gain energy at a different rate from those that are decelerated. The second-order phase-averaged transfer is (Robinson, 1989; Melatos and Robinson, 1993a, 1993b)

$$L=\frac{q^2}{4m(v^{(0)})^2}\left[\tilde{E}_j(k_0)\tilde{E}_j^*(k_0)-\frac{d}{dk_0}\mathrm{Im}\left(\hat{v}_s^{(0)}\tilde{E}_j^*(k_0)\frac{\partial\tilde{E}_s}{\partial x_j}(k_0)\right)\right], \tag{5.42}$$

where there are implicit sums over $j,s=1,2,3$. Figure 19 shows Eqs. (5.40) and (5.42), evaluated in one dimension for the field of Eq. (5.30) with a Gaussian profile. This shows that transit-time damping cuts in strongly for $a\lesssim 5v/\omega_p$.

An alternative treatment of transit-time interactions in terms of coherent Landau damping theory was given by Bingham *et al.* (1994) and Tsytovich (1995), implicitly taking into account local modifications to the particle distribution due to the field. The results are very similar to the above, and the predicted arrest scale is only slightly changed, so we do not discuss this approach here. DuBois *et al.* (1995a) have also considered local modifications to the damping operators.

3. Alternative arrest mechanisms

If Langmuir waves are intense enough, they can give even an initially stationary particle a high enough oscillating (or "quiver") velocity that it can interact resonantly with the field (Kruer, 1988). The *wave-breaking amplitude* at which this occurs is given by $qE/m\omega_p\approx\omega_p/k$ (Dawson, 1959; Kruer, 1988). If we estimate $k\approx 1/a$ we find the condition

$$W\gtrsim a^2/\lambda_D^2 \tag{5.43}$$

for wave breaking to be important. Thus, since transit-time damping halts collapse at $W\lesssim 1$ and $a\gtrsim 15\lambda_D$, wave breaking is not expected to be relevant to wave collapse. The condition (5.43) is essentially equivalent to Eq. (2.22), since $k\sim a^{-1}$ (Mounaix *et al.*, 1991).

Another suggested mechanism for halting collapse is the onset of higher-order nonlinearities not included in the Zakharov equations. These include second-harmonic responses arising from beats at $2\omega_p$, nonquasineutral effects occurring when ions lag behind electrons due to rapid evolution of the collapsing field, and other corrections of order $|\mathbf{E}|^4$ in Eqs. (2.17) and (2.18) (Vladimirov *et al.*, 1995). It is known that these nonlinearities do not contribute in the one-dimensional case, due to cancellations between the relevant terms (Khakimov and Tsytovich, 1976; Kuznetsov, 1976; Škorić and ter Haar, 1980; Malkin, 1986; Newman *et al.*, 1990; Vladimirov *et al.*, 1995). Newman *et al.* (1990) found that the predominantly one-dimensional character of the field near the center of a collapsing wave packet also gives rise to a near cancellation of these terms, with the result that higher-order nonlinearities are certainly not relevant for $W\lesssim 1$. Mounaix *et al.* (1991) found that there were further cancellations even in the multidimensional case, leading to Eq. (5.43) as the relevant criterion for the validity of the Zakharov equations in the absence of dissipation.

The ion response in Eq. (2.18) can give rise to unphysical negative densities if W is large enough. Newman *et al.* (1990) modified the ion response to prevent the development of such features, but found that this did not dramatically affect the evolution of the Langmuir waves in the high-W regime and certainly did not halt collapse. They found that the main source of discrepancies between the Zakharov equations and particle-in-cell simulations was localized heating due to dissipation during burnout (see above).

G. Relaxation and renucleation

The bulk of the Langmuir energy in a collapsing packet dissipates very near the time of arrest. As a result, the associated density well is no longer supported by the Langmuir ponderomotive force and it begins to dissipate and relax, essentially linearly. Ultimately, it re-

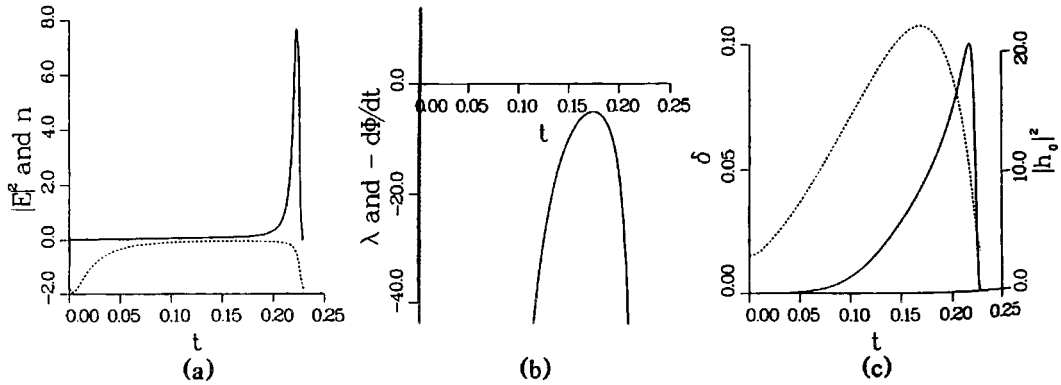

FIG. 20. Evolution of a scalar-field wave packet and associated density depression vs time, adapted from DuBois *et al.* (1988): (a) E^2 (solid) and n (dashed); (b) lowest eigenvalue; (c) squared amplitude $|h_0|^2$ (solid) and effective radius δ (dashed) of the ground state.

laxes back to the point where a trapped Langmuir eigenstate can again couple effectively to the driver and/or background turbulence and nucleate more energy. Such occurrences of renucleation have been found to account for the formation of most Langmuir wave packets that subsequently collapse provided the ion-sound-wave damping given by Eq. (2.6) is not too small (Doolen *et al.*, 1985; Russell *et al.*, 1988; Robinson *et al.*, 1988). If the ion-sound-wave damping is very small, the relaxing well can simply propagate away as a pulse of radiated ion sound waves (Russell *et al.*, 1988), in which case nucleation is either irrelevant or occurs in randomly formed density wells related to the random "hot spots" that initiate two-dimensional laser self-focusing into filaments in laser plasmas (Rose and DuBois, 1993a, 1993b). In most applications to date, however, the ion-sound-wave damping is strong enough that renucleation is the dominant mechanism of formation of localized coherent packets.

DuBois *et al.* (1988, 1990) and DuBois and Rose (1991) have studied the wave-packet cycle of nucleation, collapse, arrest and burnout, relaxation, and renucleation, using a scalar, spherically symmetric version of the Zakharov equations. The details are not the same as for the full vector equations, but the main features of the wave-packet cycle are as described above. Figure 20(a) shows the evolution of the central energy density $W(0,t)$ and density $n(0,t)$ vs time. At first, the density well is relaxing after a previous burnout and W is very small. Figure 20(b) shows that, during this time, the eigenfrequency of the lowest state rises steadily toward zero. Once the waves couple efficiently to the driver, W rises (in this case a clamp drive tuned to a small negative frequency was used). At the same point n levels off due to the increasing ponderomotive force that results. Around $t=0.18$ the collapse threshold is passed, n begins to decrease again, and the eigenfrequency again moves down as collapse proceeds. A short way into collapse, the packet effectively decouples from the driver due to frequency detuning (see Sec. V.C). Subsequently, free collapse ensues, with W and n increasing rapidly in magnitude until the point of arrest at $t\approx 0.22$. Figure 20(c) shows the decrease in the packet size and the increase in the amplitude of the localized ground state during collapse. After arrest, the energy density then drops precipitously during burnout, leaving an unsupported density well. The cycle then recommences (not shown).

VI. STRONG TURBULENCE

Section V concentrated on the physics of a single collapsing wave packet. In turbulent systems, such as those shown in Fig. 2, many such localized coherent packets are present, coexisting with propagating waves. The two types of waves are coupled via nonlinear interactions in the nucleation phase of the wave-packet cycle. In addition, the pump is coupled to one of the classes of waves, while dissipation is dominated by burnout of wave packets at arrest. This motivates a treatment in which the turbulence is treated as a two- or three-component system (see Sec. IV.C and Fig. 12) with the components linked via the decay cascade and/or nucleation. In this section it is shown that, once the rate of energy input from the driver and rate of dissipation from the coherent component are calculated, imposition of global power balance permits the steady-state scalings of many mean properties of the plasma to be calculated as functions of the driver strength or mean Langmuir energy density. Wave-collapse theory then yields statistical distributions and spectra of the fields. It should be noted that this few-component approach is not derived from a more fundamental statistical theory; however, as demonstrated below, it has shown excellent agreement with the results of numerical simulations.

Before discussing recent work on two- and three-component models of strong Langmuir turbulence, it is worth briefly considering earlier work along these lines. The earliest analyses of this type were one-dimensional studies of the undamped, undriven nonlinear Schrödinger equation using the inverse scattering transform (Zakharov and Shabat, 1971). These showed that an arbitrary initial state would evolve into a uniquely defined

sum of localized solitons and radiated plane waves—a neat two-component division. A similar picture of solutions of the undamped, undriven, 1D Zakharov equations was developed in the 1970s (Gibbons *et al.*, 1977; Thornhill and ter Haar, 1978). Pictures based on a driven, dissipative "soliton gas" in one or more dimensions were also developed around the same time or subsequently (Kingsep *et al.*, 1973; Galeev *et al.*, 1975, 1977a, 1977b; Degtyarev *et al.*, 1980; Pelletier, 1982; Shapiro and Shevchenko, 1984). However, the role of nucleation was not recognized in these analyses, and they usually assumed that all the energy initially in a collapsing wave packet is ultimately dissipated (strong collapse). An exception to the latter point was Zakharov's (1984) analysis, which allowed for the possibility of weak collapse in some regimes.

An alternative approach to the study of strong Langmuir turbulence has been via statistical closure methods based on the direct interaction approximation, first developed by Kraichnan (1959, 1964) for fluid turbulence. Despite significant progress, renormalization approaches have faced formidable difficulties for reasons such as the intermittent nature of Langmuir collapse (Pelletier, 1980a, 1980b; DuBois and Rose, 1981).

A. Power input and dissipation

Figures 12 and 13 show schematics of the energy flows in strong turbulence in block and spectral form, respectively. The first step in analyzing the statistical properties of turbulence is to calculate the rates at which power enters the system from the driver and the rate at which it is dissipated due to burnout.

1. Power input

The rate of power input depends on the type of driver. Here we consider two specific types.

A beam instability gives rise to wave growth at a rate $\Gamma(\mathbf{k}_b)$ at a wave number denoted $\mathbf{k}_b$ (in general, Γ will be positive over some small range of wave numbers $\Delta\mathbf{k}_b$ centered on $\mathbf{k}_b$). The rate of power input is then

$$P_{\rm in}=2\Gamma(\mathbf{k}_b)W(\mathbf{k}_b)|\Delta\mathbf{k}_b|, \tag{6.1}$$

where $|\Delta\mathbf{k}_b|$ is the volume occupied by the driven modes in k space. Two possibilities then present themselves: either the beam couples directly to the condensate near $k=0$ or the beam-driven waves decay via the electrostatic decay cascade. In the former case, there is no significant cascade component and $W(\mathbf{k}_b)\propto\langle W\rangle$, since the instability drives the condensate as a whole (Robinson and Newman, 1990a; Robinson, 1996a). In this case

$$P_{\rm in}\propto\Gamma(\mathbf{k}_b)\langle W\rangle. \tag{6.2}$$

When $k_b>k_*/2$ [see Eq. (3.5)], a decay cascade occurs, unless the driver is so strong, and $\Delta\mathbf{k}_b$ so small, that a direct modulational instability of the driven waves can occur under the criteria discussed in Sec. III.C, thereby truncating the cascade before it reaches $k=0$. In the cascade case, one has [see the discussion following Eq. (3.15)]

$$\Gamma_{\rm decay}\propto W(\mathbf{k_b}). \tag{6.3}$$

In the steady state $\Gamma(\mathbf{k}_b)=\Gamma_{\rm decay}$. Hence, in this case,

$$P_{\rm in}=2\Gamma(\mathbf{k}_b)^2|\Delta\mathbf{k}_b|, \tag{6.4}$$

since the number of modes involved is proportional to $|\Delta\mathbf{k}_b|$. If the driver is nearly monochromatic, coherent decay may occur, with Eq. (3.6) yielding

$$P_{\rm in}\propto\Gamma(\mathbf{k}_b)^3|\Delta\mathbf{k}_b|. \tag{6.5}$$

Note that, in the work presented here, we do not consider beam modifications to the dispersion of the Langmuir waves.

Beam driving is not the only possibility. In many laser-plasma and ionospheric-modification experiments, Langmuir waves are driven by a fixed-amplitude "clamp" field $\mathbf{E}_C$, as in Eqs. (5.17) and (5.18). In this case, if the driver is strong enough and its frequency is well above the plasma frequency, a parametric decay cascade can occur. In most relevant laser-plasma and ionospheric-modification experiments, the coherent decay rate in Eq. (3.6) is the relevant one, yielding

$$P_{\rm in}\propto\Gamma(k_C)^3\propto W(k_C)^{3/2}, \tag{6.6}$$

where k_C is the wave number of a freely propagating wave with $\omega=\omega_C$. For smaller values of the clamp strength and/or frequency, direct nucleation of wave packets can occur, with (DuBois *et al.*, 1990)

$$P_{\rm in}\propto E_C^3. \tag{6.7}$$

The cascade regime in Eq. (6.5), with k_b replaced by k_C, applies for a dimensionless clamp frequency

$$\omega_C>\Omega_{\rm crit}=\max[3/4,2E_C^2(2E_C^2+1)], \tag{6.8}$$

which defines $\Omega_{\rm crit}$ (Hanssen *et al.*, 1992). The first term on the right is the kinematic limit of the decay cascade where the wave number k_C resonant with the clamp satisfies $k_C=k_*/2$, while the second defines the regime in which the decay instability has a higher growth rate than the modulational instability. If the first criterion is fulfilled, but not the second, the waves can undergo direct modulational instability without first cascading to form a condensate.

2. Power dissipation

In the absence of significant damping at low k (see Robinson, Newman, and Rubenchik, 1992), power dissipation is dominated by the burnout phase at the end of collapse. The power dissipated is thus (Zakharov, 1984; Robinson and Newman, 1990a; Robinson, 1996a)

$$P_{\rm out}=N_P U/T, \tag{6.9}$$

where N_P is the number density of collapse sites, U is the energy dissipated at the end of collapse, and T is the characteristic time between collapses at a particular site.

The number density of collapse sites can be estimated from the characteristic length scales at the start of collapse, which is assumed here to begin in the subsonic regime. For direct modulational instability and collapse from near-monochromatic Langmuir waves of energy

density W, Eqs. (3.9) and (3.11) give $N_P \propto W^{D/2}$. In the case of nucleation, the characteristic separation between packets $\langle W\rangle^{-1/2}$ also determines the characteristic nucleation scale because energetic considerations favor close-packed wave packets with initial energy densities $W_i \approx \langle W\rangle$ (Robinson and Newman, 1990a; Robinson, 1996a; Robinson, Wouters, and Broderick, 1996). Briefly, the argument is that collapse is favored for small W_i because $n \sim -W_i$ at the collapse threshold and nucleation is most effective for small n (see Sec. V.C). However, W_i cannot be less than $\langle W\rangle$ or regions outside the nucleating wells would be favored to collapse. Typically, the central value of W_i is of order $5\langle W\rangle$ (Robinson and Newman, 1990a; Robinson, Wouters, and Broderick, 1996), with a typical value one scale length a from the center being $\approx\langle W\rangle$. This argument yields

$$N_P \propto \langle W\rangle^{D/2}. \tag{6.10}$$

By assuming that nucleating wave packets are close packed, Robinson, Wouters, and Broderick (1996) estimated their number density in D dimensions to be

$$N_P \approx \frac{\langle W\rangle^{D/2}}{(2\pi c_S^2 \lambda_D)^D D^{D/2}}, \tag{6.11}$$

where the factor 2π was obtained by requiring consistency with the results of Shen and Nicholson (1987) for the spacing between solitons in one dimension. The close-packed assumption was shown to minimize the collapse threshold, leading to a mean interpacket separation a little greater than $2a$, which compares well with the value of $\approx 3a$ obtained from numerical simulations by Robinson and Newman (1990a). It should be stressed that close packing does not contradict some experimental reports of a high-field "filling factor" of 1–10 percent; this factor refers to fields well above the rms value.

The scalings of Eq. (5.27) imply that the characteristic time of subsonic collapse is

$$T \propto \langle W\rangle^{-1}, \tag{6.12}$$

since $W \sim \langle W\rangle$ at threshold. Even if the collapse eventually becomes supersonic, the subsonic phase occupies most of the overall duration. Robinson (1996a) also showed that the collapse time dominates over the relaxation time, thus determining the overall interval between collapses at a given site (i.e., the characteristic period of the wave-packet cycle).

The energy dissipated at the end of collapse is (Robinson and Newman, 1990a)

$$U \approx W_f a_f^D N_e k_B T_e \propto \Theta a_f^{D-2} \lambda_D^2 N_e k_B T_e, \tag{6.13}$$

which is constant. Subsonic collapse has been assumed in Eq. (6.13), and the steep rise in transit-time dissipation with decreasing a means a_f is at most weakly dependent on W_i [see Eqs. (5.31) and (5.37)]. In two dimensions, collapse is strong and the energy dissipated is proportional to the initial energy in the collapsing packet. However, in three dimensions, subsonic collapse is weak and most of the energy is radiated during collapse, with only a fraction $\propto \langle W\rangle^{1/2}$ being dissipated. If a transition to strong supersonic collapse occurs at some scale a_t, the independence of $\langle W\rangle$ in Eq. (6.13) is unchanged (Robinson and Newman, 1990a).

Substitution of Eqs. (6.10), (6.12), and (6.13), into Eq. (6.9), with W replaced by $\langle W\rangle$ in Eq. (6.10), yields

$$P_{\rm out} \propto \langle W\rangle^{1+D/2}. \tag{6.14}$$

This result should be contrasted with the case in which strong collapse is assumed, seeded by modulational instability or nucleation. In that case, $P_{\rm out} \propto \langle W\rangle^2$ is predicted, independent of D. Studies of systems of different dimensionality are thus essential to distinguish between the two theories.

DuBois *et al.* (1990) argued that, in the case of a clamp drive that couples directly to nucleating states, $P_{\rm out}$ is modified to the form

$$P_{\rm out} \propto \langle W\rangle^{3/2}, \tag{6.15}$$

in three dimensions. It should be noted that DuBois *et al.*'s (1990) numerical simulations did not fully verify this and other scalings for clamp-driven turbulence [see Eqs. (6.33)–(6.36) below] and more work is needed in this area.

B. Scalings of averaged quantities

The evolution of the mean energy density obeys the equation

$$\frac{d\langle W\rangle}{dt} = P_{\rm in} - P_{\rm out}. \tag{6.16}$$

In the steady state, $P_{\rm in}$ is transferred to the system, reaching the collapsing packets either directly or via the cascade and/or condensate component(s), as shown in Figs. 12 and 13. It is then dissipated during burnout. By applying power balance $P_{\rm in} = P_{\rm out}$ in Eq. (6.16), one can calculate the mean levels of various quantities in steady-state turbulence. Alternatively, if $P_{\rm in} = 0$, the decay of undriven turbulence can be studied.

In this section attention is chiefly focused on the case in which the driver is of the instability type given in Eq. (6.2), coupled directly to the condensate with no intermediate cascade. Energy thus enters the condensate, is transferred to localized packets during nucleation, and is dissipated at burnout. This case has been the most extensively studied statistically to date, with detailed statistical properties derived and verified numerically by Robinson and Newman (1990a, 1990b, 1990c) and Robinson (1996a) in both two and three dimensions.

1. Langmuir energy density

In the steady state, Eqs. (6.2) and (6.14) imply

$$\langle W\rangle \propto \Gamma^{2/D} \tag{6.17}$$

(Robinson and Newman, 1990a). Likewise, for $P_{\rm in} = 0$ one finds (Robinson and Newman, 1990a)

$$\langle W\rangle \propto (t - t_0)^{-2/D}, \tag{6.18}$$

where t_0 is a constant.

Robinson and Newman (1990a) investigated the scalings predicted above using 2D and 3D simulations of the

TABLE I. Scalings in strong turbulence driven by a small-k instability. Predicted scalings $A \propto B^C$ vs numerical results in two and three dimensions, with subsonic scalings assumed during collapse (after Robinson and Newman, 1990a, 1990b). Notes: (1) steady state; (2) decay; (3) depends on high-k damping; (4) extra factor of $\ln(W_f/\langle W\rangle)$ in two dimensions; (5) a correction has been made to Robinson and Newman's (1990b) 2D result, based on the work of Robinson (1996a).

A	B	C (pred.)	C [a]	C [b]	Notes
$\langle W\rangle$	Γ	$2/D$	1.015 ± 0.025	0.664 ± 0.009	1
$\langle W\rangle$	$t-t_0$	$-2/D$	-0.99 ± 0.04	-0.71 ± 0.10	2
$P_{\rm out}$	$\langle W\rangle$	$(2+D)/2$	2.01 ± 0.04	2.41 ± 0.20	1
U	$\langle W\rangle$	0	0.06 ± 0.05	0.02 ± 0.07	1
N_P	$\langle W\rangle$	$D/2$	0.95 ± 0.09	1.60 ± 0.28	1
T	$\langle W\rangle$	-1	-1.00 ± 0.18	-0.8 ± 0.5	1
a_f	$\langle W\rangle$	≈0	-0.06 ± 0.014	0.018 ± 0.025	1,3
$\langle n^2\rangle$	$\langle W\rangle$	2	1.9 ± 0.1	1.91 ± 0.09	1,4,5

[a]Two-dimensional, numerical.
[b]Three-dimensional, numerical.

Zakharov equations with strong damping at high k to mimic the effects of transit-time dissipation. The form of the driver used was

$$\Gamma(\mathbf{k})=\Gamma(\mathbf{k}_b)\exp\left(-\frac{(k_x-k_b)^2}{2\Delta k_\parallel^2}-\frac{k_y^2+k_z^2}{2\Delta k_\perp^2}\right), \tag{6.19}$$

where $\mathbf{k}_b$ is assumed to be parallel to the x axis, without loss of generality, k_z is omitted in 2D cases, and $\Delta k_\parallel$ and $\Delta k_\perp$ are widths of the driver in the parallel (i.e., x) and perpendicular directions, respectively. This form can be used to approximate a beam driver, where $k_b=\omega_p/v_b$ for resonance with a beam of velocity v_b.

Using $\Delta k_\parallel=\Delta k_\perp=\Delta k$, $k_b=0$, and $c_S^2=1.6$, Robinson and Newman (1990a) found the results shown in the first 7 lines of Table I. The exponents are all consistent with the theoretical predictions above in both two and three dimensions. Figures 21(a) and 21(b) show results corresponding to the steady state and decay scalings of Eqs. (6.17) and (6.18), respectively.

In dimensional units, best fits to Robinson and Newman's (1990a) numerical results using the theoretical exponents are (Robinson and Newman, 1990c)

$$\langle W\rangle\approx300\frac{\Gamma(0)}{\omega_p}\left(\frac{\Delta k}{k_D}\right)^{0.57}, \tag{6.20}$$

$$P_{\rm out}\approx0.02\langle W\rangle^2 Nk_BT_e\omega_p, \tag{6.21}$$

$$U\approx160Nk_BT_e\lambda_D^2, \tag{6.22}$$

$$N_P\approx2\times10^{-3}\langle W\rangle\lambda_D^{-2}, \tag{6.23}$$

$$T\approx20\langle W\rangle^{-1}\omega_p^{-1}, \tag{6.24}$$

in two dimensions. Note that there is as yet no theoretical explanation of the exponent 0.57 in Eq. (6.20) or in Eq. (6.25) below, for the case $k_b\approx0$; unlike the case of large k_b, wave-wave couplings in the condensate modify the exponent substantially from the value of 1 that would apply in the large-k_b case. The values of U and N_P in Eqs. (6.22) and (6.23) are in semiquantitative agreement with the approximate theoretical results of Eqs. (5.23), (6.11), and (6.13).

In three dimensions, best fits to the simulation results are

$$\langle W\rangle\approx14\left(\frac{\Gamma(0)}{\omega_p}\right)^{2/3}\left(\frac{\Delta k}{k_D}\right)^{0.57}, \tag{6.25}$$

$$P_{\rm out}\approx0.2\langle W\rangle^{5/2}Nk_BT_e\omega_p, \tag{6.26}$$

$$U\approx9\times10^4Nk_BT_e\lambda_D^3, \tag{6.27}$$

$$N_P\approx1\times10^{-4}\langle W\rangle^{3/2}\lambda_D^{-3}, \tag{6.28}$$

$$T\approx40\langle W\rangle^{-1}\omega_p^{-1}. \tag{6.29}$$

Again, the values of U and N_P in Eqs. (6.27) and (6.28) are in semiquantitative agreement with theory.

2. Density fluctuations

Empirically, the mean-square level of density fluctuations in strong turbulence is dominated by contributions from density wells produced during wave collapse. It can be calculated by averaging n^2 over a wave-packet cycle, then multiplying by the number density of collapse sites N_P. Robinson and Newman (1990b) and Robinson (1996a) showed that this average is dominated by the collapse phase. Hence, if the subsonic scaling $n\propto-|\mathbf{E}|^2$ is used and the volume of the collapsing packet a^D is allowed for, one finds (Robinson and Newman, 1990b; Robinson, 1996a)

$$\langle n^2\rangle\propto\langle W\rangle^2 f(\langle W\rangle), \tag{6.30}$$

with $f(\langle W\rangle)=1$ for $D=3$ and $f(\langle W\rangle)=\ln(W_f/\langle W\rangle)$ for $D=2$, where W_f is the peak energy density at arrest. Here, variations in the arrest scale a_f with $\langle W\rangle$ have been ignored.

Robinson and Newman (1990b) studied the steady-state scalings of $\langle n^2\rangle$ using the same system as in the previous subsection. They found the scalings shown in the last line of Table I, in approximate agreement with theory. Figure 22 shows $\langle n^2\rangle$ vs $\langle W\rangle$ in three dimensions (Robinson and Newman, 1990b). The agreement with theory was improved if the weak variation of a_f with

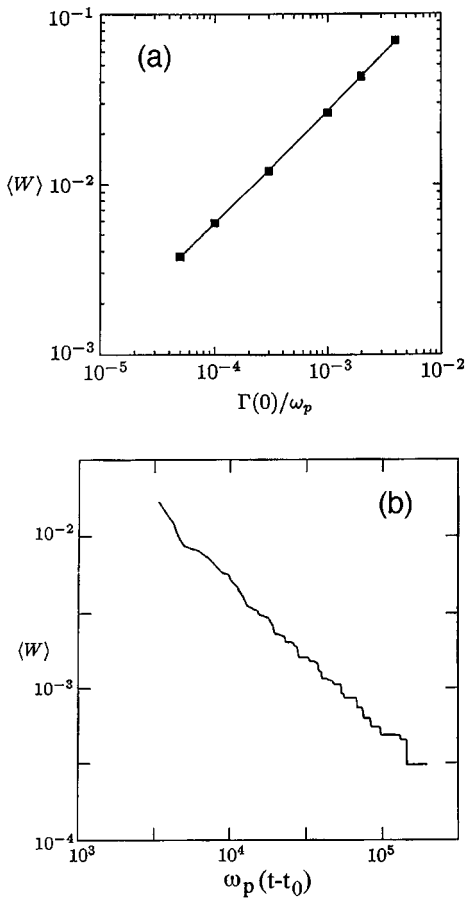

FIG. 21. Average energy density from simulations of strong turbulence (Robinson and Newman, 1990a): (a) steady-state $\langle W\rangle$ vs $\Gamma(0)$ from a three-dimensional system driven with $\mathbf{k}_b=0$; (b) the decay of $\langle W\rangle$ with time in a two-dimensional system in the absence of driving. The steplike features represent rapid loss of energy during burnouts of individual wave packets.

$\langle W\rangle$ was incorporated; however, since this variation depends on the form of the high-k damping, we do not consider it here. The best dimensional fits to Robinson and Newman's (1990b) results, with the theoretical exponents, are

$$\langle(\delta N_e)^2\rangle \approx 0.3\langle W\rangle^2 \ln(W_f/\langle W\rangle)N_e^2 \tag{6.31}$$

in two dimensions for $W_f \approx 0.3$ and

$$\langle(\delta N_e)^2\rangle \approx 0.4\langle W\rangle^2 N_e^2 \tag{6.32}$$

in three dimensions.

3. Beam-driven turbulence

The case of turbulence driven by a beam instability with $k_b > k_*/2$ has been studied numerically by Weatherall *et al.* (1983) and Robinson and Newman (1989, 1990a). Their results in two dimensions confirmed the theoretical scaling $\langle W\rangle \propto \Gamma(\mathbf{k}_b)\Delta k$, obtained from Eqs. (6.4) and (6.14) in the steady state (Robinson and Newman, 1990a), but 3D simulations of this regime have not been performed.

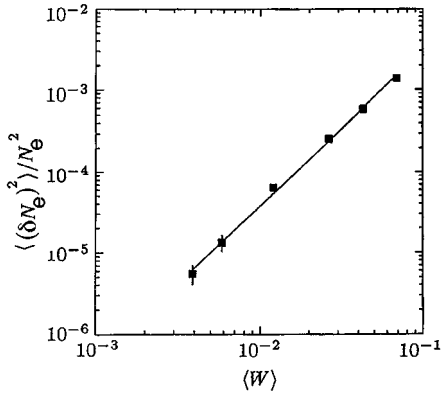

FIG. 22. Scaling of $\langle n^2\rangle$ with $\langle W\rangle$ in simulations of steady-state, three-dimensional Langmuir turbulence (Robinson and Newman, 1990b).

4. Clamp-driven turbulence

DuBois *et al.* (1990) studied the nucleation cycle for a scalar-field 3D model of turbulence in which nucleating packets couple directly to a clamp driver of the form introduced in Eqs. (5.17) and (5.18). They found the results contained in Eqs. (6.7) and (6.15) for $P_{\rm in}$ and $P_{\rm out}$ in the case in which the density wells survive long enough to renucleate further collapses. These results yielded scalings approximately of the form

$$\langle W\rangle \propto E_C^2, \tag{6.33}$$

$$P_{\rm out} \propto E_C^3 \propto \langle W\rangle^{3/2}, \tag{6.34}$$

$$N_P \propto E_C^3 \propto \langle W\rangle^{3/2}, \tag{6.35}$$

$$T \propto E_C^{-1} \propto \langle W\rangle^{-1/2}, \tag{6.36}$$

in three dimensions. The scaling of the nucleation time T is different from the case of pumping via a plasma instability and results in corresponding modifications to the scalings of $P_{\rm out}$ and $\langle W\rangle$. In numerical simulations of the scalar Zakharov equations, DuBois *et al.* (1990) found reasonable agreement with Eqs. (6.35) and (6.36), but their contradictory result $P_{\rm out} \propto E_C^2$ and a lack of power-law behavior in some regimes implies that more work is needed in this area. In particular, verification against simulations of vector-field turbulence would be desirable.

C. Probability distribution of electric-field strengths and density fluctuations

In a few-component model, knowledge of the temporal evolution of collapsing packets can be used to calculate the statistical distributions of large Langmuir field strengths and density fluctuations. At low values of $|\mathbf{E}|$ and n, the corresponding quantities can be calculated from linear wave theory. In this section, we deal for simplicity with the case of turbulence driven by a plasma instability near $k_b=0$ to eliminate the need to consider a decay-cascade component.

1. Electric-field strengths

In two-component turbulence, fields well below $\langle W\rangle^{1/2}$ in magnitude are primarily due to incoherent

TABLE II. Scalings in steady-state strong turbulence driven by a small-k instability. Predicted subsonic scalings $A \propto B^C$ vs numerical results in two and three dimensions (after Robinson and Newman, 1990a). Notes: (1) low E; (2) inertial range; (3) high-k tail.

A	B	C (pred.)	C [a]	C [b]	Notes
$P(E)$	E	$2D-1$	2.85 ± 0.24	5.0 ± 0.5	1
$P(E)$	E	$-(D+2)$	-3.89 ± 0.11	-5.12 ± 0.18	2
$P(n)$	n	$-(D+3)/2$	-2.48 ± 0.11	$-(2.6+)$	2,3
$W(k)$	$\langle W\rangle$	$(2+D)/2$	2.04 ± 0.14	2.39 ± 0.17	3
$W(k)$	k	$-2D$	-4.1 ± 0.3	...	2
$\lvert n(k)\rvert^2$	$\langle W\rangle$	$(2+D)/2$	2.04 ± 0.14	2.41 ± 0.11	3
$\lvert n(k)\rvert^2$	k	$2-2D$	-1.86 ± 0.19	$-(4.1\pm0.3)$	2,3

[a]Two-dimensional, numerical.
[b]Three-dimensional, numerical.

waves, while higher fields are chiefly found within collapsing wave packets. A useful diagnostic of such turbulence is the probability distribution $P(E)$, with $E=|\mathbf{E}|$. For $E\ll\langle W\rangle^{1/2}$, $P(E)$ can be found by noting that in isotropic turbulence, the real and imaginary parts of the D components of $\mathbf{E}$ are identically distributed. If each component has a distribution that peaks at zero field, one immediately finds (Robinson and Newman, 1990a)

$$P(E)\propto E^{2D-1}. \tag{6.37}$$

For $E\gg\langle W\rangle^{1/2}$, $P(E)$ is obtained by averaging over collapse, with appropriate weightings for the size of the wave packet [$\sim a^D\sim(t_c-t)^{\chi D}$], and the time it spends at each characteristic central field strength ($\sim|dt/dE_0|$). This gives (Robinson and Newman, 1990a; Robinson, 1996a)

$$P(E)\propto\int_0^{t_c}P(E,t)dt, \tag{6.38}$$

$$\propto\int_0^{\infty}v^{-2}g(v)a^D\left|\frac{dt}{dE_0}\right|dv, \tag{6.39}$$

where E_0 is the central field, $v=E/E_0(t)$, and $g(v)$ is a function that depends on the self-similar profile of the packet. The factor v^{-2} in Eq. (6.39) arises from the change of variable from t to v, and the bounds have been extended to 0 and ∞ in Eq. (6.39), which is a reasonable approximation in the inertial range $\langle W\rangle\ll W\ll1$ where the packet collapses freely. The scalings in Eqs. (5.24) and (5.27) then give

$$P(E)\propto E^{-(D+2)}, \tag{6.40}$$

for subsonic collapse. At the very highest fields, at and above the arrest level, $P(E)$ is chiefly determined by the statistical distribution of energies U [cf. Eq. (6.13)], which does not have a unique value for packets collapsing amid turbulence. The central limit theorem implies that this distribution will be approximately Gaussian, with

$$P(E)\propto\exp(-E^2/2E_{f0}^2), \tag{6.41}$$

$$\frac{\epsilon_0E_{f0}^2}{2N_ek_BT_e}\approx\frac{2\Theta\lambda_D^2}{a_f^2}\approx\frac{\Theta}{200}\sim1 \tag{6.42}$$

(Robinson and Newman, 1990c). Note that the distribution of U only manifests itself in the inertial range as a scatter about the mean behavior, without changing the scalings derived above.

Robinson and Newman (1990a) found $P(E)$ from Zakharov-equation simulations of strong turbulence driven at $k=0$, as described in Sec. VI.B. They found the results shown in the first two lines of Table II, consistent with Eqs. (6.37) and (6.40) for subsonic collapse. Note that their results ruled out supersonic collapse in three dimensions, at least for $W\lesssim1$, because the numerically determined exponent was inconsistent with the supersonic analog of Eq. (6.40). At the highest E their results were also consistent with Eq. (6.41), although the statistics were not well determined. Figure 23 shows $P(E)$ vs E for a series of 2D simulations with varying $\Gamma(0)$. In each case, the distribution peaks close to $\langle W\rangle^{1/2}$ and takes on its asymptotic forms (linear segments in this figure) within a factor of ~2 above or below this point. This implies that the low- and high-E components are fairly sharply separated, as assumed in the analytic model. It also implies that the initial energy density in a collapsing packet satisfies $W_i\lesssim4\langle W\rangle$, con-

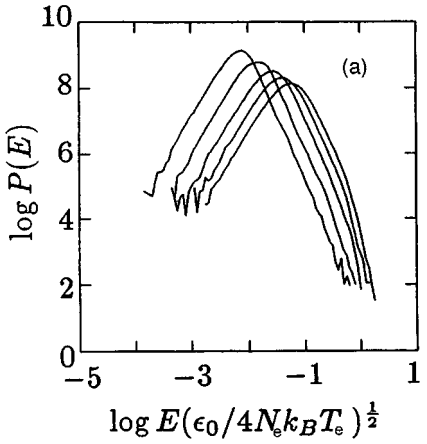

FIG. 23. Electric-field distributions from two-dimensional simulations of strong Langmuir turbulence (Robinson and Newman, 1990a). Values of the growth rate $\Gamma(0)$ are, from left to right, $5\times10^{-5}\omega_p$, $10^{-4}\omega_p$, $2\times10^{-4}\omega_p$, $5\times10^{-4}\omega_p$, and $10^{-3}\omega_p$.

sistent with the discussion in Sec. VI.A.

The scalings derived above can be used to obtain an estimate of the crossover point from subsonic to supersonic collapse. The scaling in Eq. (6.24), with $T \approx t_c$, implies $\omega_p t_c \approx 100/W_i$ in two dimensions. Using the definition $\Theta = W_i a_i^2/\lambda_D^2$, with $\Theta \approx 150$, we find $\omega_p t_c \approx a_i^2/\lambda_D^2$. Hence $a \approx [\omega_p(t_c - t)]^{1/2}\lambda_D$ in the subsonic regime. If we assume that the crossover to supersonic collapse occurs where $|da/dt| = v_S$, we then find $a \approx (m_i/4m_e)^{1/2}\lambda_D \approx 20\lambda_D$ and $W \approx 4\Theta m_e/m_i \approx 0.2$–$0.5$ at the crossover. The corresponding calculation in three dimensions yields the same result. These results imply that crossover does not occur until W and a are near their values at arrest, i.e., well above the simple estimate of $W \approx m_e/m_i$.

2. Density fluctuations

Averaging of the volume-weighted (negative) density response over collapse gives a scaling in the inertial range of

$$P(n) \propto (-n)^{-(D+3)/2}, \tag{6.43}$$

for subsonic collapse (Robinson and Newman, 1990b). The third line in Table II shows that Robinson and Newman's (1990b) numerical results were consistent with this prediction, although they were not conclusive in three dimensions.

D. Wave-number spectra of Langmuir waves and density fluctuations: instability-driven case

In this section, the power spectra of electric fields and density fluctuations are calculated in the inertial range for cases in which there is no cascade. Above and below the inertial range of k, the spectra depend sensitively on the precise forms of the collapsing packets and the incoherent turbulence, respectively. When cascade is important, the spectrum of this component must also be added.

1. Electric-field spectra

The Langmuir power spectrum $W(k) = \langle |\mathbf{E}(k)|^2 \rangle$ of an ensemble of collapsing wave packets is obtained by averaging the instantaneous power spectrum of the self-similar solution [Eq. (5.24)] over collapse:

$$W(k) = \frac{1}{t_c}\int_0^{t_c} N a^D W_i(ka/a_i)\,dt. \tag{6.44}$$

Here, W_i is the initial spectrum of a collapsing packet, rescaled to allow for self-similar contraction during collapse, and N is the total number of quanta given in Eq. (2.30). More precisely, W_i is the mean initial spectrum of the ensemble of collapsing packets. The factor Na^D allows for changes in the energy content in the packet during collapse and the spreading of the packet energy over an increasing k-space volume. This yields (Robinson and Newman, 1990a)

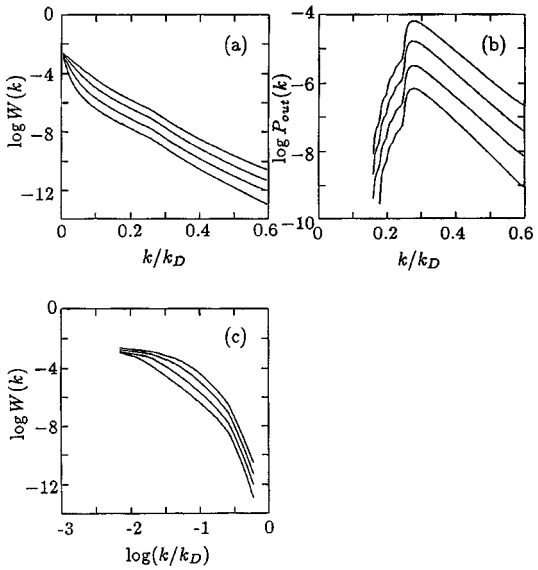

FIG. 24. Langmuir spectra and dissipation spectra from two-dimensional simulations of strong Langmuir turbulence (Robinson and Newman, 1990a). The driving instability growth rates are, from bottom to top, $10^{-4}\omega_p$, $2\times10^{-4}\omega_p$, $5\times10^{-4}\omega_p$, and $10^{-3}\omega_p$. (a) spectrum $W(k)$ vs k; (b) dissipation spectrum $2\gamma(k)W(k)$, showing the exponential tail predicted by Eqs. (6.47) and (6.48); (c) spectrum $W(k)$ vs k (log-log scale), showing the inertial range as a straight segment at intermediate k in each case.

$$W(k) \propto k^{-2D}\int_{ka_f}^{ka_i} u^{2D-1} W_i(u/l_i) \tag{6.45}$$

$$\propto \langle W \rangle^{1+D/2} k^{-2D} \tag{6.46}$$

for subsonic collapse, where the bounds in Eq. (6.45) have been extended to 0 and ∞ in obtaining Eq. (6.46), a reasonable approximation in the inertial range $1/a_i \ll k \ll 1/a_f$. The prediction of Eq. (6.46) contradicts some earlier theoretical scalings, but is confirmed by numerical results (see below).

At the highest k, the spectrum is determined by the form of the shortest-scale, highest-field packets at the point of arrest, the rate per unit volume R at which collapsing packets form ($\propto P_{\rm out}$ in the case considered here), and the damping rate. The steady-state dissipation spectrum is given by

$$P_{\rm out}(k) \propto R W_f(k), \tag{6.47}$$

where W_f is the spectrum of a packet at the arrest scale. Fourier-transforming the "standard" packet, given by Eqs. (5.4) and (5.10) with $a_{00} = 0$, then yields

$$W(k) \propto \langle W \rangle^{1+D/2} \exp(-2ka_f)/\gamma_L(k). \tag{6.48}$$

Robinson and Newman's (1990a) numerical results for the scalings of $W(k)$ and $P_{\rm out}(k)$ were consistent with Eqs. (6.46)–(6.48), as shown in Table II and Fig. 24. In particular, Figs. 24(b) and 24(c) show the exponential dependence of the dissipation spectrum and the power-law behavior of $W(k)$ in the inertial range, respectively. Fits of the exponent in Eq. (6.48) to numerical results

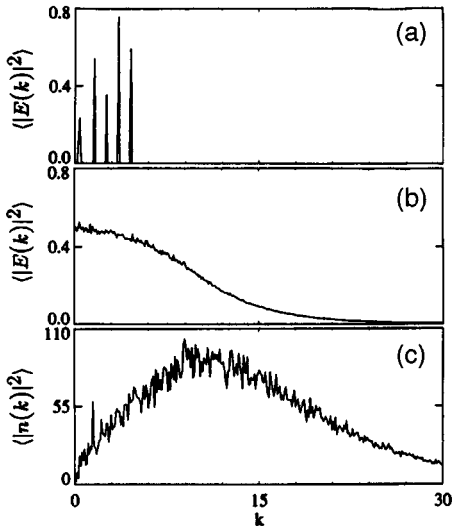

FIG. 25. Spectra from clamp-driven turbulence with $\omega_C<\Omega_{\rm crit}$ (Hanssen *et al.*, 1992). Axes are labeled with dimensionless units: (a) weak-turbulence spectrum $W(k)$; (b) strong-turbulence spectrum $W(k)$ from simulations using the Zakharov equations; (c) density spectrum $\langle|n(k)|^2\rangle$ corresponding to (b).

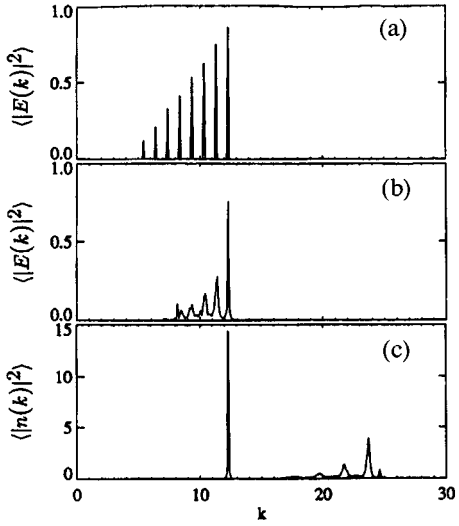

FIG. 26. Spectra from clamp-driven turbulence with $\omega_C>\Omega_{\rm crit}$ (Hanssen *et al.*, 1992). Axes are labeled with dimensionless units: (a) weak-turbulence spectrum $W(k)$; (b) strong-turbulence spectrum $W(k)$ from simulations using the Zakharov equations; (c) density spectrum $\langle|n(k)|^2\rangle$ corresponding to (b).

were used by Robinson and Newman (1990a) to determine the mean arrest scale a_f in their simulations.

2. Density-fluctuation spectra

Power spectra of density fluctuations can be obtained by procedures similar to those for Langmuir spectra. This yields (Robinson and Newman, 1990b; Robinson, 1996a)

$$|n(k)|^2\propto\langle W\rangle^{1+D/2}k^{2-2D} \tag{6.49}$$

in the inertial range for subsonic collapse. Table II shows that this result was confirmed by Robinson and Newman's (1990b) numerical simulations.

E. Spectra of Langmuir waves and density fluctuations: clamp-driven case

This section reviews recent work on the structure of spectra in the case of strong turbulence driven by clamp-type drivers, which are important in ionospheric-modification and laser-plasma experiments (DuBois *et al.*, 1990; DuBois *et al.*, 1991; DuBois and Rose, 1991; Hanssen *et al.*, 1992; DuBois *et al.*, 1993a, 1993b).

1. Wave-number spectra

The criterion $\omega_C<\Omega_{\rm crit}$ [see Eq. (6.8)] for the prevalence of nucleation has been explored by Hanssen *et al.* (1992) and DuBois *et al.* (1993a, 1993b) using simulations of the Zakharov equations with a clamp driver. Figure 25(b) shows an electric-field spectrum for a case with $\omega_C<\Omega_{\rm crit}$ in Eq. (6.8), showing a broad low-k condensate, but no evidence of the decay peaks seen in the corresponding weak-turbulence spectrum of Fig. 25(a). Figure 25(c) shows the corresponding density spectrum, which is broad and essentially featureless. Figure 26 shows weak turbulence and Zakharov-equation Langmuir spectra for a case with $\omega_C>\Omega_{\rm crit}$, showing a truncated decay cascade in the Zakharov case (Hanssen *et al.*, 1992). This truncation may be due to modulational instability of the propagating waves at the lower end of the cascade, enhanced damping due to scattering off enhanced short-wavelength density fluctuations, or direct nucleation from the bottom end of the observed cascade (Hanssen *et al.*, 1992). The precise truncation mechanism is not fully understood and its nature may affect the scaling properties of strong turbulence in this regime. The density spectrum in Fig. 26(c) shows a peak at k_C due to beating between the driven free modes and the uniform pump [cf. Eq. (5.18)] plus peaks just below $2k_C$ corresponding to ion sound waves generated in the decay cascade [cf. Eq. (3.7)].

2. Frequency spectra

One of the key predictions of strong-turbulence theory is that a substantial fraction of the Langmuir energy should be trapped in localized states with frequencies below the mean plasma frequency (Doolen *et al.*, 1985). Cheung *et al.* (1989, 1992), DuBois *et al.* (1990), and DuBois and Rose (1991), obtained frequency spectra at fixed $\mathbf{k}$ from 2D Zakharov simulations of clamp-driven turbulence, with $\omega_C>0$ (dimensionless frequencies are measured relative to the mean plasma frequency). Such spectra, shown in Fig. 27, correspond to those of waves on vertical cuts through Fig. 13(a) at fixed k, with Fig. 27(a) having lower ω_C and k_C than Fig. 27(b). They exhibit a "free-mode" peak at $\omega=k^2$ (in dimensionless units), due to propagating linear waves. For $\omega\lesssim 0$, there is also a broad feature that corresponds

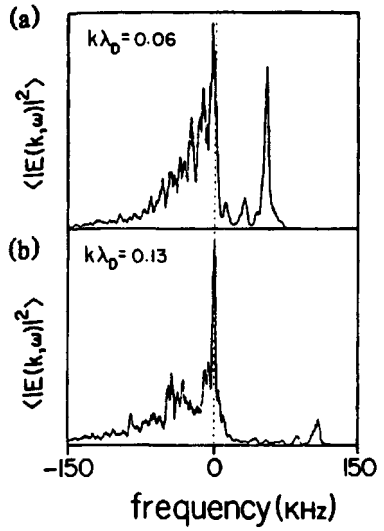

FIG. 27. Frequency spectra at fixed **k** from simulations of clamp-driven strong Langmuir turbulence with $\omega_C - \omega_p = 1.7 \times 10^{-3} \omega_p$ (Cheung *et al.*, 1989). Frequencies are measured relative to the heater frequency: (a) $k\lambda_D = 0.06$; (b) $k\lambda_D = 0.13$.

to the energy in collapsing wave packets with negative eigenfrequencies, although the discrete structure seen in Fig. 13(a) is smoothed out by averaging over many packets or over time for a single packet. Such features are also seen in simplified, scalar models of nucleation and collapse (DuBois *et al.*, 1988, 1990). The shape and scaling of the part of the spectrum with $\omega < 0$ can be calculated analytically from collapse scalings and the scaling of mean quantities in the steady state. DuBois *et al.* (1990), using their self-similar scalings, found that the spectrum behaves as $|\omega|^{-(1+3D/4)}$. Analytic calculations of the scalings of the free-mode energy in this context do not appear to have been undertaken.

VII. NUMERICAL SIMULATIONS OF WAVE COLLAPSE AND STRONG TURBULENCE

In the preceding sections, many numerical results have been cited in support of the theoretical concepts discussed. Indeed, historically, numerical calculations prompted many of the theoretical insights that have taken place. This section briefly reviews some of the main computational developments in the field of wave collapse and strong turbulence, including simulations based on the Zakharov and nonlinear Schrödinger equations, Vlasov simulations, and particle-in-cell methods, but not weak-turbulence simulations. It is not intended to provide a comprehensive review of all simulations that have been undertaken, nor is it a guide to numerical methods for carrying out such calculations.

A. Nonlinear Schrödinger and Zakharov simulations

In one dimension the initial-value problem for the undriven, undamped nonlinear Schrödinger equation can be solved analytically, via the inverse scattering transform, in terms of a superposition of solitons and plane waves (Zakharov and Shabat, 1971; Thornhill and ter Haar, 1978; Bullough and Caudrey, 1980). Likewise, 1D solutions of the Zakharov equations can be expressed in terms of a superposition of solitons and plane waves (Gibbons *et al.*, 1977; Thornhill and ter Haar, 1978). However, in 2D or 3D systems, or when driving and dissipation are introduced, such solutions are no longer possible and numerical methods are required.

The nonlinear Schrödinger equation (2.20) and the Zakharov equations (2.17) and (2.18) can be solved by finite-difference or spectral methods. One common approach is to Fourier-transform the spatial coordinates and work in k space, integrating the mode amplitudes forward in time using a leapfrog or predictor-corrector method (see Robinson and Newman, 1989, or DuBois *et al.*, 1990, for more details). This corresponds to solving the equations with periodic boundary conditions, but this constraint does not pose a problem so long as the overall system size is much greater than that of the phenomena being studied.

There are several advantages to numerical solutions of the Zakharov equations or the nonlinear Schrödinger equation: (i) In D dimensions, the size of the computational grids scales as N^D, where N is the number of grid points in each dimension. This contrasts with Vlasov simulations, where the scaling is N^{2D}, or N^{D+D_v} if D spatial dimensions and D_v components of the velocity are followed. (ii) The fast time scales ($\sim \omega_p^{-1}$) have been factored out, so large time steps $\sim \omega_p^{-1}$ can be taken if a high-accuracy time-stepping routine is used (Robinson and Newman, 1989). (iii) It is easy to incorporate arbitrary wave dispersion and k-dependent damping operators in the spectral formulation. (iv) The nonlinear terms are easily evaluated by transforming to coordinate space, multiplying the relevant terms, then transforming back. (v) Instability and clamp drivers can be straightforwardly included.

The primary disadvantage of numerical solutions of the Zakharov equations is that they incorporate all the approximations inherent in the Zakharov equations themselves, and it is not possible to test the validity of these approximations by such simulations. As a consequence, dissipation is included only approximately. Wave amplitudes are also limited to $W \lesssim 1$ to avoid density perturbations attaining unphysical negative values during strong wave collapses and because localized heating modifies the evolution near arrest otherwise. Also, the Zakharov equations do not incorporate kinetic effects, except in an *ad hoc* way via the damping operators. Some straightforward improvements to the standard Zakharov equations can be made, although we do not consider them in detail here. These include, modifying the density response to avoid unphysical negative densities (Newman *et al.*, 1990), and, more accurately incorporating kinetic effects into the ion response (Hammett and Perkins, 1990; Goldman *et al.*, 1993; DuBois *et al.*, 1995a), using multipole approximations to the

plasma dispersion functions that determine the dispersion of the waves (Robinson and Newman, 1988, and the references therein).

The first numerical solutions of the nonlinear Schrödinger equation were concerned with problems of time-independent axisymmetric self-focusing of lasers in nonlinear optical media in which the problem was reduced to a 1D calculation by symmetry (Kelley, 1965; Zakharov *et al.*, 1971; Dyshko *et al.*, 1972). Likewise, early solutions of the nonlinear Schrödinger equation or Zakharov equations in plasma contexts concentrated on demonstrating the existence and self-similar scalings of wave collapse by assuming spherical symmetry to reduce the dimensionality of the problem (e.g., Budneva *et al.*, 1975; Degtyarev *et al.*, 1975; Zakharov and Shur, 1981).

One-dimensional simulations of the Zakharov equations have also been used to study strong turbulence. First, this approach made it possible for the interaction of many solitonlike packets to be easily followed (Pereira *et al.*, 1977a) and allowed the differences between the nonlinear Schrödinger equation and Zakharov solutions to be explored (Shen and Nicholson, 1987). Second, driving and dissipation were incorporated into the basic equations to study forms of turbulence in the absence of true collapse (Pereira *et al.*, 1977a; Degtyarev *et al.*, 1980; Payne *et al.*, 1984; Doolen *et al.*, 1985). Restriction to one dimension also allowed particle acceleration in the turbulent state to be studied via an equation for the evolution of the electron distribution (Degtyarev *et al.*, 1979; 1980). Third, higher-order nonlinearities $n \propto -|\mathbf{E}|^{2m}$, with $m>1$, have been used in 1D simulations of turbulence to precipitate collapse. [Collapse occurs for $D \geqslant 2/m$ in general (Kuznetsov *et al.*, 1986; Pelletier, 1987; Zakharov, Kosmatov, and Shvets, 1989).] This approach permitted many features of strong turbulence to be elucidated, including the nucleation mechanism for the formation of coherent wave packets (Doolen *et al.*, 1985; Russell *et al.*, 1986).

Although 1D simulations enable one to study many features of wave collapse and strong turbulence, they omit much of the relevant physics. In particular, two-dimensional simulations are the smallest in which the standard Zakharov nonlinearity ($m=1$ in the previous paragraph) gives rise to true collapse.

The earliest 2D simulations of the Zakharov equations were concerned with demonstrating the existence of 2D and axisymmetric 3D wave collapse and studying their properties (Degtyarev *et al.*, 1975, 1976; Galeev *et al.*, 1975; Pereira *et al.*, 1977b). With the availability of steadily increasing computing power, subsequent work concentrated more on damped/driven turbulence, with energy input from plasma instabilities (Nicholson and Goldman, 1978; Nicholson *et al.*, 1978; Hafizi *et al.*, 1982; Weatherall *et al.*, 1983; Robinson and Newman, 1989, 1990a, 1990b, 1990c; Robinson, Newman, and Rubenchik, 1992), or clamp fields (Pereira *et al.*, 1977a, 1977b; Degtyarev *et al.*, 1984, 1989; DuBois *et al.*, 1988, 1990, 1991; Russell *et al.*, 1988; Degtyarev *et al.*, 1989; DuBois and Rose, 1991; Hanssen *et al.*, 1992; DuBois *et al.*, 1993a, 1993b). Because they embody the most essential physical effects and can be run on relatively large grids, 2D simulations have provided the most insight into wave collapse and strong turbulence over the last two decades. For example, they have demonstrated the scalings of 2D collapse, multidimensional nucleation, the two- or three-component nature of strong turbulence (see Fig. 12), the prevalence of localized states within the standard Zakharov equations, and the coexistence of weak and strong turbulence. They have also been extremely useful in applications to optics, auroral and space physics, and ionospheric-modification, laser-plasma, and beam-plasma experiments, as discussed in Secs. VIII and IX.

Despite the utility of 2D simulations, some aspects of nonlinear wave physics only manifest themselves in a fully three-dimensional geometry. For example, the D dependence of the exponents in Tables I and II can only be tested by carrying out simulations in both two and three dimensions. Also, fully three-dimensional simulations, without assumed symmetries, are necessary to test the scalings of wave collapse fully.

The first fully three-dimensional simulations using the Zakharov equations were carried out by Robinson *et al.* (1988) and Newman *et al.* (1989), whose results supported the two-component model, the nucleation scenario, and the usefulness of the spherical-harmonic decomposition of localized wave packets found in turbulence. Their work used the spectral code described in greatest detail by Robinson and Newman (1989). Using grids of up to 256^2 or 64^3 points, Robinson and Newman (1990a, 1990b, 1990c, 1991) and Newman and Robinson (1991) carried out detailed statistical studies of 2D and 3D instability-driven turbulence, establishing the validity of the scalings in Tables I and II and applying the results to beam-plasma experiments (see Sec. VIII.B).

B. Particle-in-cell simulations

In particle-in-cell (PIC) simulations, the trajectories of large numbers of electrons and ions (typically 10^4 to 10^6) are followed computationally, using forces computed from the fields due to the particle charges and currents themselves (Dawson, 1983; Birdsall and Langdon, 1985). To reduce noise and increase computational speed, the fields are computed on a grid and the particles are smoothed out over a finite spatial region. PIC simulations have the major advantages that (i) they make no small-parameter assumptions and can thus be used to check the validity of the Zakharov equations or other approximations, (ii) they incorporate kinetic effects automatically, which are only included in an *ad hoc* way in treatments based on the fluid equations, and (iii) the size of the grids involved scales as N^D in D dimensions. The chief disadvantages are that very large numbers of grid points and particles are required to model significant plasma volumes and to reduce statistical noise to acceptable levels, and that short time steps must be taken to follow individual oscillations at the plasma frequency. Currently, these considerations limit the applicability of PIC methods to study of single collapsing

wave packets—turbulence cannot be studied except in one-dimensional cases, where true collapse does not exist.

Pereira *et al.* (1977a), Anisimov *et al.* (1982, 1983), D'yachenko *et al.* (1988), Zakharov, Pushkarev, Rubenchik, Sagdeev, and Shvets (1988, 1989), and Zakharov, Pushkarev, Sagdeev, Solov'ev, Shapiro, Shvets, and Shevchenko (1989) carried out PIC simulations of 1D turbulence, and 2D and 3D wave collapse, invoking fourfold and eightfold symmetries to render tractable the 2D and 3D cases, respectively. Even so, the latter authors employed 800 000 particles in two dimensions and 1.8 million in three dimensions. They found that dissipation of the fields via interactions with electrons was the primary arrest mechanism and studied the resulting accelerated electron distribution. They obtained arrest scales of $\sim 10\lambda_D$ in two dimensions and $\sim 15\lambda_D$ in three dimensions, consistent with the values and trend with D predicted by transit-time dissipation theory (Robinson, 1991; Sec. V.F). Newman *et al.* (1990) explored the validity of the Zakharov equations by comparing Zakharov-equation simulations of wave collapse with 2D particle-in-cell simulations of the same situations. They confirmed arrest by transit-time damping at a scale of $(10–15)\lambda_D$, consistent with previous work, without invoking fourfold symmetries, and showed that the Zakharov equations remain valid for $W \lesssim 1$ (see Secs. II.B and V.F). They also found that localized heating in the core of a wave packet is the primary cause of discrepancies between the particle-in-cell and Zakharov-equation results for $W \approx 1$, consistent with the earlier results. In the context of ionospheric-modification experiments, Clark *et al.* (1992) showed that a 1D hybrid model, with electrons followed using the Zakharov equations and ions via PIC methods, gives essentially the same results as the Zakharov equations for turbulence.

C. Vlasov simulations

One-dimensional strong-turbulence and modulational instability have been studied using the coupled Vlasov-Poisson equations (Rowland, 1980, 1988; Wang *et al.*, 1994, 1995, 1996). This method involves solving the Vlasov equations for the time-dependent electron distribution function in velocity and space, subject to electric fields generated as a result of charge imbalances between the ion and electron components (Cheng and Knorr, 1976). The ions were followed using fluid equations. Major advantages of such hybrid Vlasov-fluid simulations are that they avoid the noise associated with particle-in-cell methods and most of the assumptions inherent in Zakharov equations. The chief disadvantage, numerically, is that the size of the grids involved scales as N^{2D}, where N is the number of points followed in each space and velocity dimension. It is this feature that has limited Vlasov simulations to date to one dimension.

Rowland (1980, 1988) investigated beam-plasma interactions in one dimension using the Vlasov equations for both electrons and ions. He showed that modulational instabilities can saturate the beam instability and heat ambient electrons to form a superthermal tail extending toward the beam in velocity space.

Wang *et al.* (1994, 1996) compared clamp-driven 1D Langmuir turbulence simulated with the Vlasov-fluid and Zakharov equations. They studied the formation of hot electron tails in the Vlasov case and found that localized wave packets emit "jets" of accelerated particles in phase space, as seen in particle-in-cell simulations (Zakharov, Pushkarev, Rubenchik, Sagdeev, and Shvets, 1989; Newman *et al.*, 1990) and as predicted by transit-time arrest theory (Robinson, 1991). As in the PIC simulations (Newman *et al.*, 1990), particle heating was found to be the main cause of differences between the Vlasov-fluid and Zakharov-equation simulations, with up to 200% local changes in T_e. Wang *et al.* (1995) also studied one-dimensional modulational instabilities that led to self-focusing into localized dissipative structures, and nucleation in the residual density wells remaining after burnout of such structures. Being one dimensional, these dissipative structures did not undergo true collapse.

In a complementary development, Helmerson and Mjølhus (1994) carried out 1D simulations using the first Zakharov equation to track the electrons and the Vlasov equation for the ions. They compared the results for parametric instabilities, strong turbulence, and nucleation with the Zakharov equations, finding good qualitative agreement.

VIII. EXPERIMENTAL APPLICATIONS

The first experiments on self-focusing were done in the 1960s using laser beams in solids. Plasma experiments on the analogous phenomenon of wave collapse began in the 1970s, in beam-plasma and laser-plasma contexts. During the 1970s applications to ionospheric-modification experiments and interpretation of solar radio bursts were also pursued. New areas of application in the 1980s and 1990s have involved interpretation of *in situ* observations of electrostatic waves at the planets and in the auroral regions of the Earth. Some applications to solar physics, pulsars, and other areas of astrophysics have also been proposed.

This section reviews applications of the theory of unmagnetized wave collapse and strong turbulence to phenomena in plasmas that are at most weakly magnetized (i.e., magnetic effects do not dominate during wave collapse). In order to minimize the complications at this point, analogous phenomena in more strongly magnetized plasmas are discussed in Sec. IX, along with appropriate generalizations of the unmagnetized theory. The applications considered here include beam-driven and clamp-driven wave collapse and turbulence in electron-beam, laser-plasma, ionospheric-modification, and space physics contexts. In some cases, the experiments have been carried out specifically to test the predictions of strong-turbulence theory, while in others, the theory has shed light on experiments carried out for other reasons. We do not discuss experimental techniques in any detail here.

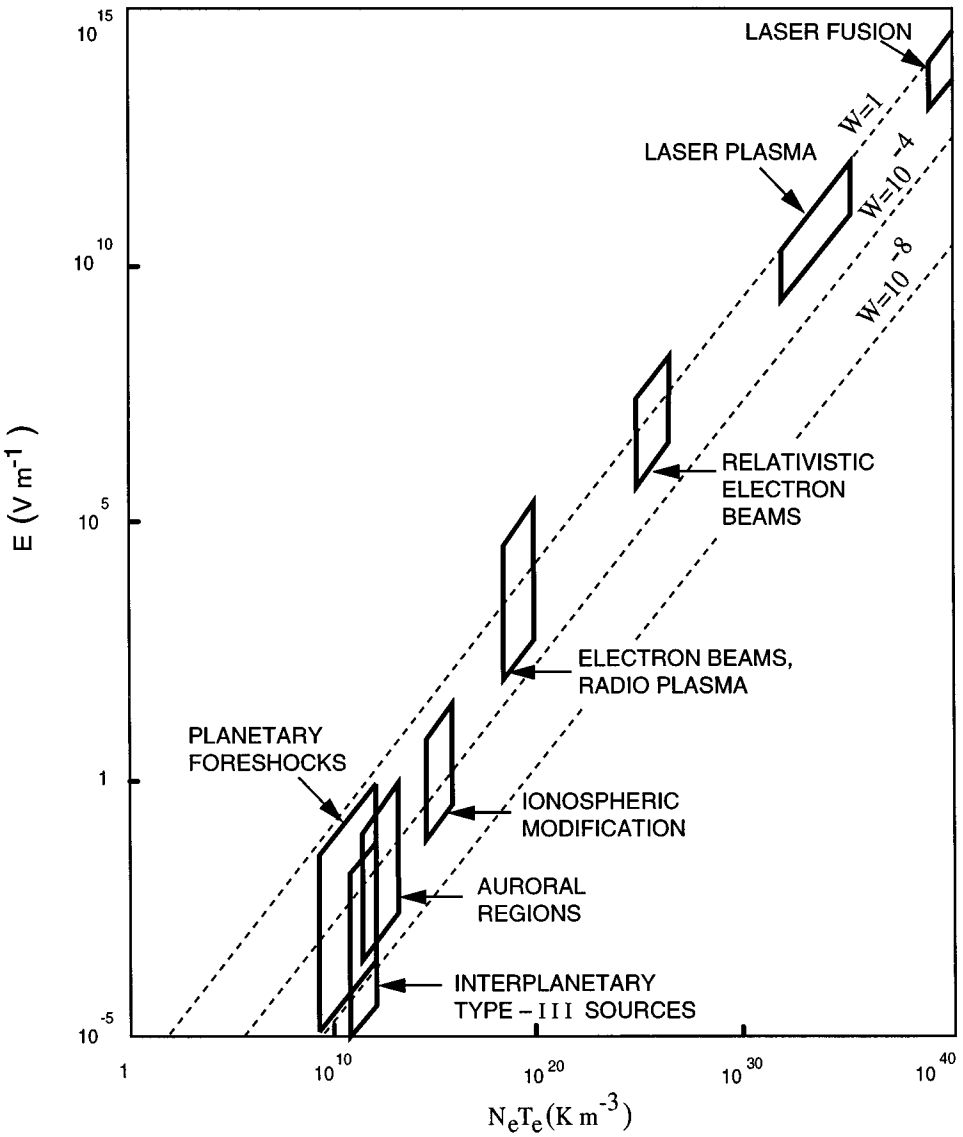

FIG. 28. Experimental regimes of wave collapse and strong turbulence, showing typical ranges of N_eT_e, E, and W (diagonal lines).

Figure 28 shows typical parameter values for some natural and laboratory plasmas in which wave collapse and/or strong turbulence are thought to exist or have been proposed. What is striking are the huge ranges of wave and particle energy densities and length scales, over which these phenomena have been observed—over 23 orders of magnitude of N_e, 4 orders in T_e, and 15 orders in E.

Before proceeding, we note that a common tendency in the literature has been to interpret strong, localized fields observed in the laboratory and nature to be collapsing wave packets. This is by no means always justified and has led to some erroneous interpretations of experimental data. For this reason, discussion of experimental applications is preceded by Sec. VIII.A, in which some key points are recapitulated and common misconceptions regarding strong turbulence and wave collapse are discussed.

A. Common misconceptions

The most striking characteristic of wave collapse and strong turbulence is the formation of intense, localized wave packets whose energy densities can approach the plasma thermal energy density and whose minimum scales can be as small as a few Debye lengths. The first common error in applications is to assume that if a field is localized and intense, it is automatically associated with wave collapse. Cairns and Robinson (1992a, 1992b, 1995a) showed that two proposed occurrences of wave collapse were not consistent with this phenomenon (see also Secs. VIII.C and VIII.D below). They noted that other mechanisms that could produce localized Langmuir waves, or field structures resembling them, include beats between parent Langmuir waves and product waves produced by electrostatic decay, Langmuir wave caustics or foci, resonant wave enhancements, ion holes, short-scale fluctuations in the Langmuir growth rate due

to beam inhomogeneities, and variations imposed by ambient density fluctuations (Robinson, 1992). Muschietti *et al.* (1995) have also suggested a kinetic mechanism for localization of beam-driven Langmuir waves.

Before assuming that a localized wave packet is associated with wave collapse, it is necessary to check that its field strength and length scale are such that it exceeds the collapse threshold $Wa_i^2/\lambda_D^2=\Theta$. It is also necessary to demonstrate that the level of background density fluctuations is not so high as to disrupt the packet before it can collapse (Cairns and Robinson, 1992a, 1995a; see also Sec. VIII.D). Another useful technique in checking for the presence of specific nonlinear wave processes is to calculate third- or fourth-order frequency cross-correlation coefficients and look for peaks corresponding to the theoretical frequency relationships (Bale *et al.*, 1996).

Sometimes it is suspected that plane waves are subject to a modulational instability that gives rise to spatial clumping of waves. In this case, it is particularly important to apply the instability criterion $\Gamma>\Delta\omega$ [see Eq. (3.16)], using the growth rate for the correct region in Fig. 3. Second, one must be sure that no other instability has a higher growth rate [see the discussion of Eq. (6.8)]. Many errors have been made in the literature by applying the wrong criterion or by omitting this step entirely. One should also be careful that plane-wave criteria are appropriate—many turbulent systems are modulationally stable, but undergo wave collapse via the nucleation mechanism (see Secs. V.A, V.C, and Russell *et al.*, 1988). Collapse directly from beam-driven waves, for example, seems to be very difficult unless the waves are extremely intense. Rather, parametric decay usually first carries the energy into a low-k condensate, whence it nucleates into collapsing packets or, if the beam wave number is not too high, it can nucleate directly.

A third area in which many errors are made is the assumption that wave-collapse theory predicts the existence of a predominance of packets with scales of a few Debye lengths (i.e., near a_f). Although such scales are possible near the point of arrest, they represent a very small fraction of packets, since collapse accelerates as the scale decreases, and dissipation is extremely rapid near arrest. By far the majority of packets have scales near the nucleation scale a_i, with

$$a_i\approx(\Theta/\langle W\rangle)^{1/2}\lambda_D\gg a_f, \tag{8.1}$$

from Sec. VI.A. The apparent reason for errors of this type is a confusion with the existence of stable solitons a few Debye lengths in size in one-dimensional systems. Such solitons simply do not exist in two or three dimensions within the framework of the nonlinear Schrödinger equation or Zakharov equations. Nor do higher-order nonlinearities cut in soon enough to stabilize collapsing packets before they reach the arrest scale (Newman *et al.*, 1990). A related error is to assume that $a_f\approx\lambda_D$; all current analyses, simulations, and experimental results imply that the arrest scale in three dimensions is of the order of $20\lambda_D$.

Incorrect analogies with soliton solutions of the 1D dissipation-free equations have also led some authors to expect that collapsing wave packets will typically propagate at a velocity comparable to the sound velocity, where Eq. (4.5) implies that the ion response is strongest. In fact, ion inertia and damping of the ion response largely restrict packet velocities to values much less than the sound velocity (see Sec. V.B and Robinson, Wouters, and Broderick, 1996). The predominance of stationary collapsing packets then tends to rule out high rates of collisional energy exchange between them, except indirectly via particle acceleration, for example (Benford and Zhai, 1993).

A fourth category of misconception is the idea that a given physical situation corresponds to weak turbulence or strong turbulence, but never both. This has led on occasion to categorical (but often incorrect) statements that only one of the two types of turbulence can be relevant to one or another particular application. In reality, it is quite possible for one part of a Langmuir spectrum to be describable by weak turbulence, while another involves strongly turbulent interactions (see Secs. III.C, IV.C, and VI.A). The classic example is turbulence driven at high k, where a weak-turbulence cascade carries the energy to a low-k condensate that feeds wave collapse. A related misconception is that strong- and weak-turbulence theories are somehow complementary theories of interactions between Langmuir waves and ion sound waves. In reality, the Zakharov equations contain the relevant three-wave parametric interactions of electrostatic decay and coalescence, whose rates also pass over to the correct random-phase limits as the bandwidths increase. Hence the Zakharov equations generalize the weak-turbulence equations. In the limit of low W, the Zakharov equations also have the linear wave modes as solutions (see Secs. II.C and III.A).

Other errors sometimes made in the literature include the following. (i) The assumption that 3D collapse is strong, i.e., energy conserving. In most cases, at least the initial stages of 3D collapse are subsonic and hence weak (see Sec. V.E). It should also be recalled that the most commonly discussed supersonic scalings, Eqs. (5.27) and (5.28), are based on an *assumption* of strong collapse. (ii) The assumption that the crossover from subsonic to supersonic collapse occurs precisely where $W=m_e/m_i$. Numerical and analytic evidence points to the transition occurring at a large multiple of this value (see Secs. V.E and VI.C).

B. Electron-beam experiments

Some of the most direct evidence for self-focusing and wave collapse in plasmas has come from experiments in which an electron beam is fired into a long cylinder of plasma. Wong and Quon (1975) fired a beam into a plasma with $N_e=10^{14}$–10^{15} m^{-3}, $T_e=2\times10^4$ K, and a beam velocity $v_b=(5$–$10)V_e$. Beam-driven Langmuir waves were observed to decay electrostatically. The parent and product waves then beat to produce a 1D standing-wave pattern. The peaks of this pattern were

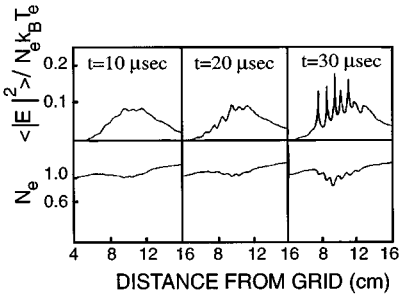

FIG. 29. Evolution of localized Langmuir field spikes and corresponding density depressions seen by Wong and Quon (1975). Density N_e is measured in units of the mean value.

then seen to steepen and form localized spikes with scales of $\sim 10\lambda_D$, separated by half a wavelength of the initial waves (see Fig. 29). Peak energy densities of $W \approx 0.2$ were seen in density wells having depths of up to 15% of the unperturbed density, and the electron beam was strongly scattered when the localized packets were seen. Wong and Quon argued that this was evidence for a modulational instability of the standing waves and of transit-time interactions between electrons and the localized packets. Several similar experiments were carried out in the 1970s, finding evidence for trapping of Langmuir waves in large, apparently self-generated, density depressions due to ion sound waves, and for associated transit-time interactions with beam electrons (Quon *et al.*, 1974; Ikezi *et al.*, 1976; Kiwamoto *et al.*, 1977). Wong *et al.* (1977) studied interactions of beam electrons with 1D localized packets excited by a radio-frequency field (see Sec. VIII.E). They found that the packets were coherent and their scattering of electrons was consistent with one-dimensional transit-time interaction theory (see Sec. V.F).

Further observations of nonlinear Langmuir interactions in 1D geometries were carried out by Cheung *et al.* (1982), who observed density depressions of up to 50% on a scale of $12\lambda_D$. They also saw electromagnetic emission at harmonics of a basic frequency of $\approx 0.7\omega_p$, which they interpreted as the frequency of a localized eigenstate trapped in the density depression. Leung *et al.* (1982) set up a 1D standing Langmuir wave using two counterpropagating electron beams. This removed the role of electrostatic decay in setting up the standing wave. Again, they observed the formation of spiky, solitonlike Langmuir peaks with a scale of $\sim 7\lambda_D$, a density perturbation of $\sim 10\%$, and $W \approx 0.1$–0.2. Simultaneous transit-time acceleration of electrons occurred, with the formation of a high-energy tail on the electron distribution, and it was inferred that these interactions arrest collapse.

All of the above experiments involved Langmuir fields that varied in only one dimension, leading to the formation of reasonably stable localized soliton structures. Wong and Cheung (1984) succeeded in studying the collapse of three-dimensional Langmuir wave packets in a beam-driven plasma by averaging over many shots in a highly reproducible system with $N_e = (2$–$3) \times 10^{15}$ m^{-3} and $T_e \approx 10^4$ K. In this experiment, they measured the dimensions and intensity of a packet as it collapsed from an initial scale of $(150$–$500)\lambda_D$ to a final scale of $(20$–$40)\lambda_D$, with $W \approx 1$ as shown in Fig. 30. They found different power-law scalings of the packet size, depending on which dimension of the packet was observed, but the inertial range was not sufficiently well developed for these to constitute a definitive test of the predicted scaling exponents. They also saw significant beam scattering by the packet prior to collapse, followed by decoupling of the collapsing waves from the beam as collapse proceeded. This was consistent with the theory in Sec. V.C and with Cheung *et al.*'s (1982) observation that the frequency of a state in a density well is lowered, leading to decoupling from the beam.

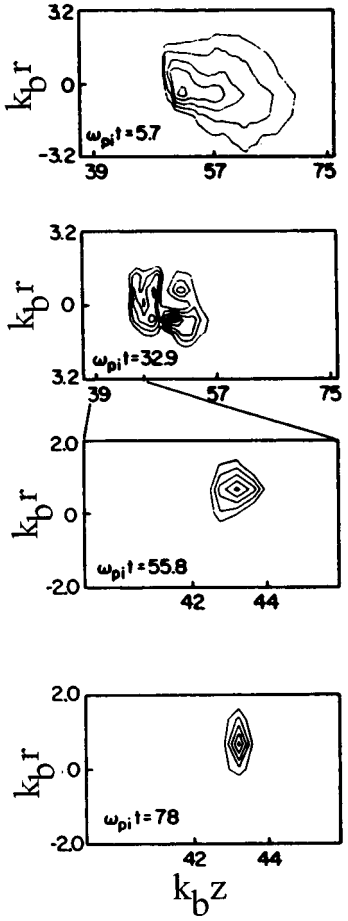

FIG. 30. Collapsing packet seen by Wong and Cheung (1984), showing contour plots of Langmuir energy density. Time increases toward the bottom. Note the different scales on the two axes, where $k_0 = 0.03 k_D$ is the beam-driven wave number.

Cheung and Wong (1985) used the same apparatus as Wong and Cheung (1984) to study the long-time evolution of nonlinear Langmuir waves initially excited by a beam instability. Their results showed repeated renucleation of collapsing wave packets at a nearly fixed location. Each packet formed, collapsed, and decoupled from the beam, then burned out, leaving a localized density well that relaxed and renucleated further waves. After each burnout, the Langmuir activity was observed to

be very low and deep density wells were found to suppress beam-plasma coupling, as found by Wong and Cheung (1984).

At the same time as Wong and Cheung's (1984) work on individual wave collapses, other beam-plasma experiments also began to shed light on strong Langmuir turbulence, consisting of many collapsing wave packets with scales much smaller than those of the apparatus (unlike the previous beam-plasma experiments, described above). Janssen, Bonnie, Granneman, Krementsov, and Hopman (1984), Janssen, Granneman, and Hopman (1984), and Hopman and Janssen (1984) carried out a series of experiments in which an electron beam was accelerated by an 800-kV potential and injected into a 2.5-m-long preionized plasma. Stark shifts were used to estimate electric-field strength distributions, while angular and energy analyzers were used to determine the pitch angle and energy distributions of the electron beam. Typical plasma parameters were $N_e = 5\times10^{19}$ m^{-3} and $T_e = 1\times10^6$ K, much higher than in the experiments discussed above. These experiments found typical amplitudes of beam-driven Langmuir waves to be on the order of 10^6 V m^{-1}, but the scattering of the beam (in both energy and angle) was found to be far too great to be accounted for by a model in which the waves were uniformly distributed. Instead, a model in which the waves were largely confined to small regions of much higher fields was proposed, implying the existence of intense localized packets. Field strengths of up to $\sim10^8$ V m^{-1} were inferred on the basis of minimum length scales of $10\lambda_D$. Hopman and Janssen (1984) concluded that the localized packets inferred were consistent with strong Langmuir turbulence.

Robinson and Newman (1990c) and Newman and Robinson (1991) applied their two-component theory of strong Langmuir turbulence to the relativistic-electron-beam experiments described in the previous paragraph. They found the scattering of beam electrons in energy (net scattering typically ±100 keV) to be consistent with random transit-time interactions with a steady-state population of collapsing wave packets corresponding to the typical observed value of $\langle W\rangle\approx0.014$ and peak fields of $\sim2\times10^7$ V m^{-1}. However, they found values of angular scattering of only 0.1–0.4 times the observed values of 10°–20°. Melatos *et al.* (1996) reanalyzed this problem using a more sophisticated Fokker-Planck formulation, which treated angular scattering more accurately. They reached essentially the same conclusions as Robinson and Newman (1990c) and suggested that the discrepancy in angular scattering is chiefly connected with transverse gradients of the beam, which were not taken into account in their analysis.

Levron *et al.* (1987) investigated the distribution of electric-field strengths in beam-driven strong Langmuir turbulence, using an experimental setup and plasma parameters similar to those employed by Hopman and Janssen (1984). They found a distribution of fields consistent with Eq. (6.41) in the regime $0.6\lesssim W\lesssim3$, which they termed *superstrong turbulence*. Benford (1987) proposed a model of collisional energy exchange between moving collapsing packets that yielded such a statistical distribution. However, given the strong tendency of collapsing wave packets to be stationary, collisions at the necessary rate appear unlikely unless they are of some other type, e.g., mediated indirectly via particle interactions (Benford and Zhai, 1993). Robinson and Newman (1990c) and Newman and Robinson (1991) noted that, for collapse amid turbulence, the value of $W_i a_i^2/\lambda_D^2$ is not always precisely equal to the collapse threshold Θ for an isolated wave packet. Rather, turbulent interactions randomize the value of the collapse threshold about a characteristic value of this order, leading to a distribution of the form of Eq. (6.41) in the superstrong regime where fields are attributed to packets at or near arrest. Fitting Eq. (6.41) to Levron *et al.*'s (1987) results and reexpressing E_{f0} in terms of the arrest scale a_f, they found $a_f=(16\pm5)\lambda_D$, in good agreement with 3D particle-in-cell simulations (see Sec. VII.B) and transit-time damping estimates (see Sec. V.F), and reasonable agreement with Wong and Cheung's (1984) estimate of $(30\pm10)\lambda_D$. The peak energy densities at the arrest scale were estimated to be $W\sim1$, consistent with observations.

Benford *et al.* (1991) reported an exponential decay of the high-E tail of the electric-field distribution, after the end of beam driving, with

$$P(E)\propto\exp(-E^2/2E_{f0}^2)\exp(-t/\tau), \tag{8.2}$$

where $\tau\approx10^{-6}$ s. Benford and Zhai (1993) argued that nucleation and wave collapse would yield too low a value of τ and proposed an alternative model in which wave packets undergo indirect "collisions" via wave or particle exchange and obtained constraints on the magnitude and functional form of the effective collision frequency. However, this decay behavior has yet to be fully explained.

C. Solar type-III radio sources

Energy release during solar flares heats and accelerates coronal electrons. Electrons on open magnetic-field lines can then escape into the interplanetary medium to form so-called type-III electron beams. These beams move at typical velocities of $0.1c$–$0.3c$ by the time they reach one astronomical unit (1 AU $\approx1.50\times10^{11}$ m) from the Sun, but have been observed to have speeds anywhere from $0.03c$–$0.99c$ nearer the Sun (Hoang *et al.*, 1994; Poquerusse, 1994). Figure 31 is a schematic of the zone swept out by a type-III electron beam travelling along interplanetary field lines.

Type-III beams have been observed by satellites *in situ* to generate intense, highly clumpy Langmuir waves (Gurnett and Anderson, 1976, 1977; Lin *et al.*, 1981, 1986). Electromagnetic emission has been seen, with observations showing fundamental ($\omega\approx\omega_p$) and harmonic ($\omega\approx2\omega_p$) radiation, sometimes simultaneously (Wild, 1950; Dulk, Steinberg, and Hoang, 1984; Suzuki and Dulk, 1985). Remote sensing has made it possible to follow beams from very close to the Sun out to beyond 1 AU.

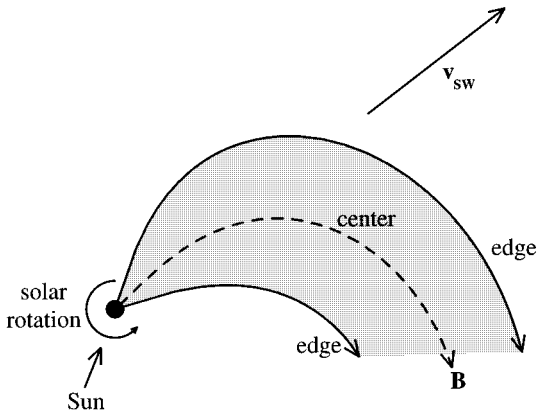

FIG. 31. Schematic of the zone swept out by a type-III solar electron beam as it streams along the Archimedean spiral formed by the interplanetary field lines (Robinson and Cairns, 1994). The solar wind flows radially outward at a speed v_{sw}.

A theoretical picture of type-III emission was first put forward by Ginzburg and Zheleznyakov (1958) and, with some modifications, the core of this picture is still current today. Briefly, a type-III beam generates Langmuir waves via a *bump-on-tail* instability, in which the presence of the beam constitutes a population inversion, giving rise to a coherent wave instability. Growth of Langmuir waves then tends to relax the beam by flattening the population inversion. Nonlinear wave-wave interactions involving these waves then lead to fundamental and harmonic radio emission. Despite general agreement on these points, the nature of the nonlinear interactions has been the subject of intense research and considerable debate over the intervening time. Two aspects of the observations have proved to be particularly important to the development of the theory and its relationship to strong-turbulence phenomena. First, Sturrock (1964) noted that, in the absence of a saturation mechanism, the bump-on-tail instability would remove energy so fast that a type-III beam would be able to propagate only a short distance (perhaps hundreds of km), rather than the 1 AU or more observed. This problem is commonly called *Sturrock's dilemma*. Second, the *in situ* observation of extremely spiky Langmuir waves (Gurnett and Anderson, 1976, 1977) suggested the operation of a dynamical localization mechanism, such as Langmuir collapse.

Strong-turbulence processes have been advanced to resolve Sturrock's dilemma. For example, Papadopoulos *et al.* (1974), Rowland and Papadopoulos (1977), Rowland (1980), and Rowland *et al.* (1981) showed that the modulational instability can rapidly remove beam-generated Langmuir waves from resonance with the beam by scattering them to different k, thereby reducing the beam's energy-loss rate and allowing it to propagate further. This mechanism gives rise to product waves at high k, where they are rapidly dissipated. In laboratory situations, this may explain observed persistence of beams (Breizman and Ryutov, 1974). However, this mechanism requires waves sufficiently monochromatic to satisfy the condition $\Gamma > \Delta\omega$ [see Eq. (3.16)]. Balance between growth and damping for typical parameters at 1 AU implies $\Gamma \approx (0.1\text{–}1)\ \mathrm{s}^{-1}$ for the modulational instability (Lin *et al.*, 1986; Robinson *et al.*, 1993). In contrast, the bandwidth of the beam-driven waves is of order $\Delta\omega \approx 3\omega_p \Delta v_b V_e^2 / v_b^3$. Typical parameters at 1 AU ($\omega_p \approx 1.5\times10^5\ \mathrm{s}^{-1}$, $\Delta v_b / v_b \approx 0.3$, $V_e \approx 1.5\times10^6\ \mathrm{m\,s}^{-1}$, and $v_b \approx 3\times10^7\ \mathrm{m\,s}^{-1}$) then yield $\Delta\omega \approx 340\ \mathrm{s}^{-1} \gg \Gamma$. Hence modulational interactions are stabilized and the proposed mechanism is ineffective in this context (Robinson, Willes, and Cairns, 1993; Cairns and Robinson, 1996). Modulational instability would require fields of order $0.1\ \mathrm{V\,m}^{-1}$, compared with the electrostatic decay threshold of $\sim 3\ \mathrm{mV\,m}^{-1}$ (Robinson, Willes, and Cairns, 1993; Cairns and Robinson, 1996).

Two-dimensional Zakharov-equation simulations of beam-driven Langmuir waves showed that energy is transferred primarily to smaller, not larger, k via a decay cascade (Nicholson and Goldman, 1978; Nicholson *et al.*, 1978; Hafizi *et al.*, 1982; Weatherall *et al.*, 1983; Goldman, 1984). This leads to formation of a condensate, which then feeds energy to collapsing wave packets. Under typical conditions relevant to type-III bursts, direct modulational instability of the beam-driven waves does not predominate. Hafizi *et al.* (1982), in particular, argued strongly against modulational-instability saturation of type-III beam instabilities.

After the main work on saturation of the beam instability via modulational interactions, it was shown that quasilinear relaxation could be substantially slowed because electrons further back in a type-III beam reabsorb waves emitted by electrons near the front (Grognard, 1982, 1985), thus partly resolving Sturrock's dilemma without recourse to strong-turbulence processes. The result was a beam that propagated close to marginal stability on average, with greatly reduced energy loss. Nonetheless, there remained the question of the source of the extreme Langmuir wave clumping observed *in situ* (Gurnett and Anderson, 1976, 1977), which has been observed on all scales from $\lesssim 100$ km to $\gtrsim 10^6$ km (Robinson, Cairns, and Gurnett, 1992, 1993). While it is tempting to invoke Langmuir collapse to account for intense, short-scale field structures, Robinson, Cairns, and Gurnett (1992, 1993) noted that the clumping occurs at all field levels, implying that the mechanism is *linear* in the Langmuir intensity. Robinson (1992) proposed a stochastic growth theory in which the beam propagates in a state close to marginal stability, with ambient density fluctuations (Celnikier *et al.*, 1983, 1987) randomly modulating the growth rate (Smith and Sime, 1979). This theory has since been able to account for most observed features of type-III Langmuir waves, as well as associated ion sound waves and electromagnetic emission, with its predictions being extensively verified against observations (Robinson, 1992, 1995, 1996; Robinson, Cairns, and Gurnett, 1992, 1993; Robinson and Cairns, 1993, 1994; Robinson, Willes, and Cairns, 1993; Cairns and Robinson, 1995c, 1996; Hospodarsky and Gurnett, 1995).

The stochastic-growth theory does not rule out a role for wave collapse or strong turbulence in type-III radio

sources at 1 AU (and, to date, makes fewer quantitative predictions at other heliospheric distances, where conditions are different and fewer *in situ* observations are available to constrain the predictions). However, it implies that such effects are not central to the observed phenomena. Evidence against wave collapse as the saturation mechanism for beam growth includes the following: (i) the highest fields seen are very close to the estimated electrostatic decay threshold and well below the collapse threshold (Robinson, Cairns, and Gurnett, 1993; Robinson, Willes, and Cairns, 1993), (ii) ion sound waves and Langmuir beats consistent with three-wave interactions, especially electrostatic decay, have been seen *in situ* (Lin *et al.*, 1986; Gurnett *et al.*, 1993; Cairns and Robinson, 1995b; Hospodarsky and Gurnett, 1995), (iii) no power-law tail is seen in the probability distribution $P(E)$ as would have been expected if wave collapse were common [see Eq. (6.40)], and (iv) ambient density fluctuations, produced by mechanisms other than strong turbulence, which have a level of a few percent, would be likely to disrupt nucleating packets before collapse could get under way (Robinson, Willes, and Cairns, 1993; Cairns and Robinson, 1995a; see next paragraph).

Recent *Ulysses* observations of millisecond spikes superposed on broad Langmuir wave packets in type-III radio sources prompted explanations in terms of wave collapse (Kellogg *et al.*, 1992; Thejappa *et al.*, 1993). In these theories it was argued that the observed spikes represented collapsed packets with scales of order $10\lambda_D$. Cairns and Robinson (1995a) compared the observed fields with predictions from wave-collapse theory and argued against this explanation on the following grounds: (i) The collapse threshold is exceeded by neither the spikes nor the underlying wave packets. In terms of observable quantities, the requirement for collapse is

$$|E(r=a)|^2 \gtrsim \frac{100Nk_BT_e}{\epsilon_0}\frac{\lambda_D^2}{a^2}, \tag{8.3}$$

where $E(r=a)$ is the typical root-mean-square field one scale size a from the center of a packet, the typical value likely to be seen by a spacecraft, given that it encounters a packet. (ii) Neither type of field satisfied the criterion

$$|E(r=a)|^2 \gtrsim \frac{100N_ek_BT_ev_S}{\epsilon_0 V_e}\frac{\lambda_D}{a}, \tag{8.4}$$

for nucleating packets to escape disruption by ambient density fluctuations, which can destroy the density well that supports the nucleating state. (iii) Wave-collapse theory does not predict a predominance of structures near the arrest scale (see Sec. VIII.A), contrary to the predominance of short-scale structures observed. Rather, a distribution of scales should be seen, in which larger scales predominate (from early stages of wave collapse), correlated with lower fields. Subsequently, Cairns and Robinson (1995a; see Sec. VIII.A) suggested several physical mechanisms that might give rise to intense fields at scales of $\lesssim 10\lambda_D$, finding only one plausible candidate among their suggestions, namely nonlinear Bernstein-Greene-Kruskal (Bernstein *et al.*, 1957) modes, called electron holes. Subsequently, Cairns (1995) argued on statistical grounds that the observed spikes are most probably an instrumental artifact.

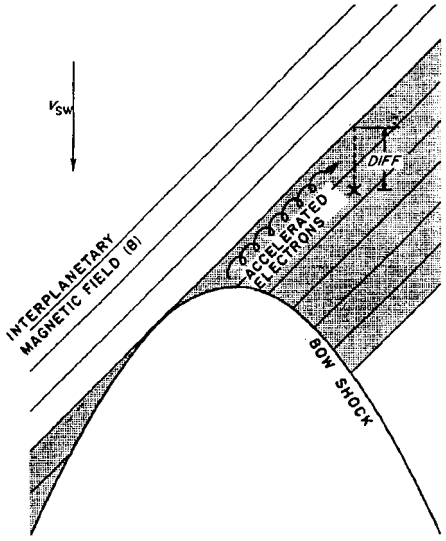

FIG. 32. Schematic of the foreshock region, showing interplanetary magnetic-field lines, the bow shock, and the downstream distance parameter DIFF (Newman, 1985; Robinson and Newman, 1991a, 1991b).

Overall, it appears that strong turbulence and wave collapse are not significant in type-III sources at 1 AU, although they are not strictly forbidden. However, it is still possible that these phenomena play a role closer to the Sun, where Langmuir energy densities are higher (as are plasma densities and temperatures, however, which mitigate against collapse). Another possible application of strong turbulence is to sources of type-II solar radio bursts, where emission is driven by beams generated at shock waves (Nelson and Melrose, 1985).

D. Planetary foreshocks

It is well known that a bow shock exists where the solar wind, carrying the frozen-in interplanetary magnetic field, impinges on the Earth's magnetic field. Dissipative processes at the shock lead to acceleration of electrons and consequent ejection of beams along interplanetary field lines, as shown in Fig. 32 (Filbert and Kellogg, 1979; Newman, 1985). The region connected to the bow shock by field lines is termed the *foreshock*. Foreshock electron beams have been observed *in situ* (Fitzenreiter *et al.*, 1984) and are believed to generate strong Langmuir waves observed by satellites such as IMP 6 and ISEE 1, shown in Fig. 33 (Fredericks *et al.*, 1968; Filbert and Kellogg, 1979; Etcheto and Faucheux, 1984). Newman (1985), Cairns and Melrose (1985), and Cairns (1987) have shown that the observed electron distributions are unstable and can lead to Langmuir wave generation via a bump-on-tail instability (see Sec. VIII.C). Newman (1985) showed that this can be followed by an electrostatic decay cascade, formation of a condensate, and wave collapse.

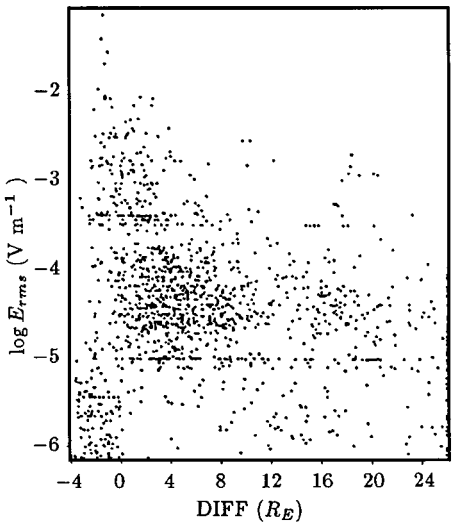

FIG. 33. Scatter plot of peak rms fields obtained by the spacecraft IMP 6 vs the downstream distance DIFF in the Earth's foreshock, as shown in Fig. 32 (Filbert and Kellogg, 1979). Here R_E is the radius of the Earth.

Peak electric fields observed by satellites appear to be too far above the typical local fields to be consistent with incoherent Gaussian field statistics like these in weak turbulence. Robinson and Newman (1991a) developed a model in which strong fields correspond to coherent wave packets that nucleate and decouple from a weak-turbulence background as they collapse. The packets then convect downstream with the solar wind velocity, simultaneously collapsing to scales as short as $a_f \approx 20\lambda_D$ and fields of $W_f \approx 1$ (see Sec. V). After correcting for observational underestimation of such short-scale fields, they found their results to be in agreement with the observed field distributions. In particular, there is an increasing fractional spread of high fields, relative to the local mean value, further downstream. In their model, this occurs because packets at a given value of the downstream distance DIFF (see Fig. 32) originated at an increasingly large range of initial values of this parameter. Robinson and Newman (1991a) also found the observed polarization of the highest fields (Filbert and Kellogg, 1979) to be in good agreement with the polarization of a "standard" linearly polarized collapsing wave packet given by Eq. (5.4), with Eq. (5.10), $a_{00}=0$, and $\alpha=1$. One shortcoming in the work of Robinson and Newman (1991a) was that they were restricted to comparisons with poorly time-resolved data. High-time-resolution observations from the spacecraft *Wind* should overcome this deficiency and provide a definitive test of the model by observing individual wave packets in enough detail to compare their fields and scales with the predictions of collapse theory.

Short-scale ($50\lambda_D$–$500\lambda_D$) Langmuir wave packets have also been seen in the Jovian foreshock by the *Voyager* spacecraft (Gurnett *et al.*, 1981), with a structure similar to that shown in Fig. 10(b). Initially, it was suggested that these short-scale modulations were the result of modulational instability or wave collapse (Gurnett *et al.*, 1981). However, reanalysis of these data within the framework of more recent strong-turbulence theory showed that the waves failed by a wide margin to satisfy the criteria of Eqs. (8.3) and (8.4) for collapse amid ambient density fluctuations (Cairns and Robinson, 1992a). However, the modulation was found to be explicable in terms of beating between a beam-driven Langmuir wave L and a wave L' resulting from the weak-turbulence electrostatic decay $L \rightarrow L' + S$, where S denotes a sound wave (Cairns and Robinson, 1992b; see Secs. III.A and III.B). Their quantitative comparison included the Doppler shift of the sound waves due to motion of the solar wind past the spacecraft, giving a modulation frequency of

$$\omega_{\rm mod} = \left(\frac{v_S}{3V_e^2} + \frac{\omega_S'}{2\omega_p |v_S - v_{sw}| \cos\theta||} \right)^{-1}, \tag{8.5}$$

$$\omega_S' = (2k_L - k_*)|v_S - v_{sw}|\cos\theta||, \tag{8.6}$$

where $\mathbf{v}_{sw}$ is the solar wind velocity and θ the angle between $\mathbf{v}_{sw}$ and the interplanetary magnetic field (which guides the beam and determines the direction of $\mathbf{k}_b$). They found this interpretation of the observations to be consistent with reasonable physical parameters and other known physical constraints. Subsequently, Gurnett *et al.* (1993) and Hospodarsky and Gurnett (1995) found evidence for similar modulations in type-III solar radio sources.

Intense, localized Langmuir waves have now been observed in the foreshocks of Venus, Earth, Mars, Jupiter, Saturn, Uranus, and Neptune, by ISEE-1, ISEE-2, *Voyager-1*, *Voyager-2*, *Phobos*, and the *Pioneer Venus Orbiter* (Gurnett *et al.*, 1989; Grard *et al.*, 1991; Cairns and Gurnett, 1992; Hospodarsky *et al.*, 1994). The case for electrostatic decay, rather than wave collapse, setting an effective upper bound to the electric-field distribution (although not prohibiting occasional wave collapses) was strengthened by Robinson and Cairns's (1995) analysis of the behavior of the highest observed fields with heliospheric distance. Figure 34 shows that this behavior corresponds reasonably closely to the trend in the electrostatic decay threshold. Foreshock-type theories for outer-heliospheric radio emissions have also been proposed (Cairns and Gurnett, 1992; Cairns *et al.*, 1993; and the references cited therein).

E. Radio experiments

The applications considered in the preceding subsections all involved driving of Langmuir turbulence by beam-plasma instabilities. In another equally important class of experiments, intense localized Langmuir waves are excited by mode conversion of an electromagnetic wave of frequency ω_R as it propagates into a region of increasing density. This method of excitation is applicable to radio-plasma, laser-plasma, and ionospheric-heating experiments. The mechanism can be understood by the following argument (Ginzburg, 1960; Kruer, 1988): If the density is a linearly increasing function of position x, the field is an Airy function of x, as shown in

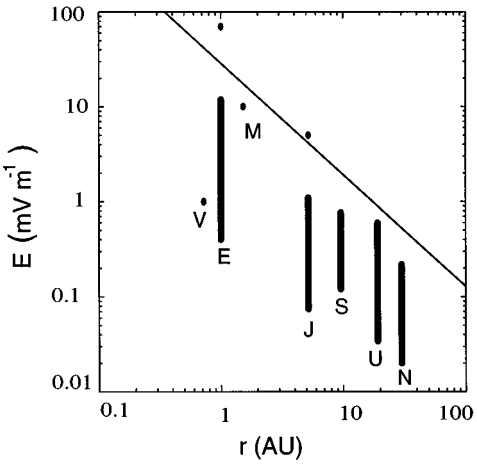

FIG. 34. Electric fields of Langmuir waves observed in the foreshocks of Venus, Earth, Mars, Jupiter, Saturn, Uranus, and Neptune vs heliospheric distance r. Robinson and Cairns's (1995) best estimate of the electrostatic decay threshold is shown as a sloping line. ISEE and *Voyager* observations are shown as solid bars, while upper bounds obtained by other spacecraft are shown as dots.

Fig. 35. A wave obliquely incident on the density gradient, at an angle θ to the normal, reflects at the *reflection point* where $\omega_p=\omega_R\cos\theta$. However, its evanescent field can tunnel through to the *resonance layer* (often called the *critical layer*) where $\omega_p=\omega_R$. If there is a component of the electric field along the density gradient at this layer (i.e., the wave is p polarized), the field can resonantly excite electron oscillations, and hence Langmuir waves, because the electrons oscillate between regions of different density (Ginzburg, 1960; Kruer, 1988). Energy is ultimately lost from the Langmuir waves, via dissipation, leading to the term *resonance absorption* to describe the overall process. If the Langmuir waves excited are sufficiently intense, they may undergo collapse, as evidenced by the particle-in-cell simulations of resonance absorption by Gavrilov *et al.* (1995).

The earliest experiment of this type was carried out by Kim *et al.* (1974), who exposed a plasma with a density

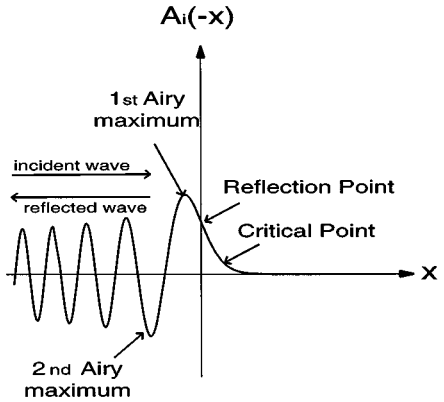

FIG. 35. Airy-function field structure for waves of frequency ω_R incident on a density gradient that increases to the right, showing the critical (or resonance) point ($\omega_p=\omega_R$) and reflection point ($\omega_p=\omega_R\cos\theta$).

gradient to a radio-frequency (rf) field with **E** parallel to the gradient. They found that the ponderomotive force of the enhanced electric field at the resonant layer generated a density depression of width $\sim 20\lambda_D$, with $\delta N_e/N_e\approx W\approx 0.25$. The density depression then trapped rf waves, further enhancing the field and leading to a deepening of the well, but not true collapse, since this was a one-dimensional geometry. The threshold for this modulational-type instability was found to be much lower than for a plane wave because of the linear localization of the rf field by the density gradient. Tanikawa *et al.* (1984) later probed the structure of trapped Langmuir fields in detail, using a very intense pump ($W\approx 10$ for the pump field). They showed the existence of at least three distinct eigenmodes in some cases. In an experiment similar to that of Kim *et al.* (1974), Ikezi *et al.* (1974) observed two different types of instabilities: a modulational instability in the region where $\omega_p>\omega_R$, near the resonance layer, and a decay instability in the underdense region $\omega_R>\omega_p$ near the reflection point. However, they found $\delta N_e\propto|\mathbf{E}|$, rather than $\delta N_e\propto|\mathbf{E}|^2$, because their field structures moved nearly at the sound speed, where the Zakharov equations must be modified to remove the divergent density response in Eq. (4.5). Bauer *et al.* (1990) found that the efficiency of formation of density cavities is highest where the density gradient is smallest and convection of Langmuir waves out of the resonant region is least effective in limiting their intensity. They found W as high as 160, well beyond the limits of validity of the Zakharov equations (see Secs. II.B, II.C, and V.F). Typical plasma parameters for these experiments were $N_e=(10^{15}$–$10^{16})$ m^{-3} and $T_e=10^4$ K.

Wong *et al.* (1977) showed the importance of transit-time interactions with localized wave packets by forming a localized packet in a density cavity using incident rf waves parallel to the density gradient, then probing it with a low-density electron beam. They found good agreement with 1D transit-time theory (see Sec. V.F) for cavities that were essentially planar in structure as a result of the experimental geometry and boundary conditions. In particular, the phase dependence in Eq. (5.40) was confirmed and it was shown that the localized field amplitude was only reduced significantly due to interaction with particles that arrived at phases corresponding to $|\cos\phi|\approx 1$.

The above radio-plasma experiments were all essentially one-dimensional in nature. Eggleston *et al.* (1982) irradiated a cylindrically symmetric plasma using a concentric external antenna consisting of 12 equally spaced rods parallel to the plasma axis. Density and field perturbations perpendicular to the density gradient were observed to grow on the ion time scale, leading to the development of a 2D structure on the critical surface. It was argued that this structure could be the precursor to wave collapse in experiments of this type, although collapse was not seen.

F. Ionospheric-modification experiments

The electron density increases with height near the bottom of the so-called F layer of the Earth's iono-

sphere, located 200–400 km above the ground (Budden, 1985), reaching a maximum of $N_e \approx (5\text{–}80)\times 10^{10}$ m^{-3} and $T_e \approx 1000$ K. Hence radio waves broadcast from the ground will be reflected back if their frequency is below the highest F-layer plasma frequency, just as in the laboratory radio-plasma experiments described in the previous section. It has long been recognized that the density and temperature of the F layer are sufficiently low that it is possible to perturb them significantly with transmitters of reasonable power ($\sim$10 MW), broadcasting at a frequency of several MHz in order to resonate with ω_p in the F layer. Some of the earliest high-frequency ionospheric-modification experiments were carried out in Colorado in 1970 by Utlaut and co-workers (Utlaut, 1970), at Arecibo in Puerto Rico (Wong and Taylor, 1971; Carlson *et al.*, 1972), and in the Soviet Union (Shlyuger, 1974). The experiments soon revealed heating of the plasma, excitation of Langmuir waves via mode conversion, and a variety of nonlinear processes, which have since provided a rich proving ground for the theory. The experimental and theoretical literature in this field is now too vast to review here in detail, so this section concentrates on aspects in which strong turbulence and wave collapse are likely to play some role and omits discussion of experimental techniques almost entirely. Previous reviews of the experiments and/or theory include those by Perkins *et al.* (1974), Fejer (1975, 1979), Fejer *et al.* (1985), DuBois *et al.* (1990), DuBois and Rose (1991), Cheung *et al.* (1992), and DuBois *et al.* (1993a, 1993b, 1996). The last six papers discuss the relevance of strong-turbulence concepts to ionospheric modification in detail.

The initial aims of ionospheric-modification experiments were to change the temperature and density of the F-layer plasma. However, very early, Wong and Taylor (1971) and Carlson *et al.* (1972) observed enhanced levels of Langmuir waves, resonantly excited by the heater. The basic observation technique was to probe the heated region using a second radar, observing waves that had backscattered off Langmuir waves via the processes shown in Fig. 36(a) and 36(b). The backscattered radar signal shows two spectra produced by Raman scattering, one upshifted in frequency due to scattering involving downgoing Langmuir waves [Fig. 36(a)] and one downshifted due to emission of upgoing Langmuir waves [Fig. 36(b)]. These processes can be written as $T(\mathbf{k}_R)+L(\mathbf{k}_L)\rightarrow T(-\mathbf{k}_R)$ and $T(\mathbf{k}_R)\rightarrow T(-\mathbf{k}_R)+L(\mathbf{k}_L)$, respectively, where $\mathbf{k}_R$ is the radar wave vector at the point of scattering and $\mathbf{k}_L=\mp 2\mathbf{k}_R$ for backscattering to the radar site. The backscattered spectra occur near $\omega_R \pm \omega_{HF}$, where ω_R is the radar frequency and ω_{HF} is the heater frequency ($\approx$ the Langmuir wave frequency produced by conversion processes). Alternative scattering processes involving scattering off ion sound waves (Brillouin scattering), are shown in Figs. 36(c) and 36(d) (Fejer, 1979).

Perkins and Kaw (1971), DuBois and Goldman (1972a, 1972b), Fejer and Kuo (1973), Perkins *et al.* (1974), and Fejer (1979) pointed out the possibility that intense Langmuir waves might undergo modulational or decay instabilities and that backscattering could probe the resulting Langmuir spectra. Despite Perkins and Kaw's (1971) initial discussion of the modulational instability, the bulk of this work concentrated on decay instabilities in which an incident heater wave T decays into a Langmuir wave L and an ion sound wave S, as in Fig. 36(e), or the related coalescence process in 36(f). Much of this analysis was concerned with the saturated spectrum of a series of decays within the framework of weak turbulence theory. However, as pointed out by Cheung *et al.* (1992) and Hanssen *et al.* (1992), for example, weak-turbulence theory is not valid for the high-energy levels seen, and strong turbulence effects must be taken into account. For example, spectra with discrete lines, as would be expected from a series of backscatter decays like those in Figs. 5 and 26, are seen only during high-duty-cycle or continuous heating, well after the onset of heating, rather than early or in less intense situations where weak-turbulence theory should provide a better approximation. Instead, the spectra seen under these latter conditions are broad, without sharp lines (Showen and Kim, 1978).

Using theory (Petviashvili, 1975, 1976) and numerical simulations, Weatherall *et al.* (1982), Sheerin *et al.* (1982), Payne *et al.* (1984), and DuBois *et al.* (1990, 1993b) discussed the possibility of modulational instability, followed by wave collapse at or near the reflection

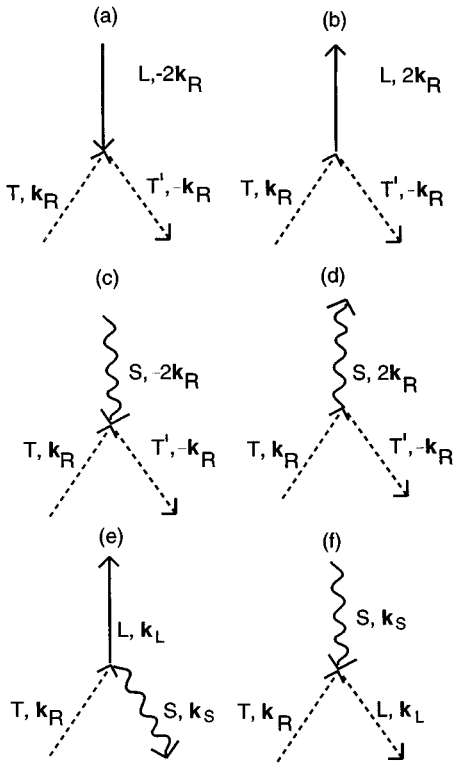

FIG. 36. Scattering processes involving electromagnetic heater waves T: (a) Raman scattering $T+L\rightarrow T'$, resulting in an upshifted spectrum; (b) Raman scattering $T\rightarrow L+T'$, resulting in a downshifted spectrum; (c) Brillouin scattering $T+S\rightarrow T'$; (d) Brillouin scattering $T\rightarrow S+T'$, where S is an ion sound wave; (e) decay, $T\rightarrow L+S$; (f) coalescence $T+S\rightarrow L$.

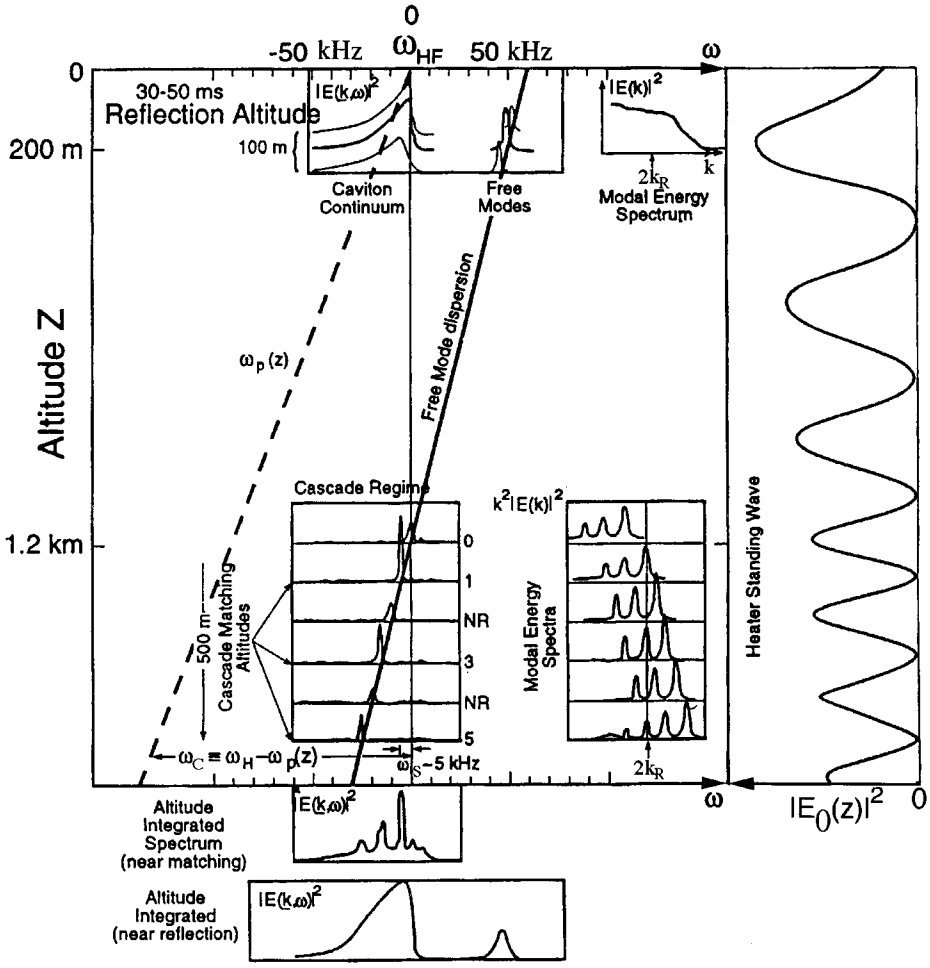

FIG. 37. Schematic of ionospheric modification, adapted from DuBois *et al.* (1993b). The Airy pattern of a vertically propagating radar is shown at the right, with the reflection altitude at the top of the figure (altitude below the reflection altitude labels the vertical axis, assuming the conditions pertaining to the Arecibo radar). The horizontal axis of the left frame of the figure is labeled by frequency relative to the heater frequency. Heavy oblique dashed and solid lines show the plasma frequency and the free-mode dispersion corresponding to the heater-excited wave number k_C, respectively. Insets near the reflection altitude show the components of the frequency spectrum corresponding to free modes and collapsing packets (the latter labeled "caviton continuum" by DuBois *et al.*, 1993b), as well as the wave-number spectrum $\langle |E(k)|^2 \rangle$. Insets at the "cascade-matching" altitudes show corresponding frequency and wave-number spectra at these heights, where cascade-type spectra are excited. Below the main part of the figure, two insets show altitude-integrated spectra corresponding to integration over ranges of height near the cascade-matching and reflection altitudes, respectively. Note that, in the wave-number spectra, the radar "sees" only the Langmuir wave at $k_r = 2k_R$, where the radar has wave number k_R.

point, i.e., within the first Airy maximum shown at the right of Fig. 37, where the Langmuir waves have such small wave vectors that they cannot satisfy the condition for decay to dominate. This corresponds to a dimensionless heater frequency (measured relative to ω_p) satisfying $\omega_C < \Omega_{\rm crit}$. At lower altitudes, where $\omega_C > \Omega_{\rm crit}$ is satisfied, one would expect decay features to be more pronounced (Hanssen *et al.*, 1992). Simulations by DuBois *et al.* (1990, 1993b), Cheung *et al.* (1992), and Hanssen *et al.* (1992) also found that nucleation and collapse occur for conditions characteristic of the first Airy maximum, while decay-like features occur for conditions elsewhere (see below). These authors also emphasized that the strong-turbulence Zakharov equations contain weak-turbulence electrostatic decay and coalescence instabilities in the appropriate limits, in addition to linear theory (see Secs. II.C, III.A, and VIII.A). Hence there can be no question of a conflict between the two sets of predictions, only a question of whether or not weak-turbulence theory is an adequate approximation to the more comprehensive theory in given situations. This point bears on the widespread misconceptions that weak and strong turbulence are somehow complementary theories and/or that strong-turbulence theory omits three-wave electrostatic decay interactions.

During the 1980s, series of experiments were carried out at Arecibo and Tromsø, Norway, using improved techniques that enabled height-resolved Langmuir spectra to be obtained (Sulzer, 1986). Time-resolved spectra were also obtained by pulsing the probe radar at various times during the heating pulse and integrating over many widely spaced heating pulses to improve the

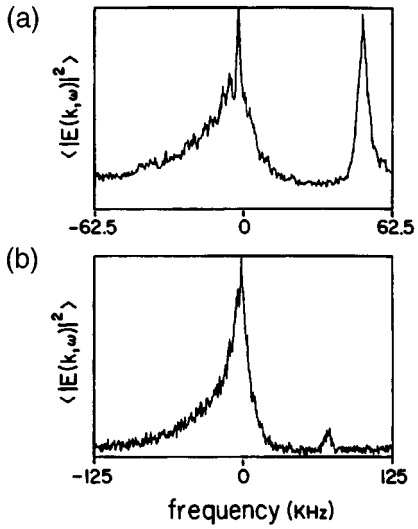

FIG. 38. Fixed-**k** frequency spectra of Langmuir waves from backscatter observations during ionospheric-modification experiments (Cheung *et al.*, 1989). Frequency is measured relative to the heater frequency: (a) experimental results from Arecibo, 0.5 ms into the heating pulse; (b) same as for (a), but 4 ms after the start of the heating pulse.

signal-to-noise ratio (Djuth *et al.*, 1986, 1994; Cheung *et al.*, 1989; Fejer *et al.*, 1991). These techniques have made it possible to test the theoretical predictions more rigorously.

In ionospheric-modification experiments, the incoming heater wave acts as a clamp field (see Sec. V.C) of fixed amplitude at a given height, with the amplitude following the Airy pattern of Fig. 37 at near-normal incidence on the density gradient. Hence the frequency mismatch $\omega_C \propto (\omega_{HF} - \omega_p)$ in Eqs. (5.17) and (5.18) decreases to zero as the reflection point (where $\omega_p \approx \omega_{HF}$) is approached, then becomes negative in the region beyond. The theory discussed in Sec. VI.A implies that a decay cascade should be prominent for low altitudes where ω_C satisfies Eq. (6.8), but that modulational instabilities and collapse should be more important near the reflection point, where the inequality (6.8) is reversed.

Cheung *et al.* (1989, 1992) published height-integrated and height-resolved backscatter frequency spectra at particular wave vectors $\mathbf{k}_L$ both early and late during heating. The value of $\mathbf{k}_L$ is $2\mathbf{k}_R$ and is thus determined by the radar frequency ω_R and ω_p at the scattering height via the electromagnetic-wave dispersion relation (2.7). Early in the heating cycle Cheung *et al.*'s (1989, 1992) observations showed the presence of linear "free-mode" waves at the frequency $\omega_L(\mathbf{k_L})$ determined by the dispersion relation of Langmuir waves in a weak magnetic field. These waves correspond to the peaks at the right of Figs. 38(a) and 38(b), seen 0.5 ms and 4 ms into the heating pulse, respectively. The positions of these peaks were consistent with free-mode dispersion of waves with $\mathbf{k}_L = 2\mathbf{k}_R$ for plasma temperatures of 900 K and 1650 K, respectively, as the ionosphere was heated. A broad spectrum was seen below the heater frequency, showing no sign of discrete cascade-type structure. Cheung *et al.*'s (1992) height-resolved measurements showed that these spectra were confined to heights near the first Airy maximum of the heater, as shown in Fig. 37. At lower altitudes, the spectra were of the "below-threshold" type, so-named because they were previously interpreted as weak-turbulence spectra below the threshold for parametric decay.

Cheung *et al.* (1989) also published the fixed-**k**, Zakharov-simulation spectra shown in Figs. 27(a) and 27(b) for conditions pertaining to regions near the first Airy maximum in Fig. 37 and two different values of k. These spectra, obtained from 2D clamp-driven Zakharov simulations, show a remarkable resemblance to the experimental results of Figs. 38(a) and 38(b). Theoretical work (DuBois *et al.*, 1988, 1990; Russell *et al.*, 1988; DuBois and Rose, 1991) has shown that the broad spectrum seen below the heater frequency under these conditions is, indeed, associated with localized, collapsing waves, which nucleate directly from the pump. For this reason, it is sometimes called the "caviton continuum." These waves are trapped in density wells with $\delta N_e < 0$, corresponding to decreased local plasma frequencies (cf. the laboratory experiments of Tanikawa *et al.*, 1984, discussed in Sec. VIII.E). In essence, the overall frequency spectrum corresponds to that of waves on a vertical cut through Fig. 13(a) at fixed k—the only modes encountered are localized-modes at $\omega < \omega_p$ and free modes that satisfy the linear dispersion equation. The localized-mode spectrum is averaged over many collapsing packets and consequently does not show a discrete structure. The free modes are pumped either by beating of the heater wave with the evolving density cavities associated with collapsing wave packets, or by coupling to the time-varying localized fields themselves (DuBois *et al.*, 1990; Cheung *et al.*, 1992). The first, direct-conversion mechanism is dominant during nucleation, while the latter dominates during collapse. Cheung *et al.* (1992) verified that the free-mode frequency offset followed the expected dependence on the radar wave number and heater frequency.

As heating progresses the form of the backscatter spectra changes, with the broad continuum increasing in intensity, while the free-mode peak broadens somewhat but does not change much in intensity (Cheung *et al.*, 1992). This point is demonstrated in the log-linear plots of early and late height-integrated spectra shown in Figs. 39(a) and 39(b), respectively. The early spectrum shows two free-mode peaks, consistent with spatially localized emission from near the first and second Airy maximums in Fig. 37, plus a featureless continuum. In the late spectrum, the free-mode peaks are still visible with similar intensity, albeit broadened. However, the continuum has increased substantially in intensity and has developed three lines, situated approximately 1, 3, and 5 times the ion acoustic frequency below ω_{HF}. Cheung *et al.* (1992) argued that this behavior explains the apparent (relative) disappearance of free-mode lines seen by them and Fejer *et al.* (1991) in some cases after 20–30 ms of heating.

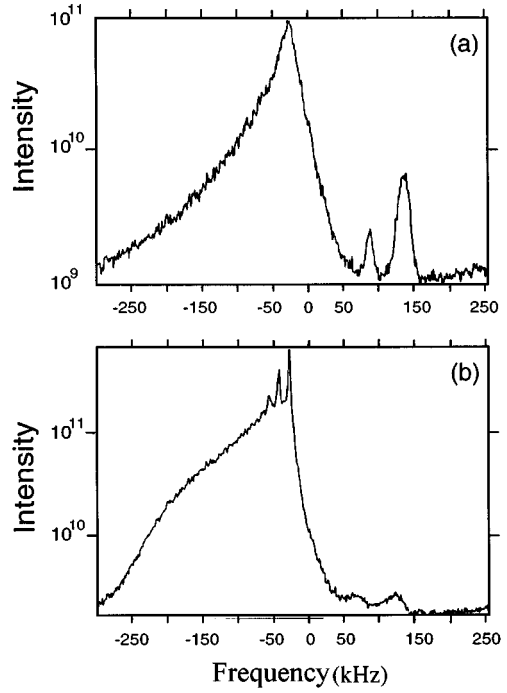

FIG. 39. Temporal evolution of Langmuir frequency spectra during long-pulse heating, from Arecibo observations (Cheung *et al.*, 1992): (a) 4 ms into the heater pulse; (b) 29 ms into the heater pulse. The heater frequency is at 0 on the horizontal axis.

In terms of strong-turbulence theory, the increasing intensity of the continuum is interpreted as being due to increasing intensity of strong turbulence in the heated region as heating continues (Cheung *et al.*, 1992). The "1:3:5" lines are interpreted as being due to scattering off Langmuir waves that have undergone repeated electrostatic decays prior to interaction with the radar. The broadening of the free-mode peaks is interpreted as being due to modification of the density gradient by the mean ponderomotive force of the Langmuir waves near the Airy peaks (Cheung *et al.*, 1992; DuBois *et al.*, 1993a, 1993b). Such modifications, estimated to be of the order of 1%, increase the range of free-mode frequencies within the Airy maximums, where strong turbulence is intense, and guarantee that matching can be achieved in these regions (see Fig. 12 of DuBois *et al.*, 1993b). Further evidence for modification of the density profile by the heater is the observation of decay spectra from altitudes that are nonmatching for these waves on the basis of an unmodified profile (Fejer *et al.*, 1991; DuBois *et al.*, 1993b).

Sulzer and Fejer (1994) carried out particularly clear height-resolved ionospheric-heating experiments at Arecibo using pulses of 5 ms each second to avoid the generation of density irregularities by the heater. They saw a weak cascade-type spectrum, followed 1–2 ms later by a spectrum of the type seen in Fig. 38, with components due to free modes and collapsing packets. In longer pulses (50 ms), decay spectra later reappeared, connected tentatively with the development of density irregularities in the plasma. These results, discussed in more detail by DuBois *et al.* (1996), were consistent with the strong-turbulence picture outlined above.

It should be stressed that weak-turbulence theory cannot predict the shapes of the spectra shown in Figs. 37–39 (DuBois *et al.*, 1990; Hanssen *et al.*, 1992; DuBois *et al.*, 1993a, 1993b). Hanssen *et al.* (1992) showed that the condition (6.8) gave a good estimate of the frequency (and hence height) offset for which decay-type spectra will be seen for a given clamp-field strength. They and DuBois *et al.* (1993b) also showed that the decay cascade is truncated to only a few peaks, as predicted from strong-Langmuir-turbulence simulations, whereas weak-turbulence theory would predict larger numbers of decays (Hanssen *et al.*, 1992; Stubbe *et al.*, 1992; DuBois *et al.*, 1993b). Hence a decay cascade and wave collapse can coexist, but the cascade does not usually extend to a $k=0$ condensate. Rather, the gaps between the decay peaks fill in and a continuum is formed, even where a cascade would kinematically be allowed (Hanssen *et al.*, 1992; DuBois *et al.*, 1993b). Observationally, Cheung *et al.* (1992) always found a number of decays consistent with the limit implied by Zakharov simulations, and often less than that predicted by weak-turbulence theory. Stubbe *et al.* (1992) also found only two decay peaks in data from Tromsø. When the decay-cascade condition of Eq. (6.8) is violated, continuum spectra with free-mode peaks were seen in simulations (Hanssen *et al.*, 1992).

Additional evidence for the occurrence of strong turbulence during ionospheric modification comes from the *ion-line* backscatter spectra. These spectra correspond to backscattering of the probe radar off low-frequency ion sound waves [see Figs. 36(c) and 36(d)] and consequently lie near the radar frequency ω_R. Weak-turbulence theory predicts two peaks at $\omega_R \pm k_S v_S$, where $k_S = 2k_R$ is the wave number of the ion sound wave responsible for the scattering. These peaks correspond to scattering off downgoing and upgoing ion sound waves, respectively. In the presence of strong turbulence, a third peak centered at ω_R is predicted to appear, due to scattering off low-k density wells associated with collapsing Langmuir packets (Hanssen *et al.*, 1992; DuBois *et al.*, 1993a, 1993b). Djuth *et al.*'s (1994) ion-line spectra showed such features, with a triple-line structure generated at the same altitudes as the broad continuum in the plasma line. No free-mode peaks were seen, but Hanssen *et al.* (1992) and DuBois *et al.* (1993a) showed that these would be unlikely to be visible because the frequencies of the probe radars used made them unresolvable or placed them in a range where the Langmuir waves would be heavily damped. Similar features were seen at Tromsø by Frey (1986) and Stubbe *et al.* (1992). At lower altitudes, only the two outer ion-line peaks were seen, in conjunction with decay-type spectra in the plasma line. These features were entirely consistent with the predictions of strong-turbulence theory (DuBois *et al.*, 1993b).

Most of the above discussion refers to Arecibo observations, particularly those by Cheung *et al.* (1989, 1992). Experiments with the EISCAT radars at Tromsø have

also provided insights into the mechanisms in operation during ionospheric modification, largely confirming those obtained from Arecibo. Some of these results have been discussed above, and further discussion is given by DuBois *et al.* (1993b). Kohl and Rietveld (1996) have recently published ion-line spectra from Tromsø that are consistent with the occurrence of strong turbulence.

Before we conclude this section, a few further points deserve mention: First, DuBois *et al.* (1990) and DuBois and Rose (1991) studied the possibility that correlations could develop between neighboring collapse sites, leading to novel spectral features resembling decay lines. DuBois *et al.* (1991) found that the special conditions required do not occur in ionospheric-heating experiments, but that related effects may be significant under less stringent conditions (DuBois *et al.*, 1993b). Second, backscatter decay peaks under strong-turbulence theory are much wider ($\sim 40°$ half-angle) than in the weak-turbulence approximation ($\sim 20°$), possibly explaining the experimental observability of backscatter spectra over a wider angular range than would otherwise be expected (DuBois *et al.*, 1990, 1993b).

G. Laser-plasma experiments

A laser beam incident on a region of increasing plasma density will undergo reflection and resonant absorption, just as for waves in radio-plasma and ionospheric-modification experiments. The principal motivation for study of laser-plasma interactions arises from attempts to achieve nuclear fusion by inertial confinement. In such experiments, a small ($\lesssim 0.1$ mm in diameter) pellet of fuel is compressed and heated by focused laser pulses with the aim of reaching fusion conditions with $N_e \gtrsim 10^{32}$ m^{-3} and $T_e \gtrsim 10^8$ K (Richardson, 1991; Yamanaka, 1991; Campbell, 1992). Early in compression, the fuel is ionized and the laser light heats and compresses the resulting plasma. Other applications are to x-ray lasers and novel particle accelerators (Tajima, 1996).

Much of the theory and experimental work on laser-plasma interactions has previously been reviewed (Sodha *et al.*, 1976; Kruer, 1988; Baldis *et al.*, 1991; Rubenchik and Zakharov, 1991; Campbell, 1992). Since some of these reviews are recent, this paper concentrates on aspects in which ponderomotive forces, nonlinear wave collapse (self-focusing), and/or strong turbulence are thought to have a role.

Rubenchik and Zakharov (1991) discussed existing experiments in which W reaches values of 0.01–0.1, or even higher. A rich variety of nonlinear processes can occur in laser-plasma interactions, including resonant absorption, electrostatic decay, modulational instabilities, stimulated Brillouin and Raman scattering, and two-plasmon decay in which a transverse wave of frequency $\omega_R \approx 2\omega_p$ decays into two Langmuir waves (Kruer, 1988; Baldis *et al.*, 1991; Campbell, 1992). Resonant absorption near the critical layer can lead to density-profile modification via the ponderomotive forces of the Langmuir waves generated (as suggested in connection with ionospheric modification), possibly followed by wave collapse or strong turbulence (Rubenchik and Zakharov, 1991). Ponderomotive effects can also split the laser beam into filaments via the so-called *filamentation instability*, in which a purely growing transverse density perturbation is driven by the electromagnetic ponderomotive force. The other processes are important to various aspects of the laser-plasma coupling, but will be largely ignored here for the reasons stated above. Figure 40 summarizes some of the main instabilities and their locations on the density profile (Kruer, 1988).

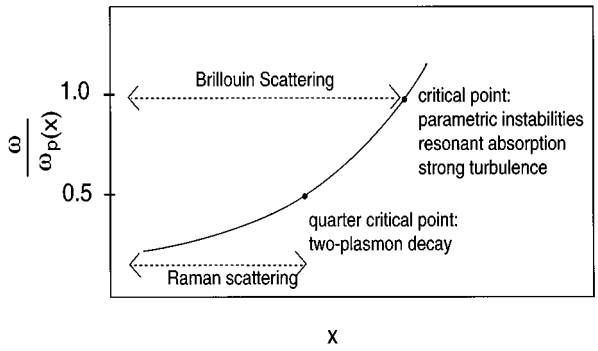

FIG. 40. Schematic of the main physical processes in laser-plasma interactions and their locations on the profile of $\omega_p(x)$ vs x. The laser frequency is ω_R.

As in radio-plasma and ionospheric-modification experiments, resonance absorption can occur at the critical layer in a laser-plasma system (Sec. VIII.E; Estabrook *et al.*, 1975; Kruer, 1988; Baldis *et al.*, 1991; Gavrilov *et al.*, 1995). Manes *et al.* (1977) confirmed that the absorption is maximal for p-polarized light at an angle where the wavelength equals the scale length along the direction of propagation, consistent with theoretical calculations by Thomson *et al.* (1978). Similar results were found by Maaswinkel *et al.* (1979). Density-profile modification by the ponderomotive force of the resulting Langmuir waves has been observed by Attwood *et al.* (1978), who also observed cratering of the critical surface at "hot spots" where the laser beam was more intense than average. Langdon and Lasinski (1983) used particle-in-cell simulations to show that density cavities can be formed near the critical surface and the *quarter-critical surface* where $\omega_R = 2\omega_p$, due to ponderomotive forces. This can lead to self-trapping of electromagnetic radiation, analogous to trapping of Langmuir waves in beam-plasma and radio-plasma experiments.

Much effort has been spent on studying the ponderomotive filamentation of laser beams in the underdense region where $\omega_R > \omega_p$. In this process, $T \rightarrow T' + S$, incident electromagnetic waves T decay into product electromagnetic waves T' plus purely growing transverse density perturbations S in the region to the left of the critical point in Fig. 40. Generation of the density perturbations is driven by the ponderomotive force of the electromagnetic waves (Kruer, 1988; Amin *et al.*, 1993; Andreev *et al.*, 1993; Chian and Rizzato, 1994) and the result is self-focusing of the transverse waves into re-

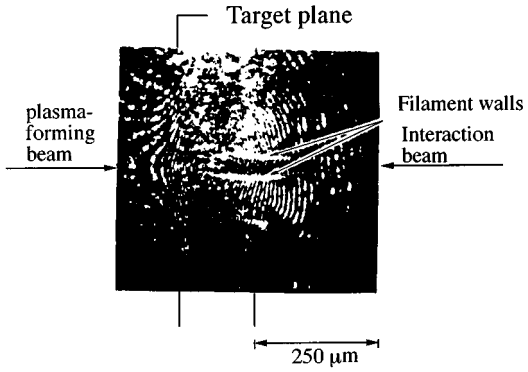

FIG. 41. Interferogram of laser-plasma experiment, showing a density channel formed by the beam, walled by regions of high density formed where material has been expelled from the channel (Wilks *et al.*, 1994).

gions of low density. This can result in the formation of laser foci in the plasma if a minimum critical power density is exceeded (e.g., Kelley, 1965; Akhmanov, 1966; Hora, 1969a, 1969b; Shearer and Eddleman, 1973; Nicholas and Sajjadi, 1986; Rubenchik and Turitsyn, 1987; Schmitt, 1991; Berger *et al.*, 1993). Alternatively, in *resonant filamentation* (Joshi *et al.*, 1982), two electromagnetic waves with frequencies much greater than ω_p and a frequency difference of ω_p beat and excite Langmuir waves L, which are then amplified by stimulated Raman scattering $T \rightarrow T' + L$. Then the ponderomotive force of the Langmuir waves drives the density variations and the formation of filaments. This process can be much more effective in forming filaments than direct filamentation because the ponderomotive force of Langmuir waves is much stronger than that of transverse waves, owing to their lower frequency [cf., the frequency dependence in Eq. (2.11)]. Formation of a focus corresponds to contraction of the filament to a singularity in the transverse direction, a process that is analogous to two-dimensional wave collapse. The minimum critical power density for focusing is analogous to the collapse threshold. We discuss these points further in Sec. IX.A.

Until recently, evidence for filamentation has been relatively scarce and indirect (Kruer, 1988). Indirect evidence has included observations of frequency shifts in reflected light (Tanaka *et al.*, 1984) and inferences from structure in x-ray pictures of the heated plasma. Filamentary structures have also been directly observed by various techniques (Baldis and Corkum, 1980; Herbst *et al.*, 1981; Stamper *et al.*, 1985; Young *et al.*, 1988; Wilks *et al.*, 1994). An example is shown in Fig. 41, showing high-density walls where material has been pushed to the edges of a low-density filament (Wilks *et al.*, 1994). Joshi *et al.* (1982) obtained strong evidence for resonant filamentation by using optical mixing of two lasers to excite Langmuir waves at their difference frequency. Raman scattering drove these waves to higher intensity and their ponderomotive force then drove filamentation.

If Langmuir waves generated by electromagnetic decay $T \rightarrow L + S$, two-plasmon decay $T \rightarrow L + L'$, or Raman scattering $T \rightarrow T' + L$ reach a sufficiently high intensity, Langmuir collapse can ensue. This can occur either near the critical layer in Fig. 40 or in the underdense region to the left, depending on the process that generates the Langmuir waves. Ultimately the state becomes turbulent if enough collapsing packets coexist (Rose *et al.*, 1987; Rubenchik and Zakharov, 1991; Sagdeev *et al.*, 1991; Kolber *et al.*, 1993; Bezzerides *et al.*, 1993; DuBois *et al.*, 1995b).

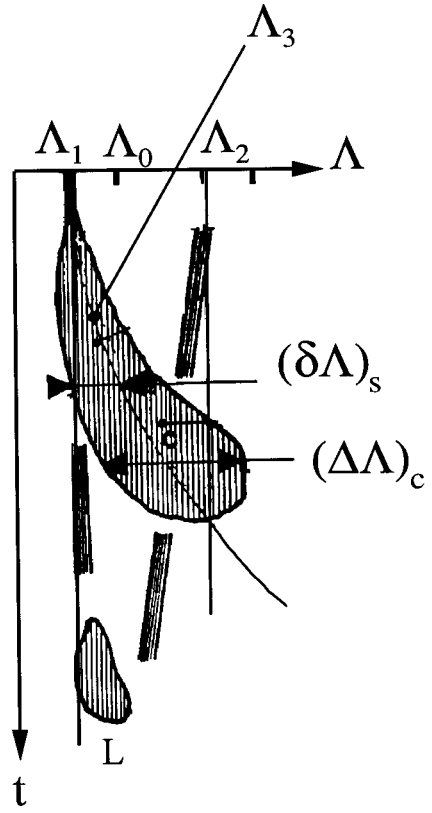

FIG. 42. Analyzed tracing of a time-resolved second-harmonic spectrum from a laser-produced plasma (Briand *et al.*, 1990), showing emitted wavelength Λ vs time t, with t increasing toward the bottom.

Baldis *et al.* (1978) saw profile steepening due to ponderomotive forces at the quarter-critical layer. Briand *et al.* (1990) and Dahmani *et al.* (1991) found evidence of Langmuir wave collapse near the critical density by observing second-harmonic spectra produced by Raman scattering,

$$T + L \rightarrow T', \tag{8.7}$$

where T denotes a pump wave, L a Langmuir wave, and T' a scattered second-harmonic wave. Figure 42 shows an analyzed tracing of a time-dependent second-harmonic spectrum obtained by Briand *et al.* (1990), with time increasing toward the bottom and wavelength toward the right. The wavelength corresponding to emission at exactly twice the laser frequency ω_R is marked Λ_0. Initially, emission is seen at Λ_1, corresponding to Eq. (8.7) for Langmuir waves L produced slightly below ω_R by the decay $T \rightarrow L + S$, where S is an ion sound wave. [This corresponds to emission of waves T'

slightly below $2\omega_R$ in Eq. (8.7), but a Doppler blueshift connected to the experimental detection conditions yields $\Lambda_1 < \Lambda_0$ in this experiment (Briand *et al.*, 1990).] At low incident intensities ($\lesssim 10^{18}$ W m^{-2}) this was the only emission seen. At higher intensities, the plasmons L underwent the electrostatic decay $L \rightarrow L' + S'$, producing emission at Λ_2 in Fig. 42. Briand *et al.* (1990) discussed ponderomotive effects that would tend to blueshift Λ_2, but not Λ_1, as seen in Fig. 42. At still higher intensities, $\sim 5\times 10^{19}$ W m^{-2}, a spectral feature Λ_3 was observed to commence at Λ_1, then redshift to larger Λ, broadening during this phase, as seen in Fig. 42. It terminated quite suddenly and was followed by another somewhat similar feature, labeled L in Fig. 42, after a brief interval. Briand *et al.* (1990) argued that the former feature was consistent with Langmuir collapse: the redshift corresponded to the progressive downshift in the frequency of collapsing Langmuir waves as their density cavity deepened (see Sec. V.E), while the broadening was attributed to dynamical effects proportional to the central density depression. Dahmani *et al.* (1991) found very similar high-intensity results to those of Briand *et al.* (1990), except that they observed two bursts of radiation subsequent to the main one, possibly connected with collapse of two separate populations of Langmuir waves.

While many aspects of the results of Briand *et al.* (1990) and Dahmani *et al.* (1991) are consistent with wave collapse, their estimate of a maximum density perturbation of $\Delta N_e/N_e = -3\times 10^{-3}$ appears very small in magnitude compared to typical values of $\gtrsim 0.1$ seen in particle-in-cell simulations, for example (see Sec. VII.B). Briand *et al.* (1990) suggested that this could possibly have been due to a transition to supersonic collapse, in which the density response is weaker.

More recently, Meyer and Zhu (1993) measured the k-space distribution of Langmuir waves excited by the two-plasmon decay instability, finding that the wave activity spreads over a wide zone. Comparison with the results of Zakharov-equation simulations (DuBois *et al.*, 1995b, 1996) showed good agreement for relevant driving parameters, with the simulations implying that this regime is probably collapse dominated to account for the broad k-space spectrum.

An important consequence of resonant absorption, filamentation, and Langmuir collapse is the formation of intense, localized, coherent fields on short scales. If electrons from the ambient plasma can cross these structures in a time of the same order as their oscillation period, strong transit-time interactions will result. These interactions can dissipate the fields rapidly (e.g., as seen in the burnout phase shown in Fig. 42) and accelerate electrons to form energetic tails (Friedberg *et al.*, 1972; Morales and Lee, 1974; Valeo and Kruer, 1974; Bezzerides and DuBois, 1975; Forslund *et al.*, 1975; Ishida and Nishikawa, 1975; DeNeef and DeGroot, 1977; Kovrizhnykh and Sakharov, 1979; Rozanov and Shumskiĭ, 1986, 1987; Gavrilov *et al.*, 1995; Melatos *et al.* 1996). Experiments have observed such acceleration, attributed to acceleration in resonance-absorption regions (Estabrook *et al.*, 1975; Kruer, 1988; Baldis *et al.*, 1991). These electrons can impede compression of inertial confinement fusion targets by penetrating and prematurely heating the core of the target. Hot electrons unequivocally associated with arrest of Langmuir collapse have not yet been observed, so we leave discussion of this topic at this point.

IX. GENERALIZATIONS AND APPLICATIONS TO RELATED SYSTEMS

Many of the ideas of Langmuir collapse and strong turbulence are applicable to other nonlinear systems involving waves in solids, fluids, and magnetized plasmas in which magnetic effects dominate in wave collapse and strong turbulence. Applications to optical systems, including fiber optics, have been pursued for decades, while space-plasma and auroral applications are more recent. Astrophysical applications to date have been very few, and this is a promising area for future investigation, since systems abound in which energetic waves are be generated (e.g., jets, shocks, pulsar magnetospheres). Other applications of related ideas have also been made to the dynamics of deep-water waves, for example.

This section outlines a variety of applications and potential applications of the concepts of wave collapse and strong turbulence, sketching relevant generalizations of the theory where appropriate. Some of these applications have been the subject of extensive experimental investigation, while others are still in rudimentary theoretical form. The emphasis here is primarily on the main ideas and current status of the fields in question, rather than on their historical development.

A. Nonlinear optics

Nonlinear optics has grown into a huge field since the invention of the laser in 1960 provided a ready source of high-intensity, near-monochromatic light. Some recent texts on this subject include those by Shen (1984), Butcher and Cotter (1990), Saleh and Teich (1991), and Boyd (1992).

Nonlinear refractive-index enhancements by intense electromagnetic waves were discussed in early papers by Askar'yan *et al.* (1962), Chiao *et al.* (1964), and Kelley (1965), for example, and it was noted that these enhancements could lead to self-focusing of a laser beam because of the tendency of the waves to refract toward the most intense region at the center of the beam. In dielectrics, this effect can occur because of nonlinearities in the response of atomic electrons to high fields, i.e., anharmonic restoring forces. In semiconductors, nonlinearities can be due to ponderomotive forces, energy-dependent changes in carrier mobility, or localized heating of the charge carriers, leading to their expulsion from the beam and a correspondingly lowered local plasma frequency (Sodha *et al.*, 1976). Such *thermal nonlinearities* can also be significant in laser-plasma interactions (Perkins and Valeo, 1974; Kruer, 1985, 1988; Schmitt, 1988, 1991, 1993; Baldis *et al.*, 1991; Richard-

son, 1991; Yamanaka, 1991; Ghanshyam and Tripathi, 1993). In laser-plasma contexts, the oscillation velocity of particles in the laser field can be so great that their relativistic mass increase gives rise to a significant enhancement of the refractive index by reducing the local plasma frequency, since $\omega_p \propto m_e^{-1/2}$ (Akhiezer and Polovin, 1956; Kaw and Dawson, 1970; Max *et al.*, 1974; Tsintsadze *et al.*, 1979; Berezhiani *et al.*, 1980; Kruer, 1988; Borisov *et al.*, 1990; Brandi *et al.*, 1993; Vladimirov *et al.*, 1995).

In many optical materials, the response of the medium to changes in the optical fields is essentially instantaneous, and one can write the refractive index as

$$n = n_0 + n_2 E^2, \tag{9.1}$$

where n_0 and n_2 are constants, with n_2 embodying the effects discussed in the previous paragraph. Such media are termed *Kerr media*. Assuming steady-state propagation in the z direction in a Kerr medium, the only case considered here, and slow amplitude variations in the z direction, one can write the electric field $\boldsymbol{\mathcal{E}}$ in terms of a slowly varying envelope $\mathbf{E}$ (see Sec. II.B)

$$\boldsymbol{\mathcal{E}} = \mathbf{E}(z, \mathbf{R}) e^{i(kz - \omega t)}, \tag{9.2}$$

where $\mathbf{R}$ denotes the pair of coordinates perpendicular to the z axis. One then finds the nonlinear Schrödinger equation obeyed by the envelope

$$2ik \frac{\partial \mathbf{E}}{\partial z} - \nabla_\perp^2 \mathbf{E} = \frac{n_2}{\eta_0} k^2 |\mathbf{E}|^2 \mathbf{E}, \tag{9.3}$$

with $\eta_0 = (\mu_0/\epsilon_0)^{1/2} \approx 377\Omega$ (Saleh and Teich, 1991). Note that this equation is of the same form as the two-dimensional version of the nonlinear Schrödinger equation (2.20), with $z/2k$ playing the role of time.

If the waves are initially plane polarized, Eq. (9.3) can be reduced to a scalar equation for a single-component field, which can be regarded as the linear eigenfunction of a refractive-index structure of magnitude $\propto |\mathbf{E}|^2$. Indeed, this is by far the most commonly used approximation in nonlinear optics. Another common simplification is to separate the solution into the product of a part that depends only on $\mathbf{R}$ and a part that is a function only of z. This approximation is rigorously justified in optical fibers, for example, where the fiber boundaries reduce the problem to strictly one-dimensional propagation of modes with transverse structure (however, there is no transverse self-focusing in this case). In other cases, it is only valid if the transverse structure of the beam is slowly changing.

Equation (9.3) has been extensively used to study optical self-focusing in dielectrics, semiconductors, and plasmas. It has been shown that self-focusing occurs for beam powers exceeding a critical value

$$P_{\text{crit}} \approx \frac{(1.22\lambda)^2 c}{128 n_2}, \tag{9.4}$$

for a laser wavelength λ (Chiao *et al.*, 1964; Kelley, 1965; Sodha *et al.*, 1976; Shen, 1984), this value being analogous to the collapse threshold derived in Sec. V.D, since

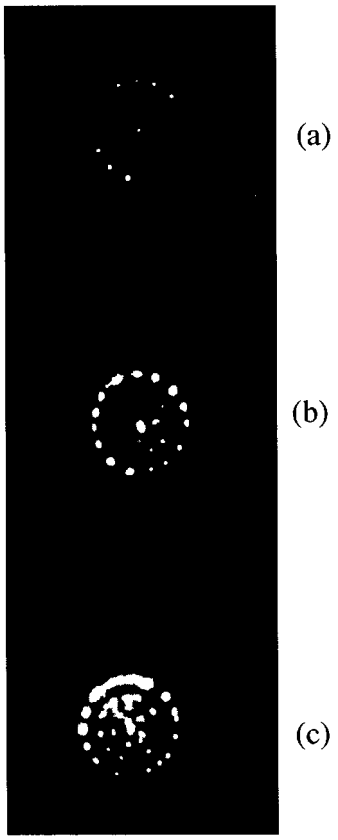

FIG. 43. Experimental results for the pattern of focal spots for a laser beam in carbon disulfide, with intensity increasing toward the bottom (from Campillo *et al.*, 1973). Some extraneous spots outside the focal region in the original figure have been removed.

$P \propto |\mathbf{E}|^2 a^2$, where a is the radius of the beam. Geometric optics and virial-type analyses similar to those yielding Eqs. (4.11) and (4.12) have been used to estimate the focusing distance z_c (Kelley, 1965; Akhmanov *et al.*, 1966; Hora, 1969a, 1969b; Lugovoĭ and Prokhorov, 1973; Sodha *et al.*, 1976). Considerable theoretical effort has been devoted to studying axisymmetric beams, sometimes following them through several foci, with the addition of dissipative processes—including large-angle scattering that removes energy from the beam—to Eq. (9.3) to prevent the formation of singularities (Dyshko *et al.*, 1972). It has also been shown that a beam with N times the critical power will break into $\sim N$ filaments. Figure 43 contains results obtained by Campillo *et al.* (1973), showing the breakup of a broad beam into numerous filaments in a cell filled with carbon disulfide. Self-focusing can lead to permanent damage to solid dielectrics and to bubble formation in liquid ones, owing to the high focal intensities attained. Dissipation of the filaments at the end of collapse can be through true dissipation and heating of the medium or simply through scattering of the light to large angles at which it escapes from the beam.

One problem that does not appear to have been studied analytically in the literature is the evolution of an initially supercritical beam that breaks into many fila-

ments, which then focus, partly dissipate, then refocus at larger z. Such a system is mathematically equivalent to undriven 2D strong turbulence governed by the nonlinear Schrödinger equation, with z playing the role of time; it is also potentially relevant to laser-plasma and laser-solid systems. The possibility of testing strong-turbulence theory using laser-solid interactions is an attractive one, since these systems are often more easily diagnosed than plasma systems. Robinson and Newman (1991b) developed a two-component theory of strong turbulence governed by the nonlinear Schrödinger equation, analogous to the theory discussed in Sec. VI for turbulence subject to the Zakharov equations. They found that the energy density in undriven turbulence decays according to

$$\langle |\mathbf{E}|^2 \rangle \propto z^{-\rho} \tag{9.5}$$

at large z, where ρ is a ratio of small integers. They were unable to determine the value of ρ theoretically because there is as yet no detailed theory of the formation of coherent wave packets within the nonlinear Schrödinger equations (see below), but found numerical values very close to 1/3 or 2/5 in two dimensions, depending on the level of $\langle |\mathbf{E}|^2 \rangle$. If experimentally observable, the power-law decay in Eq. (9.5) of the intensity of a laser beam would provide an important test of the theory and numerical calculations.

It is perhaps paradoxical that the theory of turbulence governed by the nonlinear Schrödinger equation is less developed than that for the Zakharov equations. The reason is that the nonlinear refractive index changes on the same time scale as the electric-field envelope in the nonlinear Schrödinger equation, whereas inertia in the second Zakharov equation leads to the appearance of remnant refractive-index enhancements (density wells in the plasma case; see Sec. V.G) after burnout of a collapsed field. In the latter case, it is straightforward to determine the statistics of trapped fields that are derivable from a potential, i.e., $\mathbf{E}=-\nabla\Phi$ (Newman *et al.*, 1989, 1991), but more work needs to be done if $\mathbf{E}$ is not curl free. Signs of nucleation have been seen in simulations of the nonlinear Schrödinger equation (Newell *et al.*, 1988a, 1988b), but no detailed theory exists. Robinson and Newman (1991b) have interpreted changes of exponents in the scaling of nonlinear Schrödinger equation turbulence to changes in the mechanism of wave-packet formation. For example, in some regimes, packets may form from random fluctuations in an incoherent field, and the statistics of random fields would then determine the distribution of packet structures (Rose and DuBois, 1993a, 1993b). In any event, further development of these ideas is needed to understand the field statistics. Propagation of lasers in solids or liquids provides a promising testing ground for any theoretical developments in this area.

Going beyond the nonlinear Schrödinger equation, it is possible to include inertia in the response of the refractive index to variations in the electric field. This inertia can be due to the nonzero mass of the particles that must respond, as in plasmas, thus leading to Zakharov-like equations (Rose and DuBois, 1993b; Rose, 1995). Alternatively, thermal inertia may be significant, due to the nonzero heat capacity of the material. Thermal inertia leads to a separate equation for the temperature response, analogous to the low-frequency Zakharov equation (2.18), but involving the thermal conductivity and heat capacity, rather than ion-sound-wave quantities (Sodha *et al.*, 1976; Schmitt, 1988, 1991, 1993; Kruer, 1988). Equations of these types have been extensively applied to laser-plasma interactions (see Sec. VIII.C), in which thermal and/or ponderomotive self-focusing can be significant. The general ideas developed for testing the stability of fields within the Zakharov equations can be expected to be of use in analogous optical problems. Self-similar collapse solutions are also of relevance to description of self-focusing. Other types of nonlinearities that have been studied recently include one relevant to *self-written waveguides* in which photons cause gradual buildup of damage to a material, leading to a permanent refractive-index change. In a somewhat more general case, in which the refractive-index change relaxes on a characteristic time scale τ, one has (Shen, 1984)

$$\frac{\partial n_2}{\partial t} \propto |\mathbf{E}|^2 - \frac{n_2}{\tau}. \tag{9.6}$$

Stability and evolution of such waveguides can be studied using methods analogous to those employed for the Zakharov equations. See, for example, Kuznetsov *et al.* (1986).

B. Generalizations to magnetized plasmas

An obvious direction in which to generalize the theory of Langmuir collapse is to incorporate the effects of an ambient magnetic field on the dispersion of the linear waves, the ponderomotive force, and dissipation mechanisms, particularly where these effects dominate during wave collapse. Such generalizations have been carried furthest in the case of upper-hybrid and lower-hybrid waves, but Alfvén, whistler, and other waves have also been considered. Some applications of these generalizations are considered in Sec. IX.C.

1. Upper-hybrid waves

Upper-hybrid (UH) waves are high-frequency waves in a magnetized plasma that reduce to Langmuir waves in the limit that the magnetic field $\mathbf{B}$ vanishes. Their dispersion relation is

$$\omega^2 = \omega_p^2 + 3k^2V_e^2 + \frac{\Omega_e^2\omega_p^2}{\omega_p^2-\Omega_e^2}\sin^2\theta, \tag{9.7}$$

where $\Omega_e = eB/m_e$ is the electron cyclotron frequency and θ is the angle between $\mathbf{k}$ and $\mathbf{B}$. If $\Omega_e^2/\omega_p^2 \ll 1$, magnetic effects on the low-frequency waves can be neglected and the dispersion relation (2.1) remains a good approximation. Assuming a magnetic field along the z

axis, Lipatov (1977) wrote down dimensionless equations for the envelope potential Φ. These equations were equivalent to

$$\nabla^2(i\Phi_t+\nabla^2\Phi)-\sigma\nabla_\perp^2\Phi=\nabla\cdot(n\nabla\Phi) \tag{9.8}$$

for the high-frequency oscillations, with Eq. (2.18) assumed for ion sound waves with $\hat{\gamma}_S=0$; here, $\sigma=\Omega_e^2/2\omega_p^2$ for $\omega_p^2\gg\Omega_e^2$ and $\nabla_\perp$ is the component of the gradient operator perpendicular to the z axis, which denotes the parallel direction in what follows.

Almost all analysis of upper-hybrid collapse and strong turbulence has been carried out using the adiabatic limit for the density response, in which $n=-|\nabla\Phi|^2$. However, some numerical work has solved Eqs. (9.8) and (2.18). It can be shown that upper-hybrid wave packets are unstable to collapse if they exceed a threshold of the form $Wl_\parallel^2/\lambda_D^2=\Theta$ and that they follow self-similar collapse scalings (Krasnosel'skikh and Sotnikov, 1977; Lipatov, 1977; Shapiro and Shevchenko, 1984; Kuznetsov *et al.*, 1986; Kuznetsov and Škorić, 1988a, 1988b; Hadžievski *et al.*, 1990; Robinson, 1996a). Kuznetsov and Škorić (1988a, 1988b) showed that the fastest—and hence dominant—collapse would be subsonic and weak, not energy conserving, a point confirmed by numerical calculations by Hadžievski *et al.* (1990). Moreover, nucleation tends to result in oblate wave packets, having **E** predominantly parallel to **B**, that flatten further as they collapse (Kuznetsov and Škorić, 1988a, 1988b; Robinson, 1996a). Robinson (1996a) termed such collapse *oblate collapse* and showed that it was characteristic of a broader range of wave equations. It contrasts with his class of *isotropic-collapse* models, in which the parallel and perpendicular spatial scales of a wave packet contract in proportion to one another, as typified by Langmuir collapse. Robinson, Melatos, and Rozmus (1996a, 1996b) and Melatos and Robinson (1996) discussed arrest of upper-hybrid collapse via transit-time interactions.

Lipatov (1977) studied the collapse of a single upper-hybrid wave packet using Eqs. (9.8) and (2.18) without damping. Likewise, using 2D simulations that incorporated a weak magnetic field, Goldman *et al.* (1981) showed that random upper-hybrid turbulence will evolve into oblate collapsing wave packets. They also showed that this collapse can be delayed relative to unmagnetized collapse. Note that weak magnetic fields were actually incorporated in some of the applications discussed in Sec. VIII to perturb away from the unmagnetized case; the relevant waves could be termed weakly magnetized Langmuir waves, since magnetic effects were not dominant in collapse.

Akimoto (1989, 1995) and Pelletier *et al.* (1988) showed that the nature of upper-hybrid parametric instabilities changes profoundly for $\Omega_e>\omega_p$, where the last term in Eq. (9.7) changes sign, arguing that a phase transition occurs in strong Langmuir turbulence at the point $\Omega_e=\omega_p$, with little role for collapse in the high-B limit. Newman *et al.* (1994a) confirmed this point numerically for $D=2$, with the addition of damping to Eq. (9.8), showing that beam-driven turbulence will only cascade to form a condensate for $\Omega_e<\omega_p$; otherwise, damping truncates the cascade and strong turbulence is not observed. For $\Omega_e<\omega_p$ they observed turbulence consisting of oblate collapsing wave packets amid a sea of propagating Langmuir waves, closely analogous to the case of Langmuir turbulence (see Sec. VI). It should be noted that, in the case $\Omega_e>\omega_p$, the branch of the dispersion given by Eq. (9.7) actually connects continuously to the *lower-hybrid* dispersion curve. Thus, in this case, it is more appropriate to speak of magnetized Langmuir turbulence than upper-hybrid turbulence. Robinson (1996a) developed a two-component model of strong turbulence involving oblate collapse. Restricting attention to $\Omega_e<\omega_p$, or cases in which the condensate or collapsing packets are driven directly, he found the scalings listed in the fifth column of Table III. Scalings for isotropic collapse are given in the third column for comparison.

2. Lower-hybrid waves

Magnetized plasmas also support *lower-hybrid* (LH) waves near the lower-hybrid frequency ω_{LH}, with $\omega_{LH}\approx\omega_p(m_e/m_i)^{1/2}$ for $\Omega_e\gg\omega_p$ and $\Omega_{LH}\approx\Omega_e(m_e/m_i)^{1/2}$ in the opposite limit (Melrose, 1986a). Musher and Sturman (1975), Sturman (1976), and Sotnikov *et al.* (1978) derived Zakharov-type equations for the nonlinear interaction between lower-hybrid waves and ion sound waves, taking into account magnetic modifications to the ponderomotive force (for more recent work on this topic, see Lamb *et al.*, 1983). In dimensionless form, these can be written in terms of the potential Φ as

$$\nabla_\perp^2(i\Phi_t+\nabla_\perp^2\Phi)-\rho\Phi_{zz}=i(\nabla\Phi\times\nabla n)_z, \tag{9.9}$$

$$\frac{\partial^2 n}{\partial t^2}-\nabla^2 n=i\nabla^2|\nabla\Phi^*\times\nabla\Phi|_z, \tag{9.10}$$

where damping has been omitted for simplicity and $\rho\sim(m_i/m_e)^{1/2}$ is a constant. Most theoretical investigations of lower-hybrid collapse and turbulence have used the adiabatic approximation in which $n=-i|\nabla\Phi^*\times\nabla\Phi|$. Tam and Chang (1995) noted important limitations to the use of Eqs. (9.9) and (9.10) in two dimensions, arguing that some essential terms have been omitted in that case.

Musher and Sturman (1975) showed numerically that lower-hybrid waves can collapse, in accord with theoretical analyses (Sturman, 1976; Shapiro and Shevchenko, 1984; Kuznetsov *et al.*, 1986), which yielded a threshold of the form $Wl_\perp^2/\lambda_D^2=\Theta$. Initial wave packets tend to be prolate, with their long axes along **B** and their electric fields primarily perpendicular to **B**. Kuznetsov and Škorić (1988a, 1988b) showed that the fastest collapse is weak, subsonic collapse, with progressively increasing elongation as collapse continues. Robinson (1996a) termed such collapse *prolate* and showed that it was representative of collapse under a broader range of wave equations, complementing the other classes of isotropic and oblate collapse. Using the nucleation picture,

TABLE III. Scalings $A \sim B^C$ in isotropic, prolate, and oblate wave collapse and strong turbulence, assuming the fastest collapse scenario and $m=1$ (after Robinson, 1996a). Notes: (1) inertial range; (2) steady-state turbulence; (3) small k_b; (4) large k_b; (5) relaxation of undriven turbulence; (6) additional factor of $\ln(W_f/\langle W\rangle)$ in the 2D isotropic case; (7) $E<\langle W\rangle$; (8) $\langle W\rangle<E<\langle W\rangle^{1/2}$; (9) the result in the third column corrects a misprint in Robinson's (1996a) table.

A	B	C (Isot.)	C (Prol.)	C (Obl.)	Notes
$l_\parallel$	τ	1/2	1	1/2	1
$l_\perp$	τ	1/2	1/2	1	1
$\min l_{\parallel,\perp}$	τ	1/2	1/2	1/2	1
Φ_0	τ	0	0	0	1
E_0	τ	$-1/2$	$-1/2$	$-1/2$	1
N	τ	$(D-2)/2$	$(D-1)/2$	$(2D-3)/2$	1
N_P	$\langle W\rangle$	$D/2$	$(D+1)/2$	$(2D-1)/2$	2
T	$\langle W\rangle$	-1	-1	-1	2
U	$\langle W\rangle$	0	0	0	2
P_{out}	$\langle W\rangle$	$(D+2)/2$	$(D+3)/2$	$(2D+1)/2$	2
$\langle W\rangle$	Γ	$2/D$	$2/(D+1)$	$2/(2D-1)$	2,3
$\langle W\rangle$	Γ	$4/(D+2)$	$4/(D+3)$	$4/(2D+1)$	2,4
$\langle W\rangle$	t	$-2/D$	$-2/(D+1)$	$-2/(2D-1)$	5
$\langle n^2\rangle$	$\langle W\rangle$	2	2	2	2,6
$P(E)$	E	$2D-1$	$2D-1$	$2D-1$	2,7
$P(E)$	E	$2D-1$	$2D-3$	1	2,8
$P(E)$	E	$-(D+2)$	$-(D+3)$	$-(2D+1)$	1,2
$P(n)$	n	$-(D+3)/2$	$-(D+4)/2$	$-(D+1)$	1,2
$W(\mathbf{k})$	$k_\parallel$	$-2D$	$-(D+1)$	$-2(2D+1)$	1,2
$W(\mathbf{k})$	$k_\perp$	$-2D$	$-2(D+2)$	$-(2D+1)$	1,2,9
$\lvert n(\mathbf{k})\rvert^2$	$k_\parallel$	$-2(D-1)$	$-D$	$-4(D-1)$	1,2
$\lvert n(\mathbf{k})\rvert^2$	$k_\perp$	$-2(D-1)$	$-2D$	$-2(D-1)$	1,2

he also developed a two-component model of strong lower-hybrid turbulence, which yielded the scaling exponents given in the fourth column of Table III. Shapiro *et al.* (1993, 1995) carried out extensive simulations of wave collapse and strong lower-hybrid turbulence. They confirmed theoretical predictions of prolate wave packets in two and three dimensions, followed collapse and arrest, and observed renucleation in turbulence. Robinson, Melatos, and Rozmus (1996a) showed analytically that the parallel scale of lower-hybrid collapse is so great that it is difficult for these packets to reach their self-similar form, a result that is also relevant to the perpendicular scale of collapsing upper-hybrid packets. They and Melatos and Robinson (1996) also showed that the arrest of such packets is the result of close competition between transit-time damping by ions and electrons, with the dominant mechanism depending on the precise axial ratio of the collapsing packet (Melatos and Robinson, 1996).

3. Other generalizations

A range of other systems can exhibit wave collapse and strong-turbulence effects, but space permits only the briefest of mentions here. For example, systems with higher-order nonlinearities, such as $n \propto |\mathbf{E}|^4$, can exhibit collapse (Zakharov, Kosmatov, and Shvets, 1989). A second example is the system of Taniuti and Washimi (1968), involving coupled plasma hydromagnetic waves, in which modulational instabilities were found. Hasegawa (1970) studied modulational instabilities of coupled cyclotron and magnetohydrodynamic waves in plasmas. Karpman and Stenflo (1988) showed that a system consisting of whistler and magnetosonic waves satisfies the nonlinear Schrödinger equation in an appropriate limit. Spangler and Sheerin (1982, 1983) investigated soliton formation and collapse of Alfvén waves in astrophysical contexts. Kuznetsov *et al.* (1986) and Relke and Rubenchik (1988) also discussed interaction of high- and low-frequency waves in magnetized plasmas in some detail. Stenflo and Shukla (1990) investigated modulational instability and nucleation of Langmuir waves in weakly ionized plasmas.

Leaving plasma physics and optics, Benjamin and Feir (1966) showed that trains of deep-water waves were modulationally unstable. Davey and Stewartson (1974) showed that surface waves on water of finite depth satisfy Zakharov-like equations and hence are also subject to modulational instability. Two-dimensional instabilities of plane waves have been studied by Laedke *et al.* (1982) and Blaha *et al.* (1987).

C. Applications to magnetized plasmas

We now turn briefly to some recent applications of the magnetized-plasma generalizations of Langmuir wave collapse and strong turbulence discussed in Sec. IX.B.

1. Auroral applications of lower-hybrid waves

Intense packets of lower-hybrid waves, often localized in density depressions, have been observed at auroral latitudes by the *Viking* and *Freja* satellites and sounding rockets such as TOPAZ 3, at altitudes ranging from 500 to 13 000 km (Pottelette *et al.*, 1988, 1992; Arnoldy *et al.*, 1992; Kintner 1992; Kintner *et al.* 1992; Vago *et al.*, 1992; Dovner *et al.*, 1994; Eriksson *et al.*, 1994; Lynch *et al.*, 1994). These waves appear to be localized in elongated structures, aligned with the magnetic field, with electric fields primarily perpendicular to **B**. The waves are electrostatic and their frequency is reduced inside density cavities, consistent with trapping in localized eigenmodes.

Theories based on lower-hybrid solitons have explained some aspects of particle acceleration in the auroras (Retterer *et al.*, 1986, 1994; Chang, 1993; Lynch *et al.*, 1994), but there is controversy over various aspects of the theories advanced and their relationship to observations. Specifically, some theories have assumed that the density depressions are the result of ponderomotive pressure of the localized lower-hybrid waves; however, it does not appear that the ponderomotive force is great enough to produce the observed depressions (Singh, 1994; Shapiro *et al.*, 1995; Robinson, Melatos, and Rozmus, 1996a, 1996b). Alternative theories have been advanced, in which the lower-hybrid waves nucleate in preexisting density depressions formed by some other mechanism (Robinson and Rozmus, 1994; Seyler, 1994; Singh, 1994; Robinson, Melatos, and Rozmus, 1996a, 1996b). Alternatively, it has been suggested that many collapses at a given site may ultimately deepen the density well to the observed levels, or that the discrepancy is the result of very large inaccuracies in density measurements (Shapiro *et al.*, 1995).

Robinson, Melatos, and Rozmus (1996b) recently reexamined the relationship between wave-collapse theory and *in situ* observations of localized lower-hybrid waves associated with density depressions. They found that the observed packets all matched or exceeded the predicted collapse threshold for lower-hybrid waves, while their observed scale lengths also lay between the predicted nucleation and arrest scales. Inconsistencies with theory were that the size of the density perturbations was far too large to be accounted for by the ponderomotive force of the lower-hybrid waves, and a theoretical prediction of equal numbers of positive and negative density perturbations (Shapiro *et al.*, 1993; Robinson, Melatos, and Rozmus, 1996a, 1996b) was not borne out by observations, which were dominated by density depressions. They concluded that, if wave collapse occurs, it commences with packets that have nucleated in wells produced by a mechanism other than the ponderomotive force of the trapped lower-hybrid waves themselves although this mechanism may be triggered by the trapped waves, as was Singh's (1994), mechanism. Further work is necessary to identify the mechanism that produces the observed depressions (or, alternatively, gross inaccuracies in the density measurements), and this field remains highly controversial.

Another open question in auroral physics is how to explain the 100-m scale of the finest auroral arcs, produced by localized downgoing streams of accelerated electrons (McFadden *et al.*, 1990; Borovsky, 1993). Borovsky (1993) showed that none of 22 mechanisms he considered could explain this minimum scale. Lynch *et al.* (1994), Robinson and Rozmus (1994), and Robinson, Melatos, and Rozmus (1996b) showed that lower-hybrid collapse could produce scales of this order at arrest, simultaneously accelerating electrons. Alternatively, lower-hybrid collapse may modulate a concurrently operating acceleration mechanism on scales similar to the arrest scale. This appears to be a promising area for further investigation.

2. Auroral and coronal applications of upper-hybrid waves

In auroral regions and the lower solar corona, the electron cyclotron frequency can be of the same order as the plasma frequency. Under such circumstances, magnetic effects on Langmuir dispersion are strong and it is more appropriate to consider the behavior of upper-hybrid waves excited, for example, by beam instabilities. Type-III electron beams must propagate through the lower corona, where $\Omega_e \gtrsim \omega_p$ can be satisfied, before reaching interplanetary space (see Fig. 31). Similarly, intense streams of accelerated electrons have been observed in auroral regions (McFadden *et al.*, 1990), where $\Omega_e \gtrsim \omega_p$, simultaneously with enhanced levels of waves near the plasma frequency.

Newman, Goldman, and Ergun (1994a, 1994b), Newman, Goldman, Ergun, and Boehm (1994), and Goldman and Newman (1994) simulated beam-driven upper-hybrid turbulence, using Zakharov-type equations, for various values of Ω_e/ω_p. They found that strong turbulence is only relevant to cases with $\Omega_e < \omega_p$, consistent with the results of Pelletier *et al.* (1988) and Akimoto (1989, 1995). In the opposite case, the waves are magnetized Langmuir waves rather than upper-hybrid waves, the decay cascade is truncated, and modulational instability is suppressed (see Sec. IX.B). Newman, Goldman, and Ergun (1994a) noted that this occurs in part because, unlike the usual Langmuir waves, magnetized Langmuir waves are not necessarily trapped by density depressions for $\omega_p < \Omega_e$, owing to the dependence of their frequency on θ in Eq. (9.7). Under coronal conditions, highly oblate collapsing wave packets were seen in Newman *et al.*'s (1994a) simulations for $\Omega_e < \omega_p$ (Newman, Goldman, Ergun, and Boehm, 1994). The collapse of these packets was assumed to be arrested primarily by electron transit-time damping. The central electric fields of these packets were predominantly in the direction of the magnetic field, consistent with observations. In the auroral case, the existence of an extended suprathermal background distribution was found to truncate the decay cascade before a condensate could develop, thereby precluding collapse even for $\Omega_e < \omega_p$ (Newman, Goldman, and Ergun, 1994a). Realistic parameters could then ac-

count for the observed levels of upper-hybrid waves (Newman, Goldman, Ergun, and Boehm, 1994).

3. Astrophysical applications of upper-hybrid waves

To date, the main proposed applications of strong Langmuir turbulence outside the solar system have been to pulsar magnetospheres and astrophysical jets, chiefly with a view to explaining observed electromagnetic emission. Pelletier *et al.* (1988) noted that beam-generated Langmuir waves are also likely to be important in contexts as varied as active galactic nuclei, close binaries, cataclysmic variables, and gamma bursters. They argued that strong turbulence is likely to be relevant in at least some of these situations, owing to the highly energetic nature of the phenomena involved. They further argued that magnetic effects are likely to be important in many of these contexts. However, as yet, there has been little observational evidence bearing on astrophysical strong turbulence.

Pelletier *et al.* (1988) studied the collapse of upper-hybrid waves in magnetized plasmas, arguing that modulational instabilities and wave collapse can saturate the growth of beam-driven Langmuir waves, thereby allowing the beam to propagate further than would otherwise be the case. This is closely analogous to some proposed resolutions of Sturrock's dilemma for type-III electron beams emitted by the Sun (see Sec. VIII.C). It is thus necessary also to take into account the possibility that stochastic growth of waves in an inhomogeneous medium can accomplish the same result, greatly extending the beam penetration distance, as in the type-III case (Robinson, 1992; Robinson, Cairns, and Gurnett, 1992, 1993; Robinson, Willes, and Cairns, 1993; Robinson 1995, 1996b). Stochastic-growth theory has proved to yield much better agreement with observations in the type-III case than strong-turbulence theories, but the two theories are not mutually exclusive, as pointed out by Robinson (1995), who discussed incorporation of wave collapse into stochastic-growth theory. A further prediction by Pelletier *et al.* (1988) was that there should be a sudden onset of strong upper-hybrid turbulence where a beam leaves a strong-field region and enters one with $\Omega_e < \omega_p$.

Laboratory electron-beam experiments (Kato *et al.*, 1983; Benford and Weatherall, 1992) have long shown enhanced electromagnetic emission under conditions associated with strong turbulence (see Sec. VIII.B). Newman (1985), and Benford and Weatherall (1992) interpreted this radiation as the result of Compton boosting of a beam-generated Langmuir wave into an electromagnetic wave via scattering of an electron off a coherent wave packet. Baker *et al.* (1988) argued that such interactions could provide an alternative to the usual incoherent synchrotron mechanism to explain emission from some astrophysical jets. However, it does not seem that detailed tests of this proposal have been undertaken as yet.

Early work on Langmuir waves in strongly magnetized electron-ion and electron-positron plasmas, under conditions relevant to pulsar magnetospheres, was reviewed by ter Haar and Tsytovich (1981). This work centered on the physics of one-dimensional solitons, because the magnetic fields are so strong (up to 10^8–10^9 T) that particle dynamics are essentially one-dimensional, owing to rapid loss of any perpendicular momentum through cyclotron emission. Other work has since been done by Chian and Kennel (1983), Verga and Fontan (1985), Asseo *et al.* (1990), and Asseo (1993). For example, using a 1D formulation, Asseo *et al.* (1990) and Asseo (1993) discussed emission mechanisms involving a collection of stable quasi-one-dimensional wave packets in a pulsar magnetosphere. However, as these mechanisms do not involve collapse, they are not considered further here.

4. Other space and laboratory applications

Weak magnetization of Langmuir waves was incorporated into a number of studies of type-III solar radio sources, ionospheric-modification experiments, and laboratory beam-plasma experiments, as discussed in Sec. VIII. ter Haar and Tsytovich (1981) discussed a number of proposed applications of strong turbulence to type-I, type-II, and type-IV solar radio bursts and to solar flares; however, the mechanisms proposed have been largely superseded by theories that do not involve wave collapse or strong turbulence, so these applications are not discussed further here. Section VIII.C briefly mentioned the possible occurrence of Langmuir turbulence generated by beams emitted from shock waves associated with type-II bursts.

Antipov *et al.* (1979) produced highly oblate upper-hybrid solitons in a strongly magnetized beam-plasma system with an effectively 1D geometry. They found fractional density perturbations of up to 0.3 on a scale length of $(5–6)\lambda_D$, in fair agreement with values from theory. Their solitons were stationary with respect to the plasma and were observed to form by steepening of linear parent waves, consistent with the action of a modulational instability and similar to the behavior of the Langmuir waves seen in Fig. 29.

Christiansen *et al.* (1981) observed upper-hybrid modulation forming highly prolate structures aligned parallel with the magnetic field in a beam-plasma device. The approximate parallel and perpendicular scales were 20 mm and 1 mm, respectively, and associated density depletions were also observed, consistent with a theory of upper-hybrid filamentation by Dysthe *et al.* (1978). These packets do not correspond to the oblate, collapsing solutions discussed in Sec. IX.B and found in simulations.

Magnetized beam-plasma experiments were carried out by Vyacheslavov *et al.* (1995) in a regime with $\omega_p > \Omega_e$, but where the magnetic term in Eq. (9.7) greatly exceeded the thermal one. They found a beam-driven wave spectrum strongly aligned with the beam, as expected from linear theory, with an approximately isotropic spectrum of nonresonant waves that contained roughly 30% of the wave energy. The values of W for

beam-resonant and nonresonant waves were 0.07 and 0.17, respectively, greatly exceeding the modulational instability threshold for transverse perturbations and pointing to the likelihood of wave collapse, possibly directly from the beam-driven waves.

Vyacheslavov *et al.* (1995) noted that the dispersion of the beam-driven waves (at very low k) is magnetized, despite $\omega_p \gg \Omega_e$ being satisfied. However, Robinson and Newman's (1990a, 1990c) analyses imply that the characteristic nucleation wave number is substantially larger than the beam-driven one in this case and that the dispersion is essentially unmagnetized at that value of k [see Eqs. (5), (7), and (8) of Robinson and Newman (1990c) for the relevant criteria]. This difference is important when we note that power-law wave-number spectra were observed at large wave numbers, as would be expected from wave collapse, consistent with $W(k_\perp) \sim k_\perp^{-3.6}$ and $W(k_\parallel) \sim k_\parallel^{-4.1}$ approximately. These spectra are not as steep as the ones in Table III, for any of the three classes of collapse. However, they are nearest by far to the exponent of -6 predicted for isotropic (unmagnetized) collapse in three dimensions. The cause of the discrepancy is as yet unresolved, but it appears that despite the strong magnetic fields used in this experiment (2.5 T) wave collapse is *not* strongly magnetized.

Fast electron heating was also observed by Vyacheslavov *et al.* (1995), a possible signature of arrest. There are clearly strong signs of wave collapse and strong turbulence in these experiments, but more work needs to be done to compare observations and theory in detail. One important point, mentioned by Vyacheslavov *et al.* (1995), is that the mean values of W are so high that standard strong-turbulence theory may be significantly modified, e.g., owing to localized heating.

X. CONCLUSIONS AND FUTURE DIRECTIONS

This paper has reviewed the physics and applications of wave collapse (or self-focusing) and strong turbulence, concentrating chiefly on the simplest example of unmagnetized Langmuir waves interacting with low-frequency ion sound waves in a plasma. This system is simple enough that the main features of its physics are now understood, but complex enough that it gives valuable insights into analogous processes operating in other contexts. These insights have already proved useful in understanding some other strongly nonlinear systems, such as those involving upper-hybrid and lower-hybrid waves, and much wider application appears possible. Some other wave systems reviewed in less detail include those of nonlinear optics, magnetized-plasma waves, and deep-water waves. Applications to a variety of fields have been reviewed, emphasizing tests of the basic theoretical picture, cases in which this picture has succeeded in giving an improved account of experimental results, and situations where strong turbulence or wave collapse has been seriously investigated, but found to be inapplicable.

Two extremely important areas that have been scarcely touched on in this review are those of particle acceleration in strong turbulence and secondary emission processes involving localized wave packets: (i) Wave-particle interactions seem to be chiefly responsible for the arrest of wave collapse. In addition, they can give rise to strong acceleration of electrons and the production of superthermal tails on the plasma distribution. Such electrons can be important in arresting collapse, since they interact most strongly with other packets. Transit-time acceleration may also account for some observations of accelerated particles in a range of natural and laboratory situations, including laser-plasma experiments, beam-plasma devices, and the auroral ionosphere. (ii) Interactions of waves and particles with localized wave packets are of great interest in connection with nonlinear emission mechanisms. For example, relativistic-beam electrons can scatter localized Langmuir waves to produce high-frequency electromagnetic emission. Raman and Brillouin scattering are important in the interpretation of ionospheric modification experiments, and enhanced fundamental ($\omega \approx \omega_p$) and harmonic ($\omega \approx 2\omega_p$) electromagnetic emission are possible owing to the intense coherent fields in localized wave packets. A host of applications of these and related processes exist, in both the laboratory and naturally occurring situations.

In this section we briefly recapitulate the main points discussed in earlier sections, list some open questions, and mention some promising directions for future research.

A. Main results

Some of the most significant theoretical results on Langmuir turbulence to emerge, beginning with Zakharov's (1972) original paper on Langmuir collapse, are as follows:

(i) The discovery that modulational instability of two- and three-dimensional Langmuir wave packets does not saturate with the formation of solitons, but that these solitons are unstable with respect to wave collapse if their intensity exceeds a threshold (Secs. IV.A, V.D, and V.E).

(ii) The existence and importance of self-similar solutions, with simple temporal scalings. These solutions allow the treatment of collapse to be greatly simplified and are heavily exploited in statistical theories (Sec. V.E).

(iii) The correspondence between collapsing wave packets and Langmuir eigenstates localized in the associated density well, analogous to the correspondence between discrete eigenstates of the one-dimensional nonlinear Schrödinger equation and solitons (Secs. IV.A, V.A, and V.B). This provides the basis for treating these states as nonlinear building blocks when constructing theories of strong turbulence (Sec. VI), just as solitons augment plane waves to provide a description of solutions of the one-dimensional nonlinear Schrödinger equation.

(iv) The nucleation mechanism of wave-packet formation, in which states localized in remnant density wells can accumulate energy directly from a pump or indirectly from propagating Langmuir waves (Sec. V.C). In particular, this discovery made simplified pictures of energy input to localized states possible and showed that localized packets decouple from the driver and the remainder of the turbulence as they collapse. It should be noted, however, that nucleation is not universal—collapse via direct modulational instability of waves is possible under some circumstances.

(v) Development of a simplified two-component model of strong turbulence, with one component consisting of coherent packets and another comprised of propagating waves (Sec. VI). Models of this type have allowed scaling exponents to be determined analytically for a wide variety of statistical quantities, including mean values, probability distributions of field strengths and density fluctuations, and wave-number spectra. The results obtained have underlined the usefulness of statistical measures to the study of strong turbulence.

Major numerical results obtained (see Sec. VII) have included confirmation of the existence of self-similar wave collapse, testing and verification of the Zakharov equations, identification of renucleation in turbulent systems, demonstration that coherent packets are closely packed in strong turbulence, calculation of the arrest scale of collapse, and extensive testing and verification of the scalings predicted by the two-component theory of strong turbulence. Many of the experimental applications below have relied on multidimensional simulations for their interpretation. Advances in high-speed computing in recent decades have allowed a close interplay to develop between theory and numerics.

A range of experiments discussed in Secs. VIII and IX have yielded evidence of strong turbulence and wave-collapse phenomena. Subsequently, many experiments have relied on strong-turbulence theory for their interpretation. These include the following:

(i) Low-energy beam-plasma experiments, which provided evidence for soliton formation in one dimension, collapse of individual packets in three dimensions, and transit-time interactions with electrons.

(ii) Relativistic beam-plasma turbulence experiments, whose field-strength distributions and interactions with electrons were interpreted in terms of strong turbulence. These experiments also allowed the arrest scale of collapse amid turbulence to be estimated and showed evidence of transit-time interactions.

(iii) Radio-plasma experiments, which demonstrated the existence of transit-time interactions, the formation of localized, ponderomotively supported cavities containing trapped eigenstates with reduced frequencies.

(iv) Laser-plasma experiments, which have yielded spectral evidence of many of the underlying nonlinear processes, including ponderomotive force, self-focusing, and collapse.

(v) Langmuir waves in the Earth's foreshock, the highest of which show evidence of possible wave collapse during their convection downstream from the foreshock boundary.

(vi) Ionospheric-modification experiments, whose backscatter spectra appear to be explicable in terms of collapse of Langmuir wave packets in the heated region, but not in terms of previously proposed weak-turbulence theories.

(vii) Laser-solid experiments, which exhibit self-focusing, soliton formation, and a range of other nonlinear interactions.

(viii) Observations of lower-hybrid waves at auroral latitudes, many aspects of which are consistent with wave-collapse theory, but which still pose a number of unresolved questions.

(ix) Strongly magnetized beam-plasma experiments, which have shown evidence of wave collapse and strong turbulence.

Some experimental situations in which strong turbulence has been proposed, but for which there is less evidence, have also been discussed. These include some solar radio sources, pulsar magnetospheres, and astrophysical jets.

B. Open questions

This section lists some specific open questions, mostly theoretical in nature. The next section gives a broader perspective on future directions in the theory and application of collapse and strong turbulence.

Some specific unresolved issues that could be usefully addressed in the short to medium term include the following:

(i) Better quantitative understanding of the crossover from weak to strong turbulence is needed, particularly for waves of finite bandwidth and where both forms of turbulence coexist. Such knowledge would facilitate application of the correct theory in specific experimental situations.

(ii) Quantitative understanding of the coupling of nucleating states to random-phase background turbulence is currently lacking. Coupling to a clamp driver is better understood, but a more quantitative treatment would also be useful. This is perhaps the least understood aspect of the wave-packet (renucleation) cycle.

(iii) Connected to (ii) is the question of a possible transition from nucleation-mediated collapse to direct collapse as the damping of the ion response decreases. It has been argued that there is a threshold for nucleated collapse, because nucleation must be completed before the nucleating well can disperse. Evidence for this has been found in simulations, but a quantitative theoretical description is still lacking.

(iv) Scaling theories of clamp-driven turbulence are not as advanced as those for turbulence driven via a plasma instability. Similarly, the theoretical forms of the scalings have not been verified numerically in as much detail. Quantitative calculations of the scalings of mean quantities, spectra, and field statistics in clamp-driven turbulence would thus be desirable, as would their comprehensive numerical verification. Such results are particularly important in the rescaling of numerical calculations to regimes that cannot be simulated directly.

Further analysis of the threshold for nucleation in such turbulence also seems warranted, along with more detailed study of the means by which collapsing packets form in subthreshold turbulence.

(v) An improved treatment of the effects of ambient density fluctuations on wave collapse would be useful. To date it has been argued that, if sufficiently large, such fluctuations can disrupt nucleating packets, but a detailed theory has yet to be developed. Ambient density fluctuations, generated nonponderomotively, are significant in type-III solar radio sources, ionospheric modification, and other applications.

(vi) Strong-turbulence theory has succeeded in explaining scattering of relativistic electron beams in energy, but not in angle. Observed angular scattering exceeds theoretical predictions. Because of the experimental complexities, it is not yet clear whether this is the result of geometric effects, boundary conditions, or discrepancies in interpretation, or whether it represents a failure of the theory.

(vii) The anomalous decay of beam-driven strong turbulence, after turnoff of the beam, has not been explained, although some suggestions have been made as to the mechanism, including the possibility that specifically high-W effects play a role.

(viii) The statistics of the formation of intense laser filaments should be investigated further, both theoretically and experimentally. In particular, the predicted spatial power-law decay of a beam consisting of many filaments invites an experimental test that would bear closely on the statistical properties of strong turbulence governed by the nonlinear Schrödinger equation.

(ix) Relating to (viii), the behavior of turbulence governed by the nonlinear Schrödinger equation is, somewhat paradoxically, less well understood than that of turbulence governed by the Zakharov equations. This is because refractive-index variations relax on the same time scale as the burnout of intense fields, leaving little or no remnant well. While this precludes the standard nucleation mechanism, analogs have been suggested in this case. It would be useful to resolve whether collapsing packets form via a nucleation-like mechanism and/or from random-field enhancements. As yet unexplained changes in scaling exponents for nonlinear Schrödinger turbulence imply that more than one mechanism may be relevant, depending on the turbulence level. Studies of this type could also yield predictions of the shape distributions of collapsing wave packets governed by the nonlinear Schrödinger equation or the electromagnetic Zakharov equations (nonpotential fields).

(x) More work on particle heating during strong turbulence could usefully be done using 2D particle-in-cell or Vlasov methods. Increases in computing power are making such calculations increasingly feasible.

(xi) For the purposes of treating interactions between particles or waves and localized packets theoretically, a reformulation of wave-particle and wave-wave interaction theory in terms of generalized wave eigenstates, rather than plane waves, would be advantageous. Such an approach could potentially lead to a far more compact form of analysis by exploiting the naturally occurring localized structures. Use of wavelets to represent localized states suggests itself as a promising avenue to explore.

C. Future directions

We now turn briefly from the specific questions raised in the previous section to a more general perspective on future theoretical and applied directions involving wave collapse and strong turbulence. Some of the most promising avenues involve generalizations and applications to magnetized, partially ionized, collisional, and dusty plasmas, and to optics. Generalized classes of plasmas are involved in a host of applications in the laboratory, space, and astrophysics, many of which were discussed in Sec. IX. Much work is still needed in this area before the theory reaches the same level of development as that currently achieved for Langmuir phenomena, and the huge variety of magnetized-plasma and other plasma waves calls for overarching theories, rather than *ad hoc*, case-by-case development of the necessary analysis. Optical applications of the ideas discussed here are also particularly promising. Ideas such as nucleation, originally developed in the context of Langmuir turbulence, may have application in laser-dielectric or laser-semiconductor interactions, for example.

ACKNOWLEDGMENTS

The author thanks I. H. Cairns, A. Melatos, D. B. Melrose, D. L. Newman, S. V. Vladimirov, and A. J. Willes for useful discussions and their valuable comments on this paper, I. H. Cairns and N. I. Smith for their collaboration in obtaining the numerical results presented in Figure 6, M. Roy for expert technical assistance with the figures, and L. Berge, J. Briand, P. J. Kellogg, W. Kruer, D. L. Newman, H. A. Rose, and A. Y. Wong for permission to reproduce figures from their publications. This work was supported by the Australian Research Council.

REFERENCES

Abramowitz, M., and I. A. Stegun, 1970, Eds., *Handbook of Mathematical Functions* (Dover, New York).

Akhiezer, A. I., and R. V. Polovin, 1956, Zh. Éksp. Teor. Fiz. **30**, 915 [Sov. Phys. JETP **3**, 696 (1956)].

Akhmanov, S. A., A. P. Sukhorukov, and R. V. Khokhlov, 1966, Zh. Éksp. Teor. Fiz. **50**, 1537 [Sov. Phys. JETP **23**, 1025 (1966)].

Akimoto, K., 1989, Phys. Fluids B **1**, 1998.

Akimoto, K., 1995, Phys. Plasmas **2**, 649.

Amin, M. R., C. E. Capjack, P. Frycz, W. Rozmus, and V. T. Tikhonchuk, 1993, Phys. Fluids B **5**, 3748.

Andreev, N. E., L. M. Gorbunov, S. V. Tarakanov, and A. I. Zykov, 1993, Phys. Fluids B **5**, 1986.

Anisimov, S. I., M. A. Berezovskiĭ, M. F. Ivanov, I. V. Petrov, A. M. Rubenchik, and V. E. Zakharov, 1982, Phys. Lett. A **92**, 32.

Anisimov, S. I., M. A. Berezovskiĭ, V. E. Zakharov, I. V. Petrov, and A. M. Rubenchik, 1983, Zh. Éksp. Teor. Fiz. **84**, 2046 [Sov. Phys. JETP **57**, 1192].
Antipov, S. V., M. V. Nezlin, E. N. Snezhkin, and A. S. Trubnikov, 1979, Zh. Éksp. Teor. Fiz. **76**, 1571 [Sov. Phys. JETP **49**, 797 (1979)].
Arnoldy, R. L., K. A. Lynch, P. M. Kintner, J. Vago, S. Chesney, T. E. Moore, and C. J. Pollock, 1992, Geophys. Res. Lett. **19**, 413.
Askar'yan, G. A., 1962, Zh. Éksp. Teor. Fiz. **42**, 1567 [Sov. Phys. JETP **15**, 1088 (1962)].
Asseo, E., 1993, Mon. Not. R. Astron. Soc. **264**, 940.
Asseo, E., G. Pelletier, and H. Sol, 1990, Mon. Not. R. Astron. Soc. **247**, 529.
Attwood, D. T., D. W. Sweeney, J. M. Auerbach, and P. H. Y. Lee, 1978, Phys. Rev. Lett. **40**, 184.
Baker, D. N., J. E. Borovsky, G. Benford, and J. A. Eilek, 1988, Astrophys. J. **326**, 110.
Baldis, H. A., E. M. Campbell, and W. L. Kruer, 1991, in *Handbook of Plasma Physics*, Vol. 3, edited by M. N. Rosenbluth, R. Z. Sagdeev, A. M. Rubenchik, and S. Witkowski (North-Holland, Amsterdam), p. 361.
Baldis, H. A., and P. B. Corkum, 1980, Phys. Rev. Lett. **45**, 1260.
Baldis, H. A., J. C. Samson, and P. B. Corkum, 1978, Phys. Rev. Lett. **41**, 1719.
Bale, S. D., D. Burgess, P. J. Kellogg, K. Goetz, R. L. Howard, and S. J. Monson, 1996, Geophys. Res. Lett. **23**, 109.
Bardwell, S., and M. V. Goldman, 1976, Astrophys. J. **209**, 912.
Bauer, B. S., A. Y. Wong, L. Scurry, and V. K. Decyk, 1990, Phys. Fluids B **2**, 1941.
Benford, G., 1987, Phys. Fluids **30**, 2579.
Benford, G., and J. C. Weatherall, 1992, Phys. Fluids B **4**, 4111.
Benford, G., and X.-L. Zhai, 1993, Phys. Fluids B **5**, 1914.
Benford, G., X. Zhai, and D. Levron, 1991, Phys. Fluids B **3**, 560.
Benjamin, T. B., and J. E. Feir, 1966, J. Fluid Mech. **27**, 417.
Berezhiani, V. I., N. L. Tsintsadze, and D. D. Tskhakaya, 1980, J. Plasma Phys. **24**, 15.
Berger, R. L., B. F. Lasinski, T. B. Kaiser, E. A. Williams, A. B. Langdon, and B. I. Cohen, 1993, Phys. Fluids B **5**, 2243.
Bernstein, I. B., J. M. Greene, and M. D. Kruskal, Phys. Rev. **108**, 546 (1957).
Bezzerides, B., and D. F. DuBois, 1975, Phys. Rev. Lett. **34**, 1381.
Bezzerides, B., D. F. DuBois, and H. A. Rose, 1993, Phys. Rev. Lett. **70**, 2569.
Bingham, R., V. N. Tsytovich, and U. de Angelis, 1994, Phys. Scr. **T50**, 81.
Birdsall, C. K., and A. B. Langdon, 1985, *Plasma Physics via Computer Simulation* (McGraw-Hill, New York).
Bittencourt, J. A., 1995, *Fundamentals of Plasma Physics* (National Institute of Space Research, São José dos Campos, Brazil).
Blaha, R., E. W. Laedke, and K. H. Spatschek, 1987, Phys. Fluids **30**, 264.
Boot, H., and R. Harvie, 1957, Nature **180**, 1187.
Borisov, A. B., A. V. Borovskiy, V. V. Korobkin, A. M. Prokhorov, C. K. Rhodes, and O. B. Shiryaev, 1990, Phys. Rev. Lett. **65**, 1753.
Borovsky, J. E., 1993, J. Geophys. Res. **98**, 6101.
Boyd, R. W., 1992, *Nonlinear Optics* (Academic, Boston).
Brandi, H. S., C. Manus, G. Mainfray, T. Lehner, and G. Bonnaud, 1993, Phys. Fluids B **5**, 3539.
Breizman, B. N., and D. D. Ryutov, 1974, Nucl. Fusion **14**, 873.
Briand, J., L. Berge, A. Gomes, Y. Quemener, C. Arnas, M. Armengaud, J. P. Dinguirard, and D. Pesme, 1990, Phys. Fluids B **2**, 160.
Budden, K. G., 1985, *The Propagation of Radio Waves: The Theory of Radio Waves of Low Power in the Ionosphere and Magnetosphere* (Cambridge University, Cambridge, U.K.).
Budneva, O. B., V. E. Zakharov, and V. S. Synakh, 1975, Fiz. Plazmy **1**, 606 [Sov. J. Plasma Phys. **1**, 335 (1975)].
Bullough, R. K., and P. J. Caudrey, 1980, Eds., *Solitons* (Springer, Berlin).
Butcher, P. N., and D. Cotter, 1990, *The Elements of Nonlinear Optics* (Cambridge University, Cambridge, U.K.).
Cairns, I. H., 1987, J. Geophys. Res. **92**, 2329.
Cairns, I. H., 1995, Astrophys. J. **449**, L95.
Cairns, I. H., and D. A. Gurnett, 1992, J. Geophys. Res. **97**, 6235.
Cairns, I. H., W. S. Kurth, and D. A. Gurnett, 1993, Adv. Space Res. **13**, 205.
Cairns, I. H., and D. B. Melrose, 1985, J. Geophys. Res. **90**, 6637.
Cairns, I. H., and P. A. Robinson, 1992a, Geophys. Res. Lett. **19**, 1069.
Cairns, I. H., and P. A. Robinson, 1992b, Geophys. Res. Lett. **19**, 2187.
Cairns, I. H., and P. A. Robinson, 1995a, Geophys. Res. Lett. **22**, 3437.
Cairns, I. H., and P. A. Robinson, 1995b, Astrophys. J. **453**, 959.
Cairns, I. H., and P. A. Robinson, 1995c, in *Physics of Space Plasmas 13*, edited by T. Chang and J. R. Jasperse (MIT Center for Theoretical Cosmo/Geo Plasma Physics, Cambridge, MA), p. 223.
Cairns, I. H., and P. A. Robinson, 1996, in *Physics of Space Plasmas 14*, edited by T. Chang and J. R. Jasperse (MIT Center for Theoretical Cosmo/Geo Plasma Physics, Cambridge, MA), p. 105.
Campbell, E. M., 1992, Phys. Fluids B **4**, 3781.
Campillo, A. J., S. L. Shapiro, and B. R. Suydam, 1973, Appl. Phys. Lett. **23**, 628.
Carlson, H. C., W. E. Gordon, and R. L. Showen, 1972, J. Geophys. Res. **77**, 1242.
Celnikier, L. M., C. C. Harvey, R. Jegou, M. Kemp, and P. Moricet, 1983, Astron. Astrophys. **126**, 293.
Celnikier, L. M., L. Muschietti, and M. V. Goldman, 1987, Astron. Astrophys. **181**, 138.
Chang, T., 1993, Phys. Fluids B **5**, 2646.
Cheng, C. Z., and G. Knorr, 1976, J. Comput. Phys. **22**, 330.
Cheung, P. Y., D. F. DuBois, T. Fukuchi, K. Kawan, H. A. Rose, D. Russell, T. Tanikawa, and A. Y. Wong, 1992, J. Geophys. Res. **97**, 10 575.
Cheung, P. Y., and A. Y. Wong, 1985, Phys. Rev. Lett. **55**, 1880.
Cheung, P. Y., A. Y. Wong, C. B. Darrow, and S. J. Qian, 1982, Phys. Rev. Lett. **48**, 1348.
Cheung, P. Y., A. Y. Wong, T. Tanikawa, J. Santoru, D. F. DuBois, H. A. Rose, and D. Russell, 1989, Phys. Rev. Lett. **62**, 2676.
Chian, A. C.-L., and C. F. Kennel, 1983, Astrophys. Space Sci. **97**, 9.

Chian, A. C.-L., and F. B. Rizzato, 1994, J. Plasma Phys. **51**, 61.
Chiao, R. Y., E. Garmire, and C. H. Townes, 1964, Phys. Rev. Lett. **13**, 479.
Christiansen, P. J., V. K. Jain, and L. Stenflo, 1981, Phys. Rev. Lett. **46**, 1333.
Clark, K. L., G. L. Payne, and D. R. Nicholson, 1992, Phys. Fluids B **4**, 708.
Dahmani, F., D. Ghobrini, and M. El-Mahdaoui, 1991, Phys. Fluids B **3**, 2558.
Davey, A., and K. Stewartson, 1974, Proc. R. Soc. London, Ser. A **338**, 101.
Dawson, J. M., 1959, Phys. Rev. **113**, 383.
Dawson, J. M., 1983, Rev. Mod. Phys. **55**, 403.
Degtyarev, L. M., I. M. Ibragimov, R. Z. Sagdeev, G. I. Solov'ev, V. D. Shapiro, and V. I. Shevchenko, 1984, Pis'ma Zh. Éksp. Teor. Fiz. **40**, 455 [JETP Lett. **40**, 1282 (1984)].
Degtyarev, L. M., R. Z. Sagdeev, G. I. Solov'ev, V. D. Shapiro, and V. I. Shevchenko, 1980, Fiz. Plazmy **6**, 485 [Sov. J. Plasma Phys. **6**, 263 (1980)].
Degtyarev, L. M., R. Z. Sagdeev, G. I. Solov'ev, V. D. Shapiro, and V. I. Shevchenko, 1989, Zh. Éksp. Teor. Fiz. **95**, 1690 [Sov. Phys. JETP **68**, 975 (1989)]
Degtyarev, L. M., G. I. Solov'ev, V. D. Shapiro, and V. I. Shevchenko, 1979, Pis'ma Zh. Éksp. Teor. Fiz. **29**, 543 [JETP Lett. **29**, 494 (1979)].
Degtyarev, L. M., V. E. Zakharov, and L. I. Rudakov, 1975, Zh. Éksp. Teor. Fiz. **68**, 115 [Sov. Phys. JETP **41**, 57 (1975)].
Degtyarev, L. M., V. E. Zakharov, and L. I. Rudakov, 1976, Fiz. Plazmy **2**, 438 [Sov. J. Plasma Phys. **2**, 240 (1976)].
DeNeef, C. P., and J. S. DeGroot, 1977, Phys. Fluids **20**, 1074.
Djuth, F. T., C. A. Gonzales, and H. M. Ierkic, 1986, J. Geophys. Res. **91**, 12 089.
Djuth, F. T., P. Stubbe, M. P. Sulzer, H. Kohl, M. T. Rietveld, and J. H. Elder, 1994, J. Geophys. Res. **99**, 333.
Doolen, G. D., D. F. DuBois, and H. A. Rose, 1985, Phys. Rev. Lett. **54**, 804.
Doolen, G. D., D. F. DuBois, H. A. Rose, and B. Hafizi, 1983, Phys. Rev. Lett. **51**, 335.
Dovner, P. O., A. I. Eriksson, R. Boström, and B. Holback, 1994, Geophys. Res. Lett. **21**, 1827.
DuBois, D. F., and M. V. Goldman, 1967, Phys. Rev. **164**, 207.
DuBois, D. F., and M. V. Goldman, 1972a, Phys. Rev. Lett. **28**, 218.
DuBois, D. F., and M. V. Goldman, 1972b, Phys. Fluids **15**, 919.
DuBois, D. F., A. Hansen, H. A. Rose, and D. Russell, 1993a, Phys. Fluids B **5**, 2616.
DuBois, D. F., A. Hansen, H. A. Rose, and D. Russell, 1993b, J. Geophys. Res. **98**, 17 543.
DuBois, D. F., and H. A. Rose, 1981, Phys. Rev. A **24**, 1476.
DuBois, D. F., and H. A. Rose, 1991, in *Nonlinear and Chaotic Phenomena in Plasmas, Solids, and Fluids*, edited by W. Rozmus and J. A. Tuszynski (World Scientific, Singapore), p. 266.
DuBois, D. F., H. A. Rose, and D. Russell, 1988, Phys. Rev. Lett. **61**, 2209.
DuBois, D. F., H. A. Rose, and D. Russell, 1990, J. Geophys. Res. **95**, 21 221.
DuBois, D. F., H. A. Rose, and D. Russell, 1991, Phys. Rev. Lett. **66**, 1970.
DuBois, D. F., H. A. Rose, and D. Russell, 1996, Phys. Scr. **T63**, 16.
DuBois, D. F., D. Russell, and H. A. Rose, 1995a, Phys. Plasmas **2**, 76.
DuBois, D. F., D. Russell, and H. A. Rose, 1995b, Phys. Rev. Lett. **74**, 3983.
Dulk, G. A., J.-L. Steinberg, and S. Hoang, 1984, Astron. Astrophys. **141**, 30.
D'yachenko, A. I., V. E. Zakharov, A. M. Rubenchik, R. Z. Sagdeev, and V. F. Shvets, 1988, Zh. Éksp. Teor. Fiz. **94**, 144 [Sov. Phys. JETP **67**, 513 (1988)].
Dyshko, A. L., V. N. Lugovoi, and A. M. Prokhorov, 1972, Zh. Éksp. Teor. Fiz. **61**, 2305 [Sov. Phys. JETP **34**, 1235 (1972)].
Dysthe, K. B., E. Mjølhus, H. L. Pécseli, and L. Stenflo, 1978, Plasma Phys. **20**, 1087.
Eggleston, D. L., A. Y. Wong, and C. B. Darrow, 1982, Phys. Fluids **25**, 257.
Eriksson, A. I., B. Holback, P. O. Dovner, R. Boström, G. Holmgren, M. André, L. Eliasson, and P. M. Kintner, 1994, Geophys. Res. Lett. **21**, 1843.
Estabrook, K. G., E. J. Valeo, and W. L. Kruer, 1975, Phys. Fluids **18**, 1151.
Etcheto, J., and M. Faucheux, 1984, J. Geophys. Res. **89**, 6631.
Fejer, J. A., 1975, Philos. Trans. R. Soc. London, Ser. A **280**, 151.
Fejer, J. A., 1979, Rev. Geophys. Space Phys. **17**, 135.
Fejer, J. A., C. A. Gonzales, H. M. Ierkic, M. P. Sulzer, C. A. Tepley, L. M. Duncan, F. T. Djuth, S. Ganguly, and W. E. Gordon, 1985, J. Atmos. Terr. Phys. **47**, 1165.
Fejer, J. A., and Y.-Y. Kuo, 1973, Phys. Fluids **16**, 1490.
Fejer, J. A., M. P. Sulzer, and F. T. Djuth, 1991, J. Geophys. Res. **96**, 15 985.
Filbert, P. C., and P. J. Kellogg, 1979, J. Geophys. Res. **84**, 1369.
Fitzenreiter, R. J., A. J. Klimas, and J. D. Scudder, 1984, Geophys. Res. Lett. **11**, 496.
Forslund, D. W., J. M. Kindel, K. Lee, E. L. Lindman, and R. L. Morse, 1975, Phys. Rev. A **11**, 679.
Fredericks, R. W., C. F. Kennel, F. L. Scarf, G. M. Crook, and I. M. Green, 1968, Phys. Rev. Lett. **21**, 1761.
Frey, A., 1986, Geophys. Res. Lett. **13**, 438.
Friedberg, J. P., R. W. Mitchell, R. L. Morse, and L. I. Rudsinski, 1972, Phys. Rev. Lett. **28**, 795.
Galeev, A. A., R. Z. Sagdeev, V. D. Shapiro, and V. I. Shevchenko, 1977a, Zh. Éksp. Teor. Fiz. **72**, 507 [Sov. Phys. JETP **46**, 266 (1977)].
Galeev, A. A., R. Z. Sagdeev, V. D. Shapiro, and V. I. Shevchenko, 1977b, Zh. Éksp. Teor. Fiz. **73**, 1352 [Sov. Phys. JETP **46**, 711 (1977)].
Galeev, A. A., R. Z. Sagdeev, Yu. S. Sigov, V. D. Shapiro, and V. I. Shevchenko, 1975, Fiz. Plazmy **1**, 10 [Sov. J. Plasma Phys. **1**, 5 (1975)].
Gaponov, A. V., and M. A. Miller, 1958, Zh. Éksp. Teor. Fiz. **34**, 242 [Sov. Phys. JETP **7**, 168 (1958)].
Gardner, C. S., J. M. Greene, M. D. Kruskal, and R. M. Miura, 1967, Phys. Rev. Lett. **19**, 1095.
Gavrilov, E. M., D. F. DuBois, H. A. Rose, and A. M. Rubenchik, 1995, Phys. Plasmas **2**, 1907.
Ghanshyam, and V. K. Tripathi, 1993, J. Plasma Phys. **49**, 243.
Gibbons, J., S. G. Thornhill, M. J. Wardrop, and D. ter Haar, 1977, J. Plasma Phys. **17**, 153.
Ginzburg, V. L., 1960, *Propagation of Electromagnetic Waves in Plasma* (Gordon and Breach, New York).
Ginzburg, V. L., and V. V. Zheleznyakov, 1958, Sov. Astron. AJ **2**, 694 [Sov. Astron. AJ **2**, 653 (1958)].
Goldman, M. V., 1984, Rev. Mod. Phys. **56**, 709.

Goldman, M. V., and D. L. Newman, 1994, in *Solar System Plasmas in Space and Time*, edited by J. L. Burch and J. H. Waite (American Geophysical Union, Washington, DC), p. 33.
Goldman, M. V., D. L. Newman, and F. W. Perkins, 1993, Phys. Rev. Lett. **70**, 4075.
Goldman, M. V., D. L. Newman, J. G. Wang, and L. Muschietti, 1996, Phys. Scr. **T63**, 28.
Goldman, M. V., and D. R. Nicholson, 1978, Phys. Rev. Lett. **41**, 406.
Goldman, M. V., K. Rypdal, and B. Hafizi, 1980, Phys. Fluids **23**, 945.
Goldman, M. V., J. C. Weatherall, and D. R. Nicholson, 1981, Phys. Fluids **24**, 668.
Goodman, S., 1991, Phys. Fluids B **4**, 329.
Grard, R., C. Nairn, A. Pedersen, S. Klimov, S. Savin, A. Skalsky, and J. G. Trotignon, 1991, Planet. Space Sci. **39**, 89.
Grognard, R. J.-M., 1982, Sol. Phys. **81**, 173.
Grognard, R. J.-M., 1985, in *Solar Radiophysics*, edited by D. J. McLean and N. R. Labrum (Cambridge University, Cambridge, U.K.), p. 253.
Gurnett, D. A., and R. R. Anderson, 1976, Science **194**, 1159.
Gurnett, D. A., and R. R. Anderson, 1977, J. Geophys. Res. **82**, 632.
Gurnett, D. A., G. B. Hospodarsky, W. S. Kurth, D. J. Williams, and S. J. Bolton, 1993, J. Geophys. Res. **98**, 5631.
Gurnett, D. A., W. S. Kurth, R. L. Poynter, L. J. Granroth, I. H. Cairns, W. M. Macek, S. L. Moses, F. V. Coroniti, C. F. Kennel, and D. D. Barbosa, 1989, Science **246**, 1494.
Gurnett, D. A., J. E. Maggs, D. L. Gallagher, W. S. Kurth, and F. L. Scarf, 1981, J. Geophys. Res. **86**, 8833.
Hadžievski, Lj. R., M. M. Škorić, A. M. Rubenchik, E. G. Shapiro, and S. K. Turitsyn, 1990, Phys. Rev. A **42**, 3561.
Hafizi, B., J. C. Weatherall, M. V. Goldman, and D. R. Nicholson, 1982, Phys. Fluids **25**, 392.
Hammett, G. W., and F. W. Perkins, 1990, Phys. Rev. Lett. **64**, 3019.
Hanssen, A., E. Mjølhus, D. F. DuBois, and H. A. Rose, 1992, J. Geophys. Res. **97**, 12 073.
Hasegawa, A., 1970, Phys. Rev. A **1**, 1746.
Helmerson, E., and E. Mjølhus, 1994, J. Geophys. Res. **99**, 17 623.
Herbst, M. J., J. A. Stamper, R. R. Whitlock, R. H. Lehmberg, and B. H. Ripin, 1981, Phys. Rev. Lett. **46**, 328.
Hoang, S., G. A. Dulk, and Y. Leblanc, 1994, Astron. Astrophys. **289**, 957.
Hopman, H. J., and G. C. A. M. Janssen, 1984, Phys. Rev. Lett. **52**, 1613.
Hora, H., 1969a, Phys. Fluids **12**, 182.
Hora, H., 1969b, Z. Phys. **226**, 156.
Hospodarsky, G. B., and D. A. Gurnett, 1995, Geophys. Res. Lett. **22**, 1161.
Hospodarsky, G. B., D. A. Gurnett, W. S. Kurth, M. G. Kivelson, R. J. Strangeway, and S. J. Bolton, 1994, J. Geophys. Res. **99**, 13 363.
Ikezi, H., R. P. H. Chang, and R. A. Stern, 1976, Phys. Rev. Lett. **36**, 1047.
Ikezi, H., K. Nishikawa, and K. Mima, 1974, J. Phys. Soc. Jpn. **37**, 766.
Ishida, A., and K. Nishikawa, 1975, J. Phys. Soc. Jpn. **38**, 1553.
Janssen, G. C. A. M., J. H. M. Bonnie, E. H. A. Granneman, V. I. Krementsov, and H. J. Hopman, 1984, Phys. Fluids **27**, 726.
Janssen, G. C. A. M., E. H. A. Granneman, and H. J. Hopman, 1984, Phys. Fluids **27**, 736.
Joshi, C., D. E. Clayton, and F. F. Chen, 1982, Phys. Rev. Lett. **48**, 874.
Karpman, V. I., and L. Stenflo, 1988, Phys. Lett. A **127**, 99.
Kato, K. G., G. Benford, and D. Tzach, 1983, Phys. Fluids **26**, 3636.
Kaw, P., and J. Dawson, 1970, Phys. Fluids **13**, 472.
Kelley, P. L., 1965, Phys. Rev. Lett. **15**, 1005.
Kellogg, P. J., K. Goetz, R. L. Howard, and S. J. Monson, 1992, Geophys. Res. Lett. **19**, 1303.
Khakimov, F. Kh., and V. N. Tsytovich, 1976, Zh. Éksp. Teor. Fiz. **70**, 1785 [Sov. Phys. JETP **43**, 929 (1976)].
Kim, H. C., R. L. Stenzel, and A. Y. Wong, 1974, Phys. Rev. Lett. **33**, 886.
Kingsep, A. S., L. I. Rudakov, and R. N. Sudan, 1973, Phys. Rev. Lett. **31**, 1482.
Kintner, P. M., 1992, Phys. Fluids B **4**, 2264.
Kintner, P. M., J. Vago, S. Chesney, R. L. Arnoldy, K. A. Lynch, C. J. Pollock, and T. E. Moore, 1992, Phys. Rev. Lett. **68**, 2448.
Kittel, C., 1976, *Introduction to Solid State Physics* (Wiley, New York).
Kiwamoto, Y., H. Kuwahara, and H. Tanaca, 1977, J. Phys. Soc. Jpn. **42**, 1005.
Kohl, H., and M. T. Rietveld, 1996, J. Geophys. Res. **101**, 5391.
Kolber, T., W. Rozmus, and V. T. Tikhonchuk, 1993, Phys. Fluids B **5**, 138.
Kovrizhnykh, L. M., and A. S. Sakharov, 1979, Fiz. Plazmy **5**, 840 [Sov. J. Plasma Phys. **5**, 470 (1979)].
Kraichnan, R. H., 1959, J. Fluid Mech. **3**, 32.
Kraichnan, R. H., 1964, Phys. Fluids **7**, 1163.
Krasnosel'skikh, V. V., and V. I. Sotnikov, 1977, Fiz. Plazmy **3**, 872 [Sov. J. Plasma Phys. **3**, 491 (1977)].
Kruer, W. L., 1985, Comments Plasma Phys. Controlled Fussion **9**, 63.
Kruer, W. L., 1988, *The Physics of Laser-Plasma Interactions* (Addison-Wesley, Redwood City).
Kuznetsov, E. A., 1976, Fiz. Plazmy **2**, 327 [Sov. J. Plasma Phys. **2**, 178 (1976)].
Kuznetsov, E. A., A. M. Rubenchik, and V. E. Zakharov, 1986, Phys. Rep. **142**, 103.
Kuznetsov, E. A., and M. M. Škorić, 1988a, Phys. Rev. A **38**, 1422.
Kuznetsov, E. A., and M. M. Škorić, 1988b, Phys. Lett. A **129**, 459.
Kuznetsov, E. A., and S. K. Turitsyn, 1990, Fiz. Plazmy **16**, 901 [Sov. J. Plasma Phys. **16**, 524 (1990)].
Laedke, E. W., K. H. Spatschek, and K. Zocha, 1982, Phys. Rev. Lett. **49**, 1401.
Lamb, B. M., G. Dimonte, and G. J. Morales, 1983, Phys. Fluids **27**, 1401.
Langdon, A. B., and B. F. Lasinski, 1983, Phys. Fluids **26**, 582.
Leung, P., M. Q. Tran, and A. Y. Wong, 1982, Plasma Phys. **24**, 567.
Levron, D., G. Benford, and D. Tzach, 1987, Phys. Rev. Lett. **58**, 1336.
Lin, R. P., W. K. Levedahl, W. Lotko, D. A. Gurnett, and F. L. Scarf, 1986, Astrophys. J. **308**, 954.
Lin, R. P., D. W. Potter, D. A. Gurnett, and F. L. Scarf, 1981, Astrophys. J. **251**, 364.
Lipatov, A. S., 1977, Pis'ma Zh. Éksp. Teor. Fiz. **26**, 516 [JETP Lett. **26**, 377 (1978)].

Lugovoĭ, V. N., and A. M. Prokhorov, 1973, Usp. Fiz. Nauk **111**, 203 [Sov. Phys. Usp. **16**, 658 (1974)].
Lynch, K. A., R. L. Arnoldy, P. M. Kintner, and J. L. Vago, 1994, J. Geophys. Res. **99**, 2227.
Maaswinkel, A. G. M., K. Eidmann, and R. Sigel, 1979, Phys. Rev. Lett. **42**, 1625.
Malkin, V. L., 1986, Zh. Éksp. Teor. Fiz. **90**, 59 [Sov. Phys. JETP **63**, 34 (1986)].
Manes, K. R., V. C. Rupert, J. M. Auerbach, P. Lee, and J. E. Swain, 1977, Phys. Rev. Lett. **39**, 281.
Max, C. E., J. Aarons, and A. B. Langdon, 1974, Phys. Rev. Lett. **33**, 209.
McFadden, J. P., C. W. Carlson, and M. H. Boehm, 1990, J. Geophys. Res. **95**, 6533.
Melatos, A., W. E. P. Padden, and P. A. Robinson, 1996, Phys. Plasmas **3**, 498.
Melatos, A., and P. A. Robinson, 1993a, Phys. Fluids **5**, 1045.
Melatos, A., and P. A. Robinson, 1993b, Phys. Fluids B **5**, 2751.
Melatos, A., and P. A. Robinson, 1995, J. Plasma Phys. **53**, 75.
Melatos, A., and P. A. Robinson, 1996, Phys. Plasmas **3**, 1263.
Melrose, D. B., 1986a, *Instabilities in Space and Laboratory Plasmas* (Cambridge University, Cambridge, U.K.).
Melrose, D. B., 1986b, J. Plasma Phys. **36**, 269.
Melrose, D. B., 1987a, J. Plasma Phys. **37**, 241.
Melrose, D. B., 1987b, J. Plasma Phys. **38**, 473.
Meyer, J., and Y. Zhu, 1993, Phys. Rev. Lett. **71**, 2915.
Morales, G. J., and Y. C. Lee, 1974, Phys. Rev. Lett. **33**, 1534.
Mounaix, P., G. Laval, P. Mora, and D. Pesme, 1991, Phys. Fluids B **3**, 1392.
Muschietti, L., I. Roth, and R. E. Ergun, 1995, J. Geophys. Res. **100**, 17 481.
Musher, S. L., A. M. Rubenchik, and V. E. Zakharov, 1995, Phys. Rep. **252**, 177.
Musher, S. L., and B. I. Sturman, 1975, Pis'ma Zh. Éksp. Teor. Fiz. **22**, 537 [JETP Lett. **22**, 265 (1975)].
Nelson, G. J., and D. B. Melrose, 1985, in *Solar Radiophysics*, edited by D. J. McLean and N. R. Labrum (Cambridge University, Cambridge, U.K.), p. 333.
Newell, A. C., D. A. Rand, and D. Russell, 1988a, Phys. Lett. A **132**, 112.
Newell, A. C., D. A. Rand, and D. Russell, 1988b, Physica D **33**, 281.
Newman, D. L., 1985, "Emission of Electromagnetic Radiation From Beam-Driven Plasmas," Ph.D. thesis, University of Colorado at Boulder.
Newman, D. L., M. V. Goldman, and R. E. Ergun, 1994a, Phys. Plasmas **1**, 1691.
Newman, D. L., M. V. Goldman, and R. E. Ergun, 1994b, J. Geophys. Res. **99**, 6377.
Newman, D. L., M. V. Goldman, R. E. Ergun, and M. H. Boehm, 1994, J. Geophys. Res. **99**, 6367.
Newman, D. L., and P. A. Robinson, 1991, in *Nonlinear and Chaotic Phenomena in Plasmas, Solids, and Fluids*, edited by W. Rozmus and J. A. Tuszynski (World Scientific, Singapore), p. 363.
Newman, D. L., P. A. Robinson, and M. V. Goldman, 1989, Phys. Rev. Lett. **62**, 2132.
Newman, D. L., P. A. Robinson, and M. V. Goldman, 1991, Physica D **52**, 49.
Newman, D. L., R. M. Winglee, P. A. Robinson, J. Glanz, and M. V. Goldman, 1990, Phys. Fluids B **2**, 2600.
Nicholas, D. J., and S. G. Sajjadi, 1986, J. Phys. D **19**, 737.
Nicholson, D. R., and M. V. Goldman, 1978, Phys. Fluids **21**, 1766.
Nicholson, D. R., M. V. Goldman, P. Hoyng, and J. C. Weatherall, 1978, Astrophys. J. **223**, 605.
Nishikawa, K., 1968a, J. Phys. Soc. Jpn. **24**, 916.
Nishikawa, K., 1968b, J. Phys. Soc. Jpn. **24**, 1152.
Oraevskii, V. N., and R. Z. Sagdeev, 1962, Zh. Tekh. Fiz. **32**, 1291 [Sov. Phys. Tech. Phys. **7**, 955 (1963)].
Papadopoulos, K., M. L. Goldstein, and R. A. Smith, 1974, Astrophys. J. **190**, 175.
Payne, G. L., D. R. Nicholson, R. M. Downie, and J. P. Sheerin, 1984, J. Geophys. Res. **89**, 10 921.
Pelletier, G., 1980a, J. Plasma Phys. **24**, 287.
Pelletier, G., 1980b, J. Plasma Phys. **24**, 421.
Pelletier, G., 1982, Phys. Rev. Lett. **49**, 782.
Pelletier, G., 1987, Physica D **27**, 187.
Pelletier, G., H. Sol, and E. Asseo, 1988, Phys. Rev. A **38**, 2552.
Pereira, N. R., R. N. Sudan, and J. Denavit, 1977a, Phys. Fluids **20**, 271.
Pereira, N. R., R. N. Sudan, and J. Denavit, 1977b, Phys. Fluids **20**, 936.
Perkins, F. W., and P. K. Kaw, 1971, J. Geophys. Res. **76**, 282.
Perkins, F. W., C. Oberman, and E. J. Valeo, 1974, J. Geophys. Res. **79**, 1478.
Perkins, F. W., and E. J. Valeo, 1974, Phys. Rev. Lett. **32**, 1234.
Petviashvili, V. I., 1975, Fiz. Plazmy **1**, 28 [Sov. J. Plasma Phys. **1**, 15 (1975)].
Petviashvili, V. I., 1976, Fiz. Plazmy **2**, 450 [Sov. J. Plasma Phys. **1**, 247 (1976)].
Popel, S. I., V. N. Tsytovich, and S. V. Vladimirov, 1994, Phys. Plasmas **1**, 2176.
Poquerusse, M., 1994, Astron. Astrophys. **286**, 611.
Pottelette, R., M. Malingre, A. Bahnsen, L. Eliasson, K. Stasiewicz, R. E. Erlandson, and G. Marklund, 1988, Ann. Geophys. **6**, 573.
Pottelette, R., R. A. Treumann, and N. Dubouloz, 1992, J. Geophys. Res. **97**, 12 029.
Quon, B. H., A. Y. Wong, and B. H. Ripin, 1974, Phys. Rev. Lett. **32**, 406.
Relke, I. V., and A. M. Rubenchik, 1988, J. Plasma Phys. **39**, 369.
Retterer, J. M., T. Chang, and J. R. Jasperse, 1986, J. Geophys. Res. **91**, 1609.
Retterer, J. M., T. Chang, and J. R. Jasperse, 1994, J. Geophys. Res. **99**, 13 189.
Richardson, M. C., 1991, in *Handbook of Plasma Physics*, Vol. 3, edited by M. N. Rosenbluth, R. Z. Sagdeev, A. Rubenchik, and S. Witkowski (North-Holland, Amsterdam), p. 199.
Robinson, P. A., 1989, Phys. Fluids B **1**, 490.
Robinson, P. A., 1991, Phys. Fluids B **3**, 545.
Robinson, P. A., 1992, Sol. Phys. **139**, 147.
Robinson, P. A., 1995, Phys. Plasmas **2**, 1466.
Robinson, P. A., 1996a, Phys. Plasmas **3**, 192.
Robinson, P. A., 1996b, Sol. Phys. **168**, 357.
Robinson, P. A., and I. H. Cairns, 1993, Astrophys. J. **418**, 506.
Robinson, P. A., and I. H. Cairns, 1994, Sol. Phys. **154**, 335.
Robinson, P. A., and I. H. Cairns, 1995, Geophys. Res. Lett. **22**, 2657.
Robinson, P. A., I. H. Cairns, and D. A. Gurnett, 1992, Astrophys. J. **387**, L101.
Robinson, P. A., I. H. Cairns, and D. A. Gurnett, 1993, Astrophys. J. **407**, 790.

Robinson, P. A., and P. M. Drysdale, 1996, Phys. Rev. Lett. **77**, 2698.
Robinson, P. A., A. Melatos, and W. Rozmus, 1996a, Phys. Plasmas **3**, 133.
Robinson, P. A., A. Melatos, and W. Rozmus, 1996b, J. Geophys. Res. **101**, 21545.
Robinson, P. A., and D. L. Newman, 1988, J. Plasma Phys. **40**, 553.
Robinson, P. A., and D. L. Newman, 1989, Phys. Fluids B **1**, 2319.
Robinson, P. A., and D. L. Newman, 1990a, Phys. Fluids B **2**, 2999.
Robinson, P. A., and D. L. Newman, 1990b, Phys. Fluids B **2**, 3017.
Robinson, P. A., and D. L. Newman, 1990c, Phys. Fluids B **2**, 3120.
Robinson, P. A., and D. L. Newman, 1991a, J. Geophys. Res. **96**, 17 733.
Robinson, P. A., and D. L. Newman, 1991b, Physica D **53**, 33.
Robinson, P. A., D. L. Newman, and M. V. Goldman, 1988, Phys. Rev. Lett. **61**, 702.
Robinson, P. A., D. L. Newman, and A. M. Rubenchik, 1992, Phys. Fluids **4**, 2509.
Robinson, P. A., and W. Rozmus, 1994, Prog. Astronaut. Aeronaut. **160**, 380.
Robinson, P. A., A. J. Willes, and I. H. Cairns, 1993, Astrophys. J. **408**, 720.
Robinson, P. A., M. J. Wouters, and N. G. R. Broderick, 1996, Phys. Plasmas **3**, 122.
Rose, H. A., 1995, Phys. Plasmas **2**, 2216.
Rose, H. A., and D. F. DuBois, 1993a, Phys. Fluids B **5**, 590.
Rose, H. A., and D. F. DuBois, 1993b, Phys. Fluids B **5**, 3337.
Rose, H. A., D. F. DuBois, and B. Bezzerides, 1987, Phys. Rev. Lett. **58**, 2547.
Rowland, H. L., 1980, Phys. Fluids **23**, 508.
Rowland, H. L., 1988, J. Geophys. Res. **93**, 12 916.
Rowland, H. L., J. G. Lyon, and K. Papadopoulos, 1981, Phys. Rev. Lett. **46**, 346.
Rowland, H. L., and K. Papadopoulos, 1977, Phys. Rev. Lett. **39**, 1276.
Rozanov, V. B., and S. A. Shumskiĭ, 1986, Kvantovaya Elektron. (Moscow) **13**, 1545 [Sov. J. Quantum Electron. **16**, 1010 (1986)].
Rozanov, V. B., and S. A. Shumskiĭ, 1987, Kvantovaya Elektron. (Moscow) **14**, 546 [Sov. J. Quantum Electron. **17**, 339 (1987)].
Rubenchik, A. M., and E. G. Shapiro, 1991, Pis'ma Zh. Éksp. Teor. Fiz. **54**, 20 [JETP Lett. **54**, 17 (1991)].
Rubenchik, A. M., and S. K. Turitsyn, 1987, Laser Particle Beams **5**, 3.
Rubenchik, A. M., and V. E. Zakharov, 1991, in *Handbook of Plasma Physics*, Vol. 3, edited by M. N. Rosenbluth, R. Z. Sagdeev, A. M. Rubenchik, and S. Witkowski (North-Holland, Amsterdam), p. 335.
Rudakov, L. I., and V. N. Tsytovich, 1978, Phys. Rep. **40**, 1.
Russell, D., D. F. DuBois, and H. A. Rose, 1986, Phys. Rev. Lett. **56**, 838.
Russell, D., D. F. DuBois, and H. A. Rose, 1988, Phys. Rev. Lett. **60**, 581.
Sagdeev, R. Z., 1979, Rev. Mod. Phys. **51**, 1.
Sagdeev, R. Z., V. D. Shapiro, and V. I. Shevchenko, 1991, in *Handbook of Plasma Physics*, Vol. 3, edited by M. N. Rosenbluth, R. Z. Sagdeev, A. M. Rubenchik, and S. Witkowski (North-Holland, Amsterdam), p. 271.
Saleh, B. E. A., and M. C. Teich, 1991, *Fundamentals of Photonics* (Wiley, New York).
Schiff, L. I., 1968, *Quantum Mechanics* (McGraw-Hill, New York).
Schmitt, A. J., 1988, Phys. Fluids **31**, 3079.
Schmitt, A. J., 1991, Phys. Fluids B **3**, 186.
Schmitt, A. J., 1993, Phys. Fluids B **5**, 932.
Seyler, C. E., 1994, J. Geophys. Res. **99**, 19 513.
Shapiro, V. D., and V. I. Shevchenko, 1984, in *Handbook of Plasma Physics*, Vol. 2, edited by M. N. Rosenbluth, R. Z. Sagdeev, A. A. Galeev, and R. N. Sudan (North-Holland, Amsterdam), p. 123.
Shapiro, V. D., V. I. Shevchenko, G. I. Solov'ev, V. P. Kalinin, R. Bingham, R. Z. Sagdeev, M. Ashour-Abdalla, J. Dawson, and J. J. Su, 1993, Phys. Fluids B **5**, 3148.
Shapiro, V. D., G. I. Soloviev, J. M. Dawson, and R. Bingham, 1995, Phys. Plasmas **2**, 516.
Shearer, J. W., and J. L. Eddleman, 1973, Phys. Fluids **16**, 1753.
Sheerin, J. P., J. C. Weatherall, D. R. Nicholson, G. L. Payne, M. V. Goldman, and P. J. Hansen, 1982, J. Atmos. Terr. Phys. **44**, 1043.
Shen, Y. R., 1984, *The Principles of Nonlinear Optics* (Wiley, New York).
Shen, M.-M., and D. R. Nicholson, 1987, Phys. Fluids **30**, 1096.
Sheerin, J. P., J. C. Weatherall, D. R. Nicholson, G. L. Payne, M. V. Goldman, and P. J. Hansen, 1982, J. Atmos. Terr. Phys. **44**, 1043.
Shlyuger, I. S., 1974, Pis'ma Zh. Éksp. Teor. Fiz. **19**, 274 [JETP Lett. **19**, 162 (1974)].
Showen, R. L., and D. M. Kim, 1978, J. Geophys. Res. **83**, 623.
Silin, V. P., 1965, Zh. Éksp. Teor. Fiz. **48**, 1679 [Sov. Phys. JETP **21**, 1127 (1965)].
Singh, N., 1994, Geophys. Res. Lett. **21**, 257.
Škorić, M. M., and D. ter Haar, 1980, Physica C **98**, 211.
Smith, D. F., and D. Sime, 1979, Astrophys. J. **233**, 998.
Sodha, M. S., A. K. Ghatak, and V. K. Tripathi, 1976, Prog. Opt. **13**, 169.
Sotnikov, V. I., V. D. Shapiro, and V. I. Shevchenko, 1978, Fiz. Plazmy **4**, 450 [Sov. J. Plasma Phys. **4**, 252 (1978)].
Spangler, S. R., and J. P. Sheerin, 1982, J. Plasma Phys. **27**, 193.
Spangler, S. R., and J. P. Sheerin, 1983, Astrophys. J. **272**, 273.
Stamper, J. A., R. H. Lehmberg, A. Schmitt, M. J. Herbst, E. C. Young, J. H. Gardner, and S. P. Obenschain, 1985, Phys. Fluids **28**, 2563.
Stenflo, L., and P. K. Shukla, 1990, Astrophys. Space Sci. **172**, 317.
Stix, T. H., 1992, *Waves in Plasmas* (AIP, New York).
Stubbe, P., H. Kohl, and M. T. Rietveld, 1992, J. Geophys. Res. **97**, 6285.
Sturman, V. I., 1976, Zh. Éksp. Teor. Fiz. **71**, 613 [Sov. Phys. JETP **44**, 322 (1976)].
Sturrock, P. A., 1964, in *Physics of Solar Flares*, edited by W. H. Ness, AAS-NASA Symposium, NASA SP-50 (NASA, Washington, DC), p. 357.
Sulzer, M. P., 1986, Radio Sci. **21**, 1033.
Sulzer, M. P., and J. A. Fejer, 1994, J. Geophys. Res. **99**, 15 035.
Suzuki, S., and G. A. Dulk, 1985, in *Solar Radiophysics*, edited by D. J. McLean and N. R. Labrum (Cambridge University, Cambridge, U.K.), p. 289.
Swanson, D. G., 1989, *Plasma Waves* (Academic, San Diego).

Tajima, T., 1996, Ed., *The Future of Accelerator Physics. The Tamura Symposium Proceedings*, Austin, Texas, 1994, AIP Conference Proceedings 356 (AIP, Woodbury, New York).
Tam, S. W. Y., and T. Chang, 1995, Geophys. Res. Lett. **22**, 1125.
Tanaka, K., L. M. Goldman, W. Seka, R. W. Short, and E. A. Williams, 1984, Phys. Fluids **27**, 2960.
Tanikawa, T., A. Y. Wong, and D. L. Eggleston, 1984, Phys. Fluids **27**, 1416.
Taniuti, T., and H. Washimi, 1968, Phys. Rev. Lett. **21**, 209.
ter Haar, D., and V. N. Tsytovich, 1981, Phys. Rep. **73**, 175.
Thejappa, G., D. Lengyel-Frey, R. G. Stone, and M. L. Goldstein, 1993, Astrophys. J. **416**, 831.
Thomson, J. J., W. L. Kruer, A. B. Langdon, C. E. Max, and W. C. Mead, 1978, Phys. Fluids **21**, 707.
Thornhill, S. G., and D. ter Haar, 1978, Phys. Rep. **43**, 43.
Tonks, L., and I. Langmuir, 1929, Phys. Rev. **33**, 195.
Tsintsadze, N. L., D. D. Tskhakaya, and L. Stenflo, 1979, Phys. Lett. A **72**, 115.
Tsytovich, V. N., 1977, *Theory of Turbulent Plasma* (Consultants Bureau, New York).
Tsytovich, V. N., 1995, *Lectures on Non-linear Plasma Kinetics* (Springer, Berlin).
Utlaut, W. F., 1970, J. Geophys. Res. **75**, 6402.
Vago, J. L., P. M. Kintner, S. W. Chesney, R. L. Arnoldy, K. A. Lynch, T. E. Moore, and C. J. Pollock, 1992, J. Geophys. Res. **97**, 16 935.
Valeo, E. J., and W. L. Kruer, 1974, Phys. Rev. Lett. **33**, 750.
Vedenov, A. A., and L. I. Rudakov, 1964, Dokl. Akad. Nauk SSSR **159**, 767 [Sov. Phys. Dokl. **9**, 1073 (1965)].
Verga, A. D., and C. F. Fontan, 1985, Plasma Phys. Control. Fusion **27**, 19.
Vladimirov, S. V., and S. I. Popel, 1995, Phys. Rev. E **51**, 2390.
Vladimirov, S. V., V. N. Tsytovich, S. I. Popel, and F. Kh. Khakimov, 1995, *Modulational Interactions in Plasmas* (Kluwer, Dordrecht).
Vyacheslavov, L. N., V. S. Burnasov, I. V. Kandaurov, E. P. Kruglyakov, O. I. Meshkov, and A. L. Sanin, 1995, Phys. Plasmas **2**, 2224.
Wang, J. G., G. L. Payne, D. F. DuBois, and H. A. Rose, 1994, Phys. Plasmas **1**, 2531.
Wang, J. G., G. L. Payne, D. F. DuBois, and H. A. Rose, 1995, Phys. Plasmas **2**, 1129.
Wang, J. G., G. L. Payne, D. F. DuBois, and H. A. Rose, 1996, Phys. Plasmas **3**, 111.
Weatherall, J. C., D. R. Nicholson, and M. V. Goldman, 1983, Phys. Fluids **26**, 1103.
Weatherall, J. C., J. P. Sheerin, D. R. Nicholson, G. L. Payne, M. V. Goldman, and P. J. Hansen, 1982, J. Geophys. Res. **87**, 823.
Wild, J. P., 1950, Aust. J. Sci. Res., Ser. A **3**, 541.
Wilks, S., P. E. Young, J. Hammer, M. Tabak, and W. L. Kruer, 1994, Phys. Rev. Lett. **73**, 2994.
Winglee, R. M., 1983, Plasma Phys. **25**, 217.
Wong, A. Y., and P. Y. Cheung, 1984, Phys. Rev. Lett. **52**, 1222.
Wong, A. Y., P. Leung, and D. Eggleston, 1977, Phys. Rev. Lett. **39**, 1407.
Wong, A. Y., and B. H. Quon, 1975, Phys. Rev. Lett. **34**, 1499.
Wong, A. Y., and R. J. Taylor, 1971, Phys. Rev. Lett. **27**, 644.
Yamanaka, C., 1991, in *Handbook of Plasma Physics*, Vol. 3, edited by M. N. Rosenbluth, R. Z. Sagdeev, A. Rubenchik, and S. Witkowski (North-Holland, Amsterdam), p. 1.
Young, P. E., H. A. Baldis, R. P. Drake, E. M. Campbell, and K. G. Estabrook, 1988, Phys. Rev. Lett. **61**, 2336.
Zakharov, V. E., 1972, Zh. Éksp. Teor. Fiz. **62**, 1745 [Sov. Phys. JETP **35**, 908 (1972)].
Zakharov, V. E., 1984, in *Handbook of Plasma Physics*, Vol. 2, edited by M. N. Rosenbluth, R. Z. Sagdeev, A. A. Galeev, and R. N. Sudan (North-Holland, Amsterdam), p. 81.
Zakharov, V. E., N. E. Kosmatov, and V. F. Shvets, 1989, Pis'ma Zh. Éksp. Teor. Fiz. **49**, 431 [JETP Lett. **49**, 492 (1989)].
Zakharov, V. E., and E. A. Kuznetsov, 1986, Zh. Éksp. Teor. Fiz. **91**, 1310 [Sov. Phys. JETP **64**, 773 (1986)].
Zakharov, V. E., E. A. Kuznetsov, and S. L. Musher, 1984, Pis'ma Zh. Éksp. Teor. Fiz. **41**, 125 [JETP Lett. **41**, 154 (1985).
Zakharov, V. E., S. L. Musher, and A. M. Rubenchik, 1975, Zh. Éksp. Teor. Fiz. **69**, 155 [Sov. Phys. JETP **42**, 80 (1975)].
Zakharov, V. E., S. L. Musher, and A. M. Rubenchik, 1985, Phys. Rep. **129**, 285.
Zakharov, V. E., A. N. Pushkarev, A. M. Rubenchik, R. Z. Sagdeev, and V. F. Shvets, 1988, Pis'ma Zh. Éksp. Teor. Fiz. **47**, 239 [JETP Lett. **47**, 286 (1988)].
Zakharov, V. E., A. N. Pushkarev, A. M. Rubenchik, R. Z. Sagdeev, and V. F. Shvets, 1989, Zh. Éksp. Teor. Fiz. **96**, 591 [Sov. Phys. JETP **69**, 334 (1989)].
Zakharov, V. E., A. N. Pushkarev, R. Z. Sagdeev, G. I. Solov'ev, V. D. Shapiro, V. F. Shvets, and V. I. Shevchenko, 1989, Dokl. Akad. Nauk SSSR **305**, 598 [Sov. Phys. Dokl. **34**, 248 (1989)].
Zakharov, V. E., and A. B. Shabat, 1971, Zh. Éksp. Teor. Fiz. **61**, 118 [Sov. Phys. JETP **34**, 62 (1972)].
Zakharov, V. E., and L. N. Shur, 1981, Zh. Éksp. Teor. Fiz. **81**, 2019 [Sov. Phys. JETP **54**, 1064 (1981)].
Zakharov, V. E., V. V. Sobolev, and V. C. Synakh, 1971, Zh. Éksp. Teor. Fiz. **60**, 136 [Sov. Phys. JETP **33**, 77 (1971)].